NUREG/CR-3766
BNL-NUREG-51767

TESTING OF NUCLEAR GRADE LUBRICANTS AND THEIR EFFECT ON A540 B24 AND A193 B7 BOLTING MATERIALS

Carl J. Czajkowski

March 1984

MATERIALS TECHNOLOGY DIVISION
DEPARTMENT OF NUCLEAR ENERGY, BROOKHAVEN NATIONAL LABORATORY
UPTON, LONG ISLAND, NEW YORK 11973

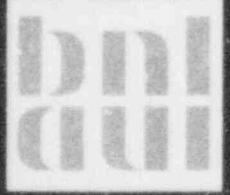

Prepared for
United States Nuclear Regulatory Commission
Office of Nuclear Regulatory Research
Contract No. DE-AC02-76CH00016

NUREG/CR-3768
BNL-NUREG-51767
AN, R-5

TESTING OF NUCLEAR GRADE LUBRICANTS AND THEIR EFFECT ON A540 B24 AND A193 B7 BOLTING MATERIALS

Carl J. Czajkowski

March 1984

MATERIALS TECHNOLOGY DIVISION
DEPARTMENT OF NUCLEAR ENERGY, BROOKHAVEN NATIONAL LABORATORY
UPTON, LONG ISLAND, NEW YORK 11973

PREPARED FOR THE UNITED STATES NUCLEAR REGULATORY COMMISSION
DIVISION OF ENGINEERING TECHNOLOGY
OFFICE OF NUCLEAR REGULATORY RESEARCH
NRC FIN. NO. A-3011

TABLE OF CONTENTS

LIST OF FIGURES

LIST OF FIGURES (CONT'D)

LIST OF FIGURES (CONT'D)

LIST OF FIGURES (CONT'D)

LIST OF FIGURES (CONT'D)

LIST OF FIGURES (CONT'D)

LIST OF FIGURES (CONT'D)

LIST OF TABLES

ABSTRACT

An increase in the number of bolting failures attributed to lubricant/coolant interaction at nuclear power plants has caused a great deal of concern regarding the more judicious use of lubricants by the nuclear power industry. An investigation was performed on eleven commonly used lubricants by the nuclear power industry. The investigation included EDS analysis of the lubricants, notched-tensile constant extension rate testing of bolting materials with the lubricants, frictional testing of the lubricants and weight loss testing of a bonded solid film lubricant. The report generally concludes that there is a significant amount of variance in the mechanical properties of common bolting materials, that MoS_2 can hydrolize to form H_2S at 100°C and cause stress corrosion cracking (SCC) of bolting materials, and that the use of copper-containing lubricants can be potentially detrimental to high strength steels in an aqueous environment. Additionally, the testing of various lubricants disclosed that some lubricants contain potentially detrimental elements (e.g. S, Sb) which can promote SCC of the common bolting materials. One of the most significant findings of this report is the observation that both A193 B7 and A540 B24 bolting materials are susceptible to transgranular stress corrosion cracking in demineralized H_2O at 280°C in notched tensile tests.

1.0 INTRODUCTION

In the first quarter of 1983, the United States Nuclear Regulatory Commission (U.S. NRC) reported [1] 44 distinct instances of bolting degradation at nuclear power plants between October 1964 to March 1982. These 44 occurrences were broken down into the following subclassifications: 19 involved a stress corrosion cracking (SCC) mechanism, 13 were attributed to boric acid wastage corrosion, 3 were fatigue induced, 1 instance of erosion-corrosion and 8 additional incidents involving material related problems or where apparent cause could not be identified. It is clearly obvious that the largest single cause of bolting degradation was SCC. (At least two [2,3] analyses involving SCC of fasteners attributed the failure to a lubricant/moisture interaction which resulted in a corrosive environment.)

It was this lubricant/moisture interaction which was of sufficient concern to the Office of Nuclear Regulatory Research (ONRR) of the U.S. NRC to provide funding to Brookhaven National Laboratory (BNL) for an investigation into the effects of lubricants on fastener degradation. The program as originally proposed by BNL consisted of four major sections:

1) Reactions of MoS_2 with steam.

2) Reactions of commercial lubricants, including those containing MoS_2, with steam.

3) Notched tensile and WOL (wedge Open Load) tests of high strength bolting materials (ASTM A-193 B-7 and A-540) in the presence of steam and either MoS_2 or commercial lubricants.

4) Fractography and EDS (Energy Dispersive Spectroscopy) surface analysis.

The original program was later modified in order to accommodate a larger scope of testing in the allowable time frame of the program. The expanded program removed WOL tests in favor of notched tensile tests, coefficient of friction testing, and weight loss testing of a bonded solid film lubricant.

2.0 CHEMICAL ANALYSIS OF THE LUBRICANTS

For purposes of this program, a total of 11 lubricants were used. Some tests were also performed on a bonded solid film lubricant. (Note: due to time restrictions and other constraints, only one type of coating was tested, and these results should not be extrapolated to other types of coating without additional testing).

These 11 lubricants were types commonly used in construction and post operational lubrication at nuclear power plants. The 11 lubricants tested were numbered one through eleven and were classified as follows:

Lubricant Number	Type
1	Chemically pure MoS_2
2	Commercially available MoS_2 spray
3	Commercial MoS_2 spray (different manufacturer)
4	Commercial MoS_2 spray (3rd manufacturer)
5	Graphite in isopropanol
6	Graphite in ammonia
7	Nickel + graphite lubricant
8	Copper + graphite lubricant
9	Anti-seizing lubricant
10	Nickel based never seizing lubricant
11	Never seizing lubricant

Each of these lubricants was either sprayed or smeared onto carbon blocks and then loaded into a scanning electron microscope (SEM) and subjected to energy dispersive spectroscopy analysis of constituents.

EDS is an analytical technique, capable of performing elemental analysis of microvolumes, typically on the order of a few cubic microns in bulk samples and considerably less in thinner sections. Analysis of X-rays emitted from a sample is accomplished by crystal spectrometers which use energy dispersive spectrometers and permit analysis by discriminating among X-ray energies.

The feature of electron beam microanalysis that best describes this technique is its mass sensitivity. For example, it is often possible to detect less than 10^{-16} grams of an element present in a specific microvolume of a sample. The minimum detectable quantity of a given element or its detectability limit varies with many factors, and in most cases is less than 10^{-16} grams/microvolume.

For purposes of this report, EDS was considered to be a satisfactory method of chemical analysis. (Note: EDS will only discern elements with atomic numbers greater than Na so certain light elements will not be detected).

Figure 1 is the EDS scan of lubricant #1. It is clearly seen that only molybdenum and sulfur (MoS_2) are present in the scan.

Figure 2 is an EDS scan of a commercially available MoS_2 (lubricant #2) spray. The scan detected both antimony and titanium in addition to the molybdenum and sulfur. The titanium is possibly used for coloring. The significance of the antimony addition is unknown.

Figure 3 is a scan of lubricant #3 which is a second manufacturer's molylube type spray and shows only molybdenum and sulfur present in the spray. This would be the expected scan of a molybdenum disulfide lubricant.

The EDS scan of lubricant #4 which is another moly-lube spray is shown in Figure 4. This scan showed only a sulfur peak with no molybdenum present at all.

Lubricant #5, which is a graphite and isopropanol lubricant, was subjected to EDS and the resultant scan is shown in Figure 5. This lubricant showed a high sulfur peak with a trace of silicon also present. The presence of sulfur would not be normally anticipated in a graphite + alcohol lubricant and might be detrimental to highly alloyed steels under the proper conditions.

Figure 6 is a scan of lubricant #6 which is graphite + ammonia. The absence of any peaks would be expected and was the final result. (C, N, H all have atomic numbers lower than sodium.)

The next five lubricants tested are all metal based with different materials used as the carrier medium.

Figure 7 is an EDS scan of the nickel + graphite lubricant #7. The scan shows only a trace of silicon with nickel present. Graphite (carbon) would not show on the scan. This scan is the expected result for this lubricant.

Lubricant #8 is a copper + graphite lubricant and Figure 8 shows a scan of only copper which would be expected for this lubricant.

Figure 9 is a photograph of the EDS scan of the anti-seize type lubricant #9. The scan showed an aluminum peak (possibly for coloration) and a silicon peak with the major constituent being copper.

The nickel based never seize type lubricant (lubricant #10) is shown in the EDS scan (Figure 10) with a predominant nickel peak and a secondary peak of aluminum.

Figure 11 is a representative EDS scan of the never seize type lubricant #11. It is clearly seen that copper is the primary constituent of the lubricant with a significant amount of both zinc and aluminum also present.

The bonded solid film type lubricant was not subjected to EDS analysis due to significant outgassing of the material when subjected to an electron beam. The manufacturer's reported chemical analysis limit of this lubricant are therefore included:

Fluoride	29 ppm
Chlorine	200 ppm
Sulfur	98 ppm
Lead	2 ppm
Mercury	1 ppm
Arsenic	0.05 ppm
Zinc	1 ppm

It can be clearly seen from the different EDS scans that there is a significant variance in the chemical analysis of even similar type lubricants. The appearance of possibly detrimental elements in lubricant #2 (antimony) and #5 (sulfur) plus the total absence of molybdenum in the moly-lube type lubricant #4 give evidence that independent chemical analysis of lubricants prior to their general use on a nuclear power plant would be a prudent course of action by a utility.

2.1 Steaming Tests on MoS_2

Prior BNL reports [2, 4, 5] had referenced various papers and reports which showed that in moist conditions, MoS_2 could hydrolize and form detrimental sulfides which could result in a SCC failure in low alloy steels.

These conditions involved frictional tests in flowing nitrogen/water mixtures. Since rubbing forces are only at work at the torqing down of a bolt and would not normally come into play during the bolts' service life; some steaming tests were performed to see if steam alone could interact with MoS_2 in order to form potentially detrimental compounds.

Three tests were performed in order to determine if a gaseous sulfide could be produced by steaming MoS_2. The first test was conducted in a stainless steel autoclave. For this test, distilled water was poured into the autoclave, after which a glass dish with chemically pure MOS_2 was suspended above the water; the autoclave head tightened down and the water then heated to 100°C. The autoclave head was vented into a plastic tube with a metering valve into a test tube of water and then into a test tube of cadmium acetate. The unbalanced chemical reaction of this experiment is:

Hydrogen Sulfide + Cadmium Acetate ▶ Cadmium Sulfide ▼ (precipitate)

The amount of cadmium sulfide produced is then weighed and sulfur also measured in the water after the experiment is completed. The results of the first experiment produced 0.889μg of sulfur from the gaseous phase and 0.911 mg of sulfur in the H_2O. Since some sulfide experiments had been performed in this autoclave prior to this run of tests, two more tests were performed in a new glass dessicator. The test conditions of the second test were basically the same as the first experiment although this time the experiment was conducted with 71.10 gms of chemically pure MoS_2 placed on two glass dishes supported above 500 ml of distilled H_2O. The water was boiled on a hot plate for five hours, after which the amount of sulfur was measured in both the gaseous and liquid phases. A blank was also run of the experiment and subtracted from the original results to take into account any sulfide which might be present in the surrounding air. This test produced 0.615μg in the gaseous phase and 142.4μg in the H_2O or approximately 2 ppm sulfur (total) produced from steaming 71.1 gms of MoS_2.

The third experiment was conducted in the dessicator using 71.10 gms of MoS_2 under similar conditions as the second test. The only variation was that the surface area of the MoS_2 open to the steam was reduced to 614 mm^2 from 1486 mm^2. This test produced 0.0 gms of sulfur in the gaseous phase and and 0.351 mg of sulfur in the liquid phase after the blanks were subtracted.

These experiments show that the steaming of MoS_2 produces hydrogen sulfide (H_2S). Since H_2S has been shown to produce SCC in low alloy steels [6]; it is considered unadvisable to use MoS_2 containing lubricants on critical components of nuclear power plants.

Because many power plants have used MoS_2 containing lubricants on bolts and other components, it was felt worthwhile to determine if previously applied MoS_2 (spray form) could be removed from a bolt's surface and if so, by what cleaning agent(s).

To this end two bolts were sprayed with lubricant #2 and allowed to dry. The bolts were then ultrasonically cleaned, one bolt in a bath of carbon disulfide (CS_2) and the other in a bath of Calfonex 78-A. The Calfonex had been previously shown [7] to remove sprayed on MoS_2 and the carbon disulfide was used as a result of discussions between the U.S. NRC-MTEB and BNL [8]. After ultrasonic cleaning for 15 minutes, the two bolts were rinsed in distilled water, and then again ultrasonically cleaned in methanol for an additional 15 minutes. The bolts were again rinsed in distilled water, hot air dried and then subjected to EDS in the SEM to determine the extent of MoS_2 removal. The results of this cleaning procedure are shown in Figures 12 and 13.

It is quite evident from the scans that the Calfonex left a residue of MoS_2 from the bolt's surface while the carbon disulfide removed the MoS_2 entirely.

Although MoS_2 has been shown to be removed by cleaning with carbon disulfide and methanol; adequate testing of the effect of carbon disulfide on the possible SCC of low alloy steels should be performed prior to this method being used in the field. It should be stressed that the pre-testing of any new lubricant or cleaning material used on critical reactor components (prior to widespread use) is the only prudent method of minimizing the potential for SCC.

3.0 COEFFICIENT OF FRICTION TESTING OF THE ELEVEN LUBRICANTS

SCC requires three separate elements to be present, namely:

1) Susceptible material
2) Corrosive environment
3) Tensile stress

If any of the aforementioned elements are missing, SCC will not occur. In the case of bolting, the material and the environment may not be able to be altered, in which case the applied tensile stress (preload) may have to be altered (if design conditions allow) to keep the applied tensile stress below a critical level. Since preload is dependent on the coefficient of friction for a given lubricant a factor of 2-3 (some lubricants have ranges given) in this frictional coefficient may throw the applied stress into the critical range of SCC susceptibility.

It was felt that since the coefficient of friction can play such an important role in the potential susceptibility of a bolt to SCC; BNL should measure the coefficient of friction for these lubricants.

The technique used for these measurements was the "sled and bed" technique. The tests performed were similar to those outlined in ASTM D 1894-75 (Static and Kinetic Coefficients of Friction of Plastic Film and Sheeting). Both static and kinetic measurements were made. Some of the lubricants were tested both wet (as sprayed or brushed) and dry (if the lubricants were of the air drying type).

The following are the results of these tests:

Lubricant No.		Coefficient of Friction	
		Static	Kinetic
1a.	dry	0.182	0.164
b.	wetted with isopropanol	0.273	0.142
2a.	dry	0.266	0.223
b.	wet	0.250	0.149
3a.	dry	0.223	-
b.	wet	0.156	-
4a.	dry	0.026	0.150
b.	wet	-	0.130
5a.	dry	0.130	0.160
b.	wet	0.185	0.190
6 .	dry	0.351	0.170
7 .	wet	-	0.149
8 .	wet	0.055	0.126
9 .	wet	0.093	0.171
10 .	wet	0.042	0.296
11 .	wet	0.049	0.268

The results show that the coefficients of friction, for even similar types of lubricants, vary widely. For example, the static values for lubricants 1-4, (All purportedly molybdenum disulfide-based lubricants), ranged from 0.026 to 0.273 dependent upon manufacturer and condition (wet or dry).

Coefficients of friction with the two graphite-based lubricants #5 and 6 in the dry static condition varied by a factor of almost 3.

This difference was also noted in the static measurements of the copper based lubricants #8, #9 and #11. Here the spread, while less, was still almost a factor of two.

The kinetic values also had some variances as shown by the nickel based lubricants #7 and #10. These also vary by almost a factor of two (0.149 - #7 and 0.296 - #10).

The wide variances in the coefficients of friction for these lubricants would certainly demand that this value be measured prior to its general use in a reactor environment. This investigation should be for the particular brand of lubricant being considered, as the same type (e.g. the moly lubes) can also show a considerable spread of value.

4.0 ENVIRONMENTAL TESTING OF BOLTING MATERIALS

4.1 Hardness Testing

Hardness measurements are a reasonable method of estimating tensile strengths of carbon and low alloy steels. This results from the fact that there exists a close relationship between compressive strength and tensile strength of these steels and that resistance to indentation (hardness testing) is related to the steel's compressive strength. Estimates of a material's tensile strength can be approximated in most cases to $\pm$ 5000 psi with a hardness test.

Due to the fact that at one nuclear site [8] a review of 12 heats of bolting materials (384 bolts) disclosed that all of the heats were essentially in violation of the hardness specifications for the bolting materials, hardness tests were performed on both the A540 B24 Cl.2 and the A193 B7 materials [Table 3] prior to commencing the notched tensile testing.

Initially, only one end of the A540 B24 Class 2 rod had hardnesses performed on it yielding an average value of 356 KN/500 gm (equivalent to approximately a 159 Ksi tensile strength) which was reasonably close to the actual tensile strength of the material 160.5 Ksi. After some disparities were noted during the testing of the specimens, additional hardnesses were performed on specimens 1, 22, 6, 27, 30, 31. These hardness values only equated to a tensile strength of approximately 143 Ksi or a drop of approximately 16 Ksi.

The hardness of A193 B7 material was also checked for each of the non-coated tests and also had a spread of values of approximately 12 Ksi (145 Ksi - 157 Ksi).

4.2 Notched Tensile Testing

In order to ascertain if bolting materials (specifically A193-B7 and A540 B24 Class 2) would have an environmental interaction with any of the lubricants and steam, constant extension rate tests (CERT) were performed at 100°C and 280°C.

The CERT method is basically the application of slow dynamic straining to a stress corrosion (tensile type) specimen while it is exposed to the environment. This particular mode of testing has the advantage of always resulting in a fracture at its completion and normally does so in a relatively short period of time (a few hours to a few days).

Another advantage of this type of testing is the ability to adjust the strain rate in the most probable range of stress corrosion crack velocities namely 10^{-6} to 10^{-9} in/sec . This strain rate is quite important as too high a strain rate would result in ductile failure by void coalescence prior to the development of the necessary corrosion reactions; while too slow a strain rate could again fall out of the range for SCC failures to occur. For these reasons, it is important to realize that the

absence of cracking in a given medium does not necessarily preclude the possibility of SCC until additional strain rate tests (both higher and lower rates) have been completed.

Since ordinary tensile tests on smooth specimens will not indicate whether a material is prone to brittle fracture in the presence of a stress concentration (similar to the threads on bolts), it was decided that a notched tensile specimen would be used. The specimens had a 50% diameter notch machined into them (Figure 14). The materials tested were A193 B7 (Table 1) and A540 B24 Class 2 (Table 2) bolting materials.

The fracture face of each of the specimens was examined by SEM after the CERT. Prior to examination by SEM, the specimens were electrolytically cleaned to remove the oxide film as follows:

A working solution of endox-214 was prepared by adding 8 ounces of endox-214 powder to 1000 ml of cold water and stirring until it was completely dissolved. A small amount of photoflow was added to the solution to aid the wetting of the specimen and eliminate some of the featuring during the electrochemical cleaning step. A glass beaker with 500 ml of the endox-214 solution was placed in an ultrasonic cleaner. The specimen was made the cathode and a platinum wire loop was used as an anode. A current density of 250 mA/cm^2 was applied for one minute. The specimen was removed from the electrolyte and ultrasonically washed in a detergent solution consisting of alconox and photoflow for another minute, then rinsed in clean water, dipped in methanol and dried in hot air. The above procedure comprises one cycle. It was occasionally necessary to repeat the above cycle several times before removing all the corrosion products. It was not possible to predetermine the exact number of cleaning cycles for any given specimen, since it depends upon the severity of the oxidation, roughness of surface, and the physical size of the sample. The specimen was observed optically after each cycle so that the process can be discontinued after the oxide or the corrosion product was removed and the specimen surface looks clean. After the specimen was thoroughly dried, it was examined immediately, since it may be prone to reoxidization at ambient atmosphere, or it was stored in a good desiccate.

This investigation involved a total of 62 notched tensile CERT. In addition to 44 tests on A193 B7 and A540 B24 materials; 18 tests were conducted on both A193 B7 and A540 B24 C1.2 material coated with a bonded solid film lubricant.

All of the tests were conducted in a stainless steel autoclave. Approximately 1000 ml of demineralized H_2O was added to the autoclave and then the specimen loaded above the water. The temperature of the solution was raised to test temperature (either 100°C or 280°C) through the use of resistance heating coils. After the required temperature was stabilized (approximately 30 minutes) the test pull was commenced. When the lubricant tests were conducted, the lubricants were either sprayed on or brushed onto the notched area of the specimen. All specimens were tested at a strain rate of $5\text{-}9 \times 10^{-7}$ sec.$^{-1}$.

4.2.1 A540 B24 Class 2 Tests

The first six specimens were tested, Figures 15-26, at 100°C in demineralized H_2O with no lubricants added and at a strain rate of approximately $5.0\text{-}9.0 \times 10^{-7}$ sec.$^{-1}$. It was seen in all of the SEM photographs that each of the fracture faces is ductile in nature (dimpled rupture). The surprising observation was in the wide range of tensile strength results (195 Ksi - 277 Ksi) considering the fact that all of the A540 B24 specimens were machined from the same bar. On these specimens, there was no discernable difference in the fracture faces to account for the different strength levels. This variation in strength level from the same bar is consistent with the hardness variations previously discussed and should be taken into account prior to critical bolting installations.

Specimen #7 was tested at 280°C in demineralized water and displayed a tensile value of approximately 210 Ksi. The fracture face (Figures 27 and 28) exhibited a typical overload failure.

The next three tests (Specimens #8, 9, 10) were also conducted at 280°C but exhibited a transgranular (quasi cleavage) area around the circumference of each specimen (Figures 29-34). The tensile strength of these specimens ranged between 189 Ksi - 216 Ksi. This area of transgranular fracture would be indicative of a brittle fracture, probably induced by the environment.

Specimens #11 and 12 (Figures 35-38) were tested at 100°C but had diametrically half of the notch coated with chemically pure MoS_2 lubricant #1. Both specimens exhibited a ductile overload failure, but differed in tensile strengths by almost 60 Ksi (#11-207 Ksi; #12-265 Ksi).

The next five specimens (tests #13-17) were all tested at 280°C with chemically pure MoS_2 on half of the notch. Specimens #13 and 14 only attained notch tensile values of 165 Ksi and 171 Ksi. The fracture faces for these tests (Figures 39-42) had transgranular areas associated with them, indicating an environmental interaction. Specimens #15-17 all attained tensile values in excess of 240 Ksi and the fracture faces (Figures 43-48) all exhibited a dimpled rupture appearance; typical of ductile overload.

Specimens #18 and 19 were tested under the same environmental conditions as the prior five tests, except the strain rate was reduced by a factor of about 2. Both specimens attained very low (144 Ksi and 120 Ksi) notch tensile strengths and their fracture faces were primarily dimpled with possibly some small areas of transgranularity evident (Figures 49-52).

Specimens #20 and 21 were tested at 100°C and 280°C respectively with lubricant #2 sprayed on half of the notch. Both specimens attained notched tensile values in excess of 200 Ksi and both specimens had fracture faces exhibiting ductile failure (Figures 53-56).

The next five specimens #22-26 were all tested using lubricant #3. Specimens 22-24 were tested at 100°C and all attained notch tensile values in excess of 230 Ksi. The fracture faces for these specimens (Figures 57-62) were all ductile in nature. Specimens 25 and 26 were tested at 280°C and both of these attained tensile values above 228 Ksi with dimpled fracture faces (Figures 63-66) also evident.

Specimen #27 was tested at 280°C using lubricant #4. There was one area of transgranularity evident (Figures 67 and 68) with the specimens attaining a value in excess of 220 Ksi. This area of transgranular fracture was considered to be induced by the environment.

Specimen #28 was tested with lubricant #5 (graphite + isopropanol) at 280°C. The fractographs of the fracture surface showed the failure to be ductile (Figures 69, 70) and the specimen attained a notched tensile value of 244.6 Ksi.

The fracture surface of Specimen #29 and #30 both showed ductile failures (Figures 71-74). These specimens were tested with lubricant #7 (nickel + graphite) at 280°C. The notch tensile strength of Specimen #29 was 251 Ksi. The tensile strength of #30 could not be determined due to recorder problems with the test.

Specimens 31 and 32 were tested with the copper + graphite lubricant #8 at 280°C. Both specimens exhibited some transgranularity (Figures 75-78) with #32 exhibiting only a 146.7 Ksi notched tensile strength. This specimen also had a circumferential crack running almost completely around the specimen. Specimens #33 and 34 were tested with lubricants #9 and 11 respectively at 280°C. Both specimens attained notched tensile strengths of 244.6 Ksi and had dimpled rupture type fracture faces (Figures 79-82).

4.2.2 A193 B7 Tests

The next ten specimens tested were machined from A193 B7 bolting material.

Specimen #35 was tested in demineralized water at 100°C. The specimen attained a notched tensile strength of 230.7 Ksi and showed a ductile failure (Figures 83 and 84).

Specimens #36-39 were all tested in demineralized water at 280°C. There was a large range of notched tensile values attained (114 Ksi - 232 Ksi). Transgranular areas were noted on specimens #38 and #39 (Figures 89-92) while the fracture faces for the other specimens were predominantly ductile in appearance (Figures 85-88). The transgranular areas plus the wide range of tensile strengthr are evidence of the susceptibility of this material to SCC in the demineralized water environment at 280°C. The lowest tensile value obtained on specimen #36 with no discernible transgranularity at this time must be considered an anomaly.

Specimens #40-#43 were all tested using chemically pure MoS_2 (lubricant #1) or one half of the notch.

Specimen #40 was tested at 100°C and attained a notched tensile strength of 231.5 Ksi and exhibited a ductile fracture mode (Figures 93 and 94).

The fracture faces of the specimens tested at 280°C with chemically pure MoS_2 (Figures 95-100) all exhibited areas of transgranular fracture. The appearance of these areas in addition to the fact that these specimens only attained notched tensile strengths of 171 Ksi - 198 Ksi denote an environmental effect on this fracture.

Specimen #44 was tested at 280°C with lubricant #8 applied to half of the notch. Portions of the fracture face were transgranular in appearance (Figures 101-102) and the specimen achieved a notched tensile strength of 256.8 Ksi.

4.3 Bonded Solid Film Lubricant Tests

A total of 18 tests were performed on bolts coated with a bonded solid film lubricant in order to determine if the lubricant would have a beneficial effect on the SCC resistance of the bolting materials tested. Twelve of the tests were performed on A540 B24 Class 2 materials and six tests were performed on A193 B7 bolting materials.

Specimens #45-49 were all tested at 280°C in demineralized water. The fracture faces of specimens #45, 47, 48, and 49 (Figures 103, 104 and 107-112) all showed ductile overload. The notch tensile strengths of these specimens ranged between 224 Ksi and 261 Ksi. Specimen #46 attained a notched tensile strength of only 171.2 Ksi and exhibited transgranular areas on the fracture face (Figures 105, 106) defining a SCC susceptibility under these conditions.

Tests were performed at 280°C with chemically pure MoS_2 on half of the notch on specimens #50-53. Specimen #50 attained a notched tensile strength of 203.8 Ksi and had transgranular areas in evidence on the fracture face (Figures 113, 114). Specimen #51 showed an entirely ductile fracture (Figures 115-116) and had a notched tensile strength of 293.5 Ksi. Specimen #52 had large areas of transgranular fracture (Figures 117-118) and only had a measured notched tensile strength of 171 Ksi. The final MoS_2 test (Specimen #53) was basically ductile in appearance (Figures 119, 120) and attained a notched tensile strength of 228.9 Ksi.

Specimen #54 tested at 280°C with lubricant #8 showed no environmental effect (Figures 121, 122) with a ductile fracture evident and a notched tensile value of 256.8 Ksi.

Since some bolts removed from power plants may have been previously exposed to MoS_2 lubricants prior to the application of a bonded solid film lubricant, two specimens (both A540, B24 material) were steamed at 100°C with MoS_2 for 1 hour; then cleaned, and sent out for coating. The two specimens #55 and #56 were tested afterward in demineralized water at 280°C. Specimen #55 exhibited a ductile fracture face (Figures 123, 124) and had a notched tensile strength of 260.9 Ksi. A 60 Ksi reduction in the notched tensile strength of specimen #56 was observed, as well as some transgranularity of the fracture face (Figures 125, 126). This specimen appeared to have suffered SCC while specimen #55 did not. Since all conditions of the two tests were constant, the difference in notched tensile strength must be attributed to the materials inconsistent mechanical properties.

The last six notched tensile tests were performed on A193 B7 material. Specimens #57-58 were tested at 100°C in demineralized water. Specimen #57 had areas of transgranular fracture evident on the fracture face (Figures 127, 128) and had a notched tensile strength of 216 Ksi. Specimen #58 achieved a tensile value of 232 Ksi and had a ductile fracture in evidence (Figures 129, 130).

Specimen #59 was tested in demineralized water at 280°C. It had an area of transgranularity on the fracture face (Figures 131, 132) and had a notched tensile strength of 216 Ksi.

Specimens #60-62 were all tested at 100°C with chemically pure MoS_2 (lubricant #1) used on half of the notch. Both specimens #60 and #61 had dimple ruptured fracture faces (Figures 133-136) with #60 attaining a 224 Ksi value in the notched tensile strength.

The last specimen (#62) was tested at 280°C with chemically pure MoS_2 on one half of the notch. The fracture face exhibited transgranular areas (Figures 137-138) and had a notched tensile strength of 220 Ksi.

5.0 WEIGHT LOSS TESTING OF BONDED FILM LUBRICANT

As previously mentioned [1], the U.S. NRC documented the bolting degradation experience in 1983. The second largest contributor to the bolting degradation problem was boric acid wastage corrosion. BNL investigated this problem for the U.S. NRC, Chemical Engineering Branch [10] (CMEB) by conducting a literature search and by performing confirmatory experiments of boric acid wastage corrosion as outlined below:

Previously published data [11] were accumulated by BNL on an AISI 4135 steel in H_3BO_3 and H_3BO_3 - KOH solutions at 70°F and 140°F. In addition, BNL work on A193-B7 and AISI 4130 material at higher temperatures was plotted to determine if extrapolations were valid. The temperature dependence of the graph (Figure 139) is evident. As temperature increases to the boiling point of water, the corrosion rate increases at much faster rates. This increase continues until the boiling point is reached and then starts to diminish, probably due to the loss of water in solution. The decrease in corrosion rate continues through at least a temperature of 352°F in H_3BO_3 + LiOH. As the higher temperatures are attained, water of hydration would also start to evaporate, which would probably deposit a lithium salt of meta-boric acid $LiBO_2$ ($LiBO_2$ has a melting point as high as 845°C in non-hydrated form). Other corrosion products may have a similar stifling effect in the case of H_3BO_3 by itself, accounting for the drop in rate after H_2O is lost, although they have not been examined in any detail.

A total of nine specimens coated with the bonded solid film lubricant were subjected to the same tests as the bare metal specimens. Five specimens were tested at 100°C (3 for 132.5 hours and 2 for 77 hours). Two specimens were also tested at 352°F (178°C) for 120 hours and two specimens at 300°F (315°C) for 130 hours. The working solution used for the testing was 4000 ppm boron (as H_3BO_3) + H_2O + LiOH titrated to a pH of 7.3.

The data generated from these tests are plotted on the graph of the original test data in Figure 139.

It is evident that the corrosion rate at 178°C and 100°C for the solid bonded film lubricant is almost an order of magnitude less than for the bare metal alone. As no data were generated for the H_3BO_3 + LiOH solution at 315°C, the corrosion rate for an A193 B7 material in 4000 ppm boron as H_3BO_3 + H_2O solution is plotted. The point almost coincides with the bonded lubricant point denoting virtually no additional protection offered by the lubricant, at this temperature.

6.0 DISCUSSION

There has been a tremendous amount of controversy over the use of molybdenum disulfide as a lubricant on nuclear power plant components. BNL's involvement over this issue was initiated during prior investigations of turbine disc failures [4,5]. During these investigations, a very extensive literature search was performed on MoS_2 and its possible role as a SCC contributor. An investigation [12] performed as a result of the Hinkley Point "A" disaster found that MoS_2 could reduce the crack initiation time of turbine steels (similar to bolting materials) by a factor of three in a steam environment. BNL tests [5] reduced the notched tensile strength of a disc steel by a factor of 3.5 over a corresponding steam test.

Other investigations [13, 14] have concluded that MoS_2 accelerates corrosive tendencies of metallic materials in moist environments.

Some of the earliest work found during this literature search [15] showed that MoS_2 could hydrolize in a moist environment to produce H_2S and that this oxidation reaction was reversible [16].

A report for the Royal Aircraft Establishment (U.K.) [17] cites accelerated corrosion of steel in contact with MoS_2 under conditions of high humidity. The formation products of this reaction are molybdenum dioxide and sulfuric acid. Sulfuric acid is very detrimental to low alloy steels.

At least five other investigations have attributed nuclear component failures to the possible use of MoS_2 [2, 18, 19, 24].

Work done by Atomic Energy of Canada Ltd. (AECL) [21] has shown that the following materials cracked under BWR conditions when contaminated by MoS_2: sensitized 304SS, sensitized Inconel 600, Inconel 718, 17-4 PH in the H1025 and H1100 conditions, PH 13-8 Mo, Custom 455 and AM 355 SCT 1000.

The AECL work is substantiated by a G.E. Report [21] which documented stress corrosion tests on a a number of materials with 12 different lubricants and partially concluded that "MoS_2 is the most aggressive lubricant. It readily cracked 17-4 PH (1100) and cold worked 304SS. After longer exposures, even annealed 304 stainless steel cracked with this lubricant."

Recent work at Combustion Engineering [22] shows that MoS_2 can produce H_2S under PWR conditions.

The chemical instability of MoS_2 in aqueous media has been discussed in an EPRI report [23]. The report states that MoS_2 is not stable at pH values greater than 4.5. The stable compounds formed are $HMoO_4^-$ or MoO_4^{-2} with $H_2S(aq.)$, HS^- or S^{-2} also formed. These compounds could quite easily induce a sulfide SCC phenomenon in critical bolting applications where moisture is present and MoS_2 has been used.

The copper bearing lubricants have also been involved in at least one report as a crack initiator [21]. The particular lubricant used, (similar to this report's #8) produced cracks in 17-4 PH specimens. This result is complementary to BNL results where significantly lower notched tensile strength values were associated with the use of this lubricant. The effect of copper on low alloy steels in as little as 1 ppm chloride solutions [25] has been observed. In this case, the copper is speculated to have shifted the potential into the cracking range in a CERT at 268°C. This potential shift might well be applicable to the lubricants.

7.0 CONCLUSIONS

1. The appearance of potentially detrimental elements in the chemical analysis (EDS scans) of the various lubricants clearly shows a marked difference in composition between supposedly similar (e.g. MoS_2 based) lubricants. For this reason, an independent chemical analysis of lubricants used on critical nuclear components prior to their application is advisable.

2. The steaming tests of the chemically pure MoS_2 show that in the presence of steam (100°C), MoS_2 will hydrolize to form detrimental gaseous sulfides (H_2S).

3. Carbon disulfide was shown to remove previously applied MoS_2 from a carbon steel fastener, by a simplified cleaning procedure. The potential for carbon disulfide to cause SCC of these steels should be investigated before this cleaning procedure is used in field applications.

4. The wide variation of measured coefficients of frictions for similar lubricants shows that generalizations of this value for "same type" (e.g. MoS_2 based, graphite-based, copper-based or nickel-based) should not be made and that the coefficient of friction should be determined (or obtained) for the specific lubricant and substrate used.

5. The notched tensile tests of the bolting materials showed that both A540 B24 Class 2 and A193 B7 materials are susceptible to a SCC failure in steam at 280°C. The use of MoS_2 or a copper + graphite lubricant appear to enhance this susceptibility to SCC, although these test results are inconclusive. However, the literature references and prior work done at BNL do show that molybdenum disulfide can have a significant material effect on low alloy steels in the presence of moisture. The use of a solid bonded film lubricant does not significantly improve the bolting materials performance with either steam or MoS_2. There may be some benefit in using the bonded film lubricant with copper bearing lubricants. This SCC susceptibility of these common bolting materials should be of tremendous concern for nuclear utilities.

6. The variation in notched tensile strengths with no discernable difference on the fracture faces of the A540 B24 Class 2 material shows that bolts cut from the same rod may exhibit different mechanical properties. This observation is upheld by field experience [9] and is adequate indication that more intensified inspections may be necessary on incoming bolting materials.

7. The weight loss experiments, using previously coated solid bonded film lubricant specimens, show a marked decrease in metal loss at 100°C and 178°C when compared to previously reported bare metal data. This lubricant protection disappears at 600°F (315°C), where the results on previously coated specimens differed little from results on bare metal specimens.

8.0 ACKNOWLEDGEMENTS

The author wishes to especially thank Dr. J. Woodward for her helpful discussions and contributions to this report. The author also wishes to thank R. Sabatini for the SEM/EDS work, L. Gerlach for the testing, A. Cendrowski and D. Horne for the hardness testing, J. Langan and O. Betancourt for their typing skills. The author also wishes to thank E. Woolridge (ONRR-USNRC) for his patience and support and Dr. J. Weeks for his constant support.

9.0 REFERENCES

1. Koo, W. H., NUREG-0943, January 1983.

2. Czajkowski, C. J., NUREG/CR-2993, July 1982.

3. Burck, L. H., Foley, W. J., Report No. IE-123, April 1981.

4. Czajkowski, C. J., BNL-NUREG-28724, October 1980.

5. Czajkowski, C. J., BNL-NUREG-29964, March 1981.

6. Hudgins, C. M., McGlasson, R. L., Mehdizadeh, P., Rosborough, W. M., Corrosion, Vol. 22, August 1966.

7. Letter Report J. R. Weeks to D. Smith (U.S. NRC)-MTEB.

8. Telecon C. D. Sellers (U.S. NRC)-MTEB.

9.0 REFERENCES (CONT'D)

9. Cipolla, R. C., Cargill, R. L., Bersin, J. M., APTECH Report AES-8-08-79 dated May 1982.

10. Czajkowski, C. J., NUREG/CR-2728, March 1982.

11. YAEC-67, Westinghouse, November 1958.

12. Thornton, D. V., Mould, P. B., Patrick, E. C., Conference on Grain Boundaries, 1976 D13 (London: The Institution of Metallurgists).

13. Calhoun, S. F., Rock Island Arsenal Report #62-2752, August 15, 1962.

14. Perna, C. Picatinny Arsenal Report #DC3-1, January 1961.

15. Haltner, A. J., Oliver, C. S., Proc. ACS Pet. Div. Symp. on Chemistry of Friction and Wear, Vol. 3, No. 4, 1958, pp. A77-84.

16. Rowe, G. W., Sci. Lubn, Vol. 11, No. 10, 1959, pp. 12-15.

17. Kay, E., Wear, 12 (1968), pp. 165-171.

18. Goldberg, A., Streit, R. D., NUREG/CR-1884, November 1980.

19. Hall, J. F., Fink, G. C., Draft Copy of Combustion Engineering Report "Examination of #2 Steam Generator Cold Leg Primary Manway Cover Studs from Maine Yankee."

20. Private Communication - E. V. Murphy (AECL) 1983.

21. Rowland, M. C., Rose, T. C., G. E. Report, APED-4422, December 1963.

22. Hall, J. F., Presentation at EPRI Seminar, "Bolting Degradation or Failure in Nuclear Power Plants," November 1983.

23. Chen, C. M., Aral, K., Theus, G. J., EPRI NP-3137 Volume 1, Project 1167-2, Final Report, June 1983.

24. Jonas, O., Draft Paper, Corrosion/84 Paper #55.

25. Czajkowski, C. J., NUREG/CR 3614, December 1983.

TABLE 1

TYPICAL CHEMICAL AND MECHANICAL PROPERTIES OF
ASTM A193 B7

Chemical Requirement		Actual Specimen Material
Carbon	0.37 - 0.49	0.44
Manganese	0.65 - 1.10	0.92
Phosphorous, max.	0.04	0.010
Sulfur, max.	0.04	0.019
Silicon	0.15 - 0.35	0.26
Chromium	0.75 - 1.20	0.87
Molybdenum	0.15 - 0.25	0.19

	Tensile Strength min.	Yield Strength 0.2 offset, min.	Elongation % in 2 in.	% Red. of Area, min.
Specification	125 Ksi	105 Ksi	16	50
Actual	147.5	136.5	19	60.8

TABLE 2

TYPICAL CHEMICAL AND MECHANICAL PROPERTIES OF
ASTM A540 B24 STEEL, CLASS 2

Chemical Requirement		Actual Specimen Material
Carbon	0.37 - 0.44	0.39
Manganese	0.70 - 0.90	0.80
Phosphorous, max.	0.025	0.020
Sulfur, max.	0.025	0.019
Silicon	0.15 - 0.35	0.26
Chromium	0.70 - 0.95	0.78
Nickel	1.65 - 2.00	1.85
Molybdenum	0.30 - 0.40	0.32

	Tensile Strength min.	Yield Strength 0.2 offset, min.	Elongation %	% Red. of Area, min.	Surface Hardness, Brinell min.	max.
Specification	155 Ksi	140 Ksi	11	40	311	401
Actual	160.5	152.0	18	58.6	311/352	

TABLE 3

HARDNESS MEASUREMENTS OF
THE BOLTING MATERIALS TESTED

A540 B24 Class 2 (All specimens tested from one rod

Knoop Hardness

358	353	361	
361	356	356	Avg. 356 KN/500 gm
351	353		(equivalent to approx. 159 Ksi
356	357		tensile strength)

Rockwell C

34.5	Avg. 34.3 R_C
34.0	
34.5	

Specimens 27, 30

Knoop Hardness

317	328	323	
319	317	317	Avg. 320 KN/500 gm
320	320		(equivalent to approx. 143 Ksi
323	319		tensile strength)

Specimens 1, 22

Knoop Hardness

328	323	323	
327	317	317	Avg. 320 KN/500 gm
319	314		(equivalent to approx. 143 Ksi
317	320		tensile strength)

Specimens 6, 31

Knoop Hardness

317	323	328	
314	331	314	Avg. 321 KN/500 gm
317	323		(equivalent to approx. 143 Ksi
327	317		tensile strength)

TABLE 3 (CONT'D)

A193 B7

Specimens 35, 40

Knoop Hardness

346	329	
341	338	Avg. 341 KN/500 gm
338	348	(equivalent to approx. 152 Ksi
343	346	tensile strength)

Rockwell C

31.5	Avg. 30.8 R_C
30.5	
30.5	

Specimens 36, 41

Knoop Hardness

341	332	
334	327	Avg. 335 KN/500 gm
332	338	(equivalent to approx. 148 Ksi
341	336	tensile strength)

Rockwell C

32	Avg. 31.7 R_C
32	
31	

Specimens 37, 42

Knoop Hardness

346	327	
343	329	Avg. 334 KN/500 gm
338	323	(equivalent to approx. 148 Ksi
334	334	tensile strength)

Rockwell C

31	
30.5	Avg. 30.5 R_C
30	

TABLE 3 (CONT'D)

Specimens 38, 43

Knoop Hardness

325	320	
332	332	Avg. 326 KN/500 gm
329	325	(equivalent to approx. 145 Ksi
318	332	tensile strength)

Rockwell C

31	Avg. 30.7 R_C
30	
31	

Specimens 39, 44

Knoop Hardness

350	355	
346	353	Avg. 349 KN/500 gm
348	348	(equivalent to approx. 157 Ksi
343	355	tensile strength)

Rockwell C

33.5	Avg. 32.8 R_C
33	
32	

TABLE 4

NOTCHED TENSILE CONSTANT EXTENSION RATE TESTS

SAMPLE NO.	TEMP.	TEST DURATION (hrs.)	TOTAL EXTENSION (in.)	EXTENSION RATE (Sec^{-1})	TENSILE STRENGTH (psi)	ENVIRONMENT
1	100°C	5:48	.010	4.8×10^{-7}	195,678	water
2	100°C	-	.028		277,056	water
3	100°C	6:40	.015	6.25×10^{-7}	228,291	water
4	100°C	6:48	.015	6.1×10^{-7}	275,580	water
5	100°C	7:01	.0225	8.9×10^{-7}	273,134	water
6	100°C	6:22	.0225	9.8×10^{-7}	240,521	water
7	280°C	7:28	.026	9.6×10^{-7}	201,303	water
8	280°C	4:56	.0245	1.38×10^{-7}	195,678	water
9	280°C	5:03	.020	1.1×10^{-6}	189,971	water
10	280°C	5:46	.0185	8.9×10^{-7}	216,877	water
11	100°C	7:08	.020	7.0×10^{-7}	207,093	molybdenum disulfide
12	100°C	6:31	.023	9.8×10^{-7}	264,981	molybdenum disulfide
13	280°C	-	.0225	-	154,912	molybdenum disulfide
14	280°C	6:43	.0175	7.2×10^{-7}	171,218	molybdenum disulfide
15	280°C	7:40	.031	1.1×10^{-6}	242,152	molybdenum disulfide
16	280°C	7:12	.027	1.0×10^{-6}	269,058	molybdenum disulfide
17	280°C	7:13	.0365	1.4×10^{-6}	242,152	molybdenum disulfide

TABLE 4 CONT'D

SAMPLE NO.	TEMP.	TEST DURATION (hrs.)	TOTAL EXTENSION (in.)	EXTENSION RATE (Sec^{-1})	TENSILE STRENGTH (psi)	ENVIRONMENT
18	280°C	15:26	.031	5.58×10^{-7}	143,846	molybdenum disulfide
19	280°C	17:47	.0225	3.5×10^{-7}	119,853	molybdenum disulfide
20	100°C	7:14	.0225	8.6×10^{-7}	203,832	lube #2
21	280°C	6:46	.026	1.06×10^{-6}	228,291	lube #2
22	100°C	5:54	.0265	1.2×10^{-6}	232,368	lube #3
23	100°C	7:25	.028	1.0×10^{-6}	252,751	lube #3
24	100°C	6:50	.026	1.0×10^{-6}	240,521	lube #3
25	280°C	7:19	.025	9.0×10^{-7}	228,291	lube #3
26	280°C	7:41	.030	1.1×10^{-6}	238,891	lube #3
27	280°C	5:53	.0225	1.06×10^{-6}	220,138	lube #4
28	280°C	7:35	.0265	9.7×10^{-7}	244,598	lube #5
29	280°C	8:12	.030	1.02×10^{-6}	252,019	lube #7
30	280°C	-	-	-	-	
31	100°C	6:24	.025	1.08×10^{-6}	228,291	lube #8
32	280°C	5:40	.0235	1.15×10^{-6}	146,700	lube #8
33	280°C	8:05	.030	1.0×10^{-6}	244,598	lube #9
34	280°C	7:00	.0265	1.05×10^{-6}	244,598	lube #11
35	100°C	6:07	.0325	1.47×10^{-6}	230,737	water
36	280°C	6:19	.013	5.0×10^{-7}	114,146	water
37	280°C	7:03	.0175	6.9×10^{-7}	232,368	water

TABLE 4 CONT'D

SAMPLE NO.	TEMP.	TEST DURATION (hrs.)	TOTAL EXTENSION (in.)	EXTENSION RATE (Sec^{-1})	TENSILE STRENGTH (psi)	ENVIRONMENT
38	280°C	4:49	.0015	8.64×10^{-8}	167,142	water
39	280°C	5:33	.0215	1.07×10^{-6}	220,138	water
40	100°C	5:33	.0265	1.3×10^{-6}	231,553	molybdenum disulfide
41	280°C	4:28	.02	1.2×10^{-6}	171,210	molybdenum disulfide
42	280°C	4:14	.0165	1.08×10^{-6}	179,372	molybdenum disulfide
43	280°C	5:04	.019	1.04×10^{-6}	198,124	molybdenum disulfide
44	280°C	7:00	.030	1.2×10^{-6}	256,828	lube #8
45	280°C	7:20	.0145	5.5×10^{-7}	244,598	water
46	280°C	14:32	.018	3.4×10^{-7}	171,218	water
47	280°C	14:43	.015	2.8×10^{-7}	224,215	water
48	280°C	14:01	.0325	6.4×10^{-7}	260,905	water
49	280°C	13:38	.021	4.3×10^{-7}	244,600	water
50	280°C	5:06	.018	9.8×10^{-7}	203,832	molybdenum disulfide
51	280°C	24:00	.032	3.7×10^{-7}	293,518	molybdenum disulfide
52	280°C	8:08	.022	7.5×10^{-7}	171,218	molybdenum disulfide
53	280°C	14:36	.0175	3.3×10^{-7}	228,291	molybdenum disulfide
54	280°C	7:09	.0075	2.9×10^{-7}	256,828	lube #8

TABLE 4 CONT'D

SAMPLE NO.	TEMP.	TEST DURATION (hrs.)	TOTAL EXTENSION (in.)	EXTENSION RATE (Sec^{-1})	TENSILE STRENGTH (psi)	ENVIRONMENT
55	280°C	7:45	.022	7.87×10^{-7}	260,905	water
56	280°C	14:27	.013	2.5×10^{-7}	203,832	water
57	100°C	12:53	.0225	4.9×10^{-7}	216,061	water
58	100°C	12:01	.012	2.8×10^{-7}	232,368	water
59	280°C	13:30	.016	3.3×10^{-7}	216,061	water
60	100°C	12:51	.0125	2.7×10^{-7}	224,215	molybdenum disulfide
61	100°C	15:13	----------N.G.----------			molybdenum disulfide
62	280°C	12:50	.025 in.	5.4×10^{-7}	220,138	molybdenum disulfide

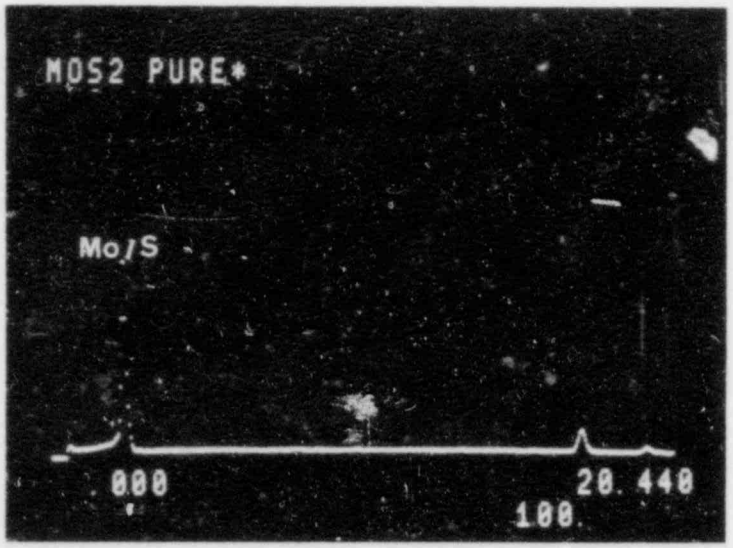

Figure 1 EDS Scan of Lubricant #1

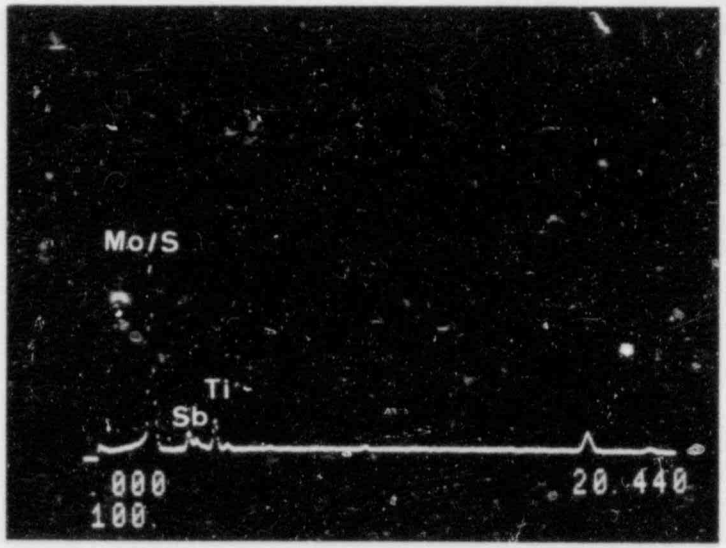

Figure 2 EDS Scan of Lubricant #2

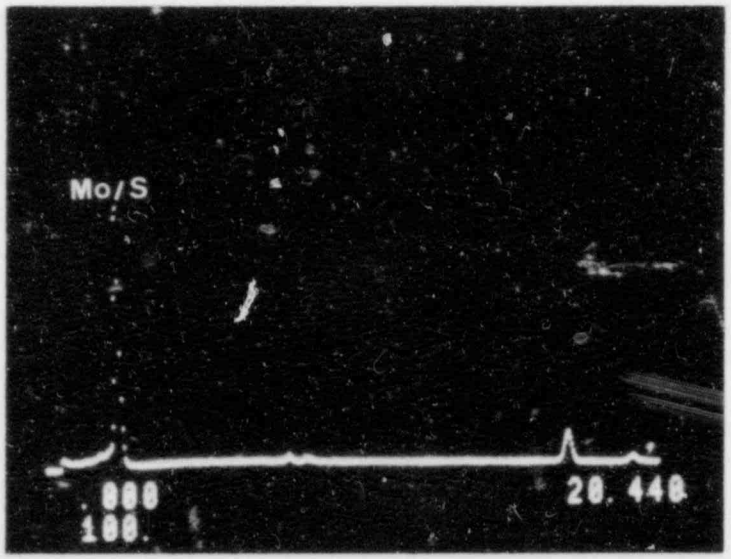

Figure 3 EDS Scan of Lubricant #3

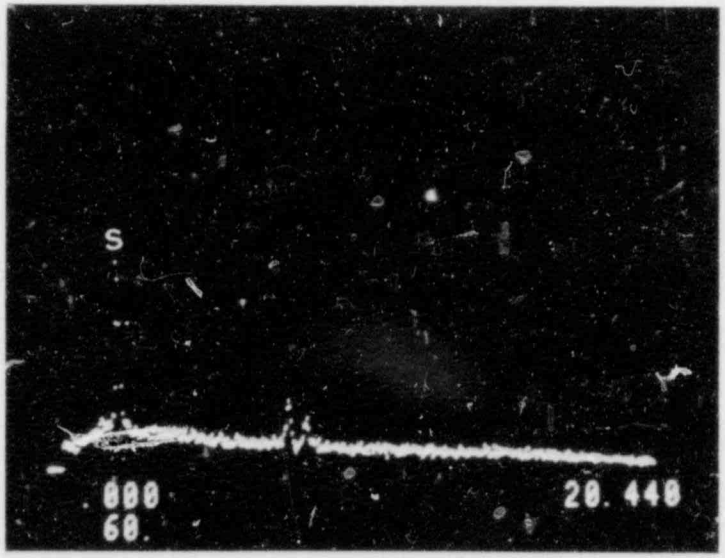

Figure 4 EDS Scan of Lubricant #4

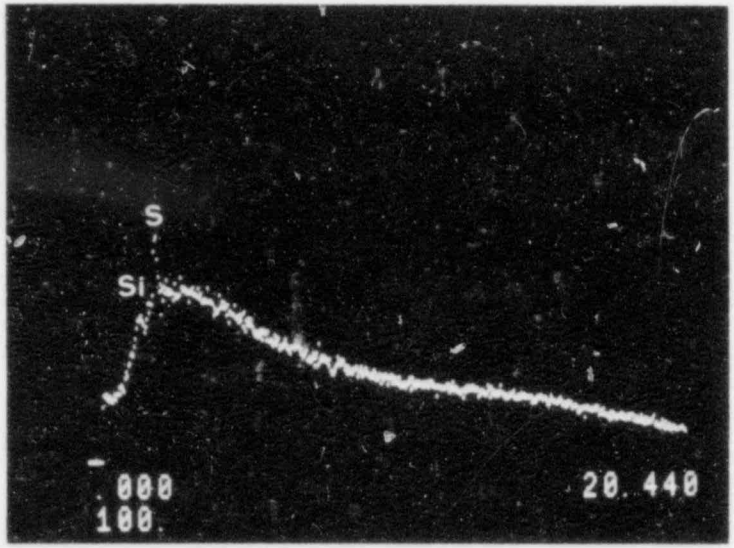

Figure 5 EDS Scan of Lubricant #5

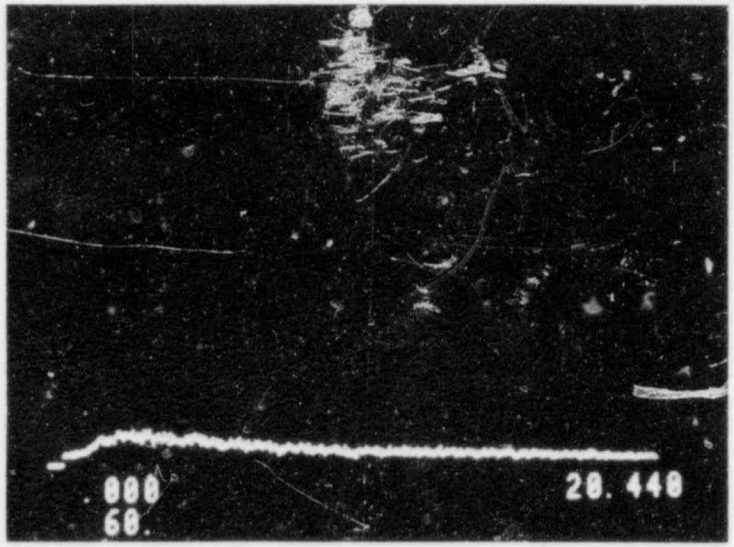

Figure 6 EDS Scan of Lubricant #6

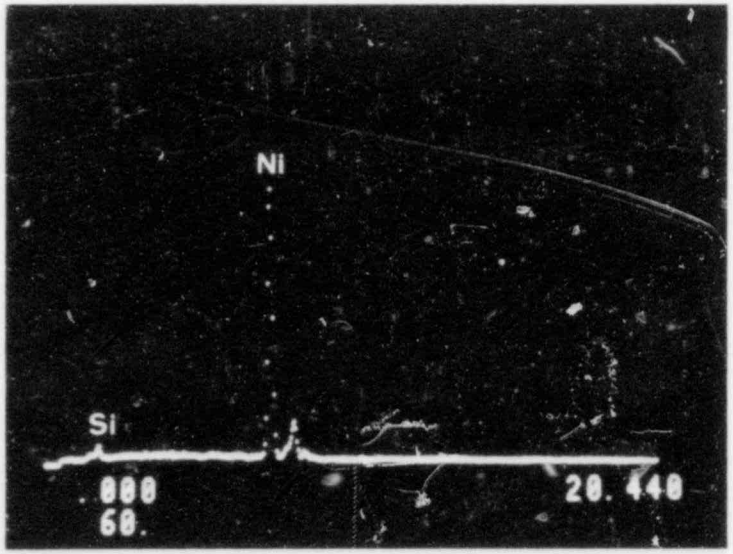

Figure 7 EDS Scan of Lubricant #7

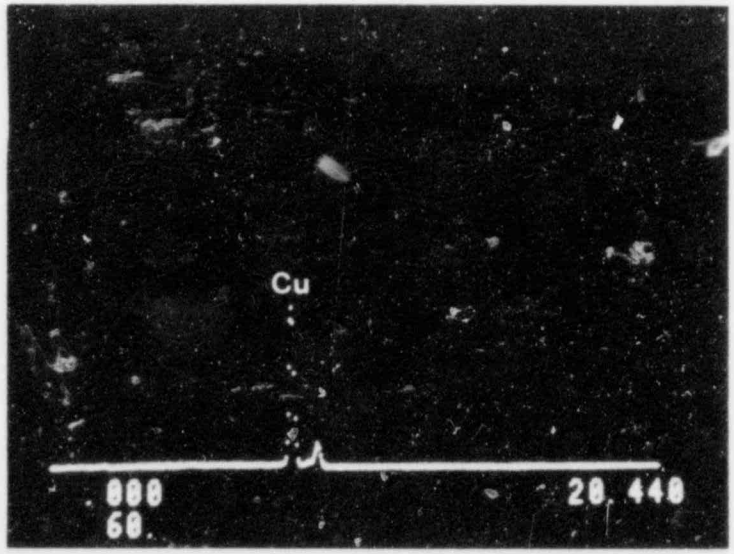

Figure 8 EDS Scan of Lubricant #8

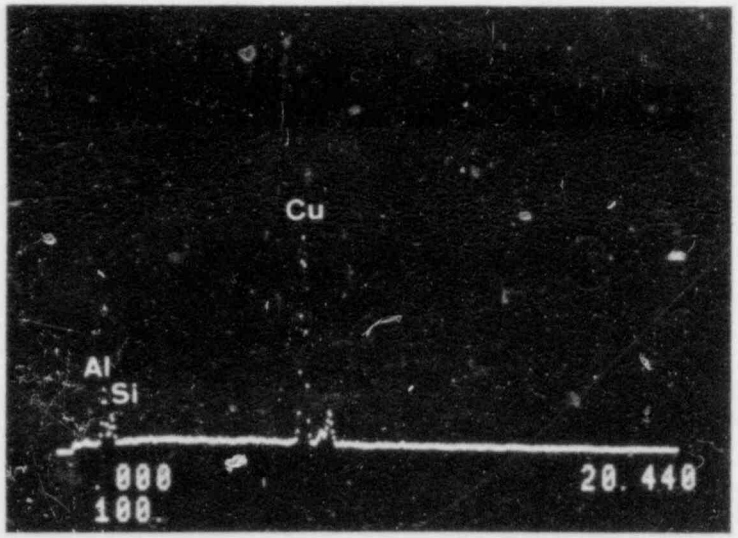

Figure 9 EDS Scan of Lubricant #9

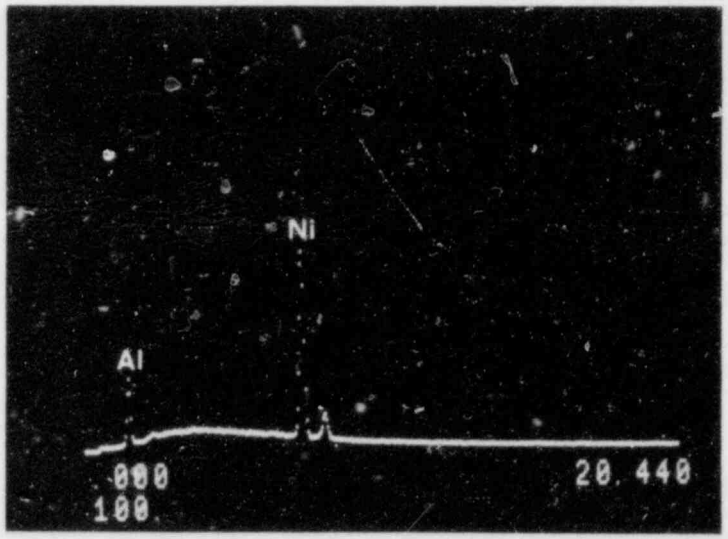

Figure 10 EDS Scan of Lubricant #10

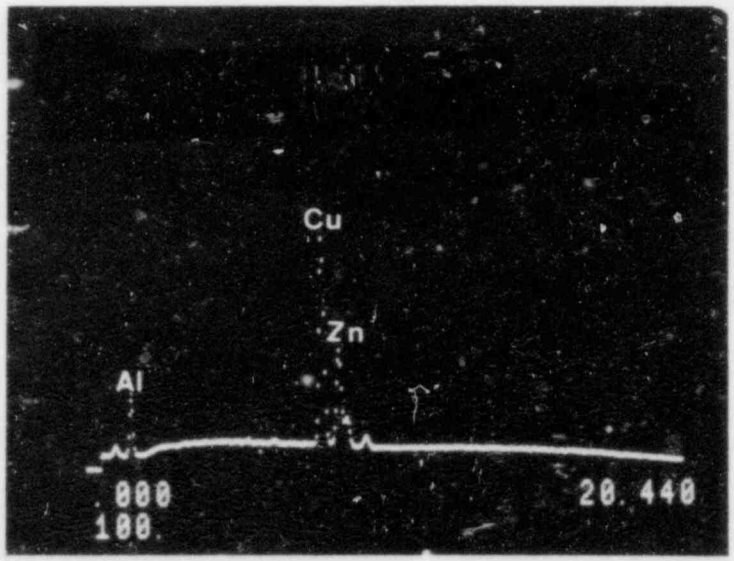

Figure 11 EDS Scan of Lubricant #11

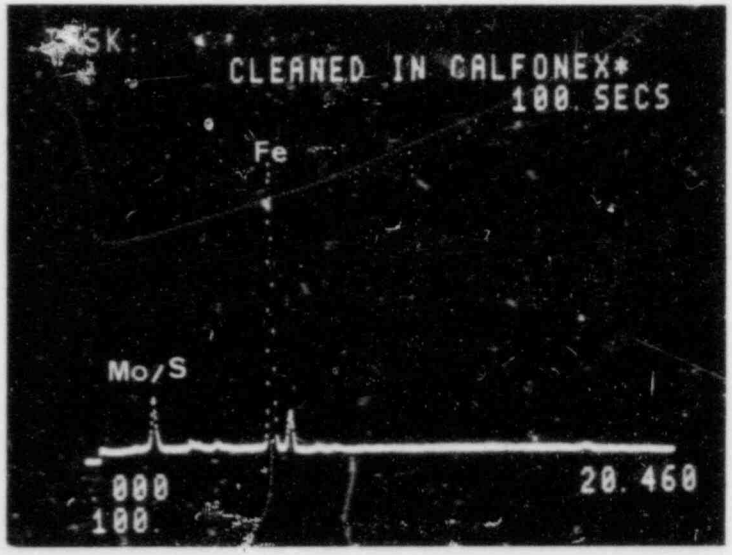

Figure 12 EDS Scan of MoS_2 Sprayed Bolt (Cleaned with Calfonex)

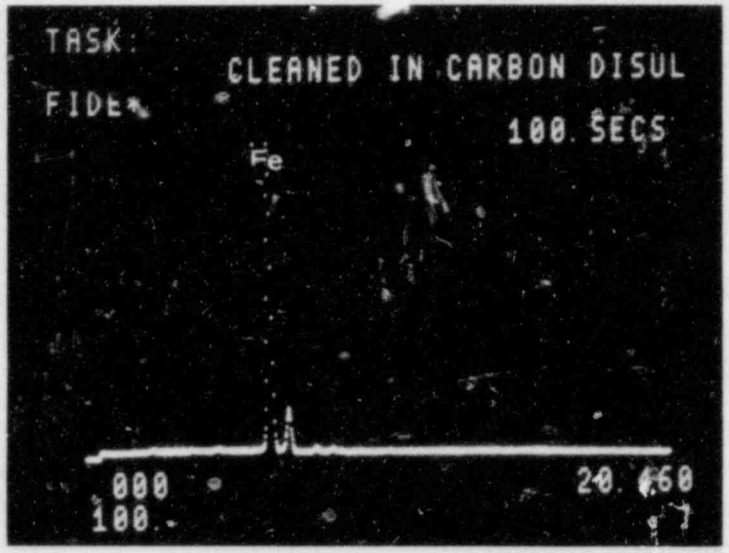

Figure 13 EDS Scan of MoS_2 Sprayed Bolt (Cleaned with Carbon Disulfide)

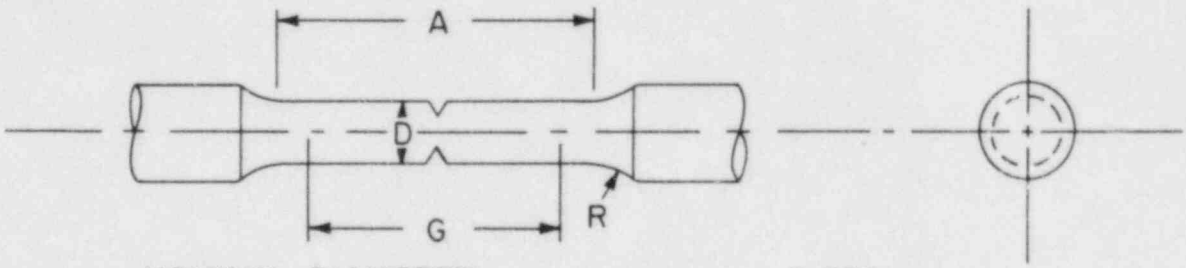

NOMINAL DIAMETER	0.250
G-GAGE LENGTH	1.000 ±0.005
D-DIAMETER	0.250 ±0.005
R-RADIUS OF FILLET, min	3/16
A-LENGTH OF REDUCED SECTION, min	1 1/4

(NOT TO SCALE)

Figure 14. Drawing of typical notched tensile specimen.

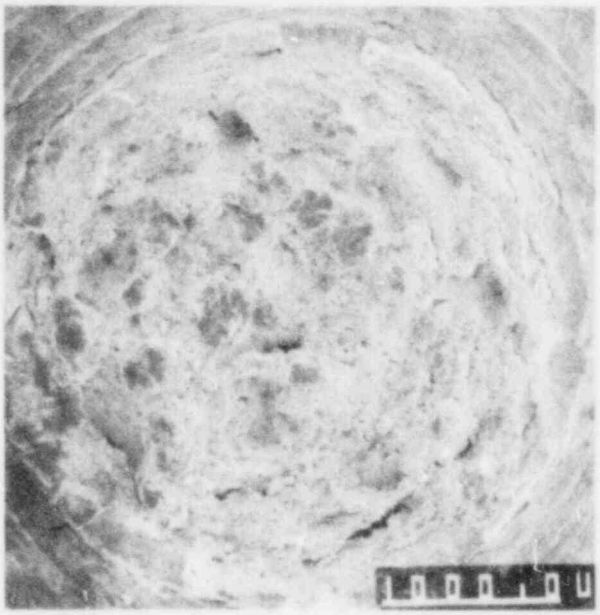

Figure 15. 27X
SEM Photo of Fracture Face for Specimen #1.

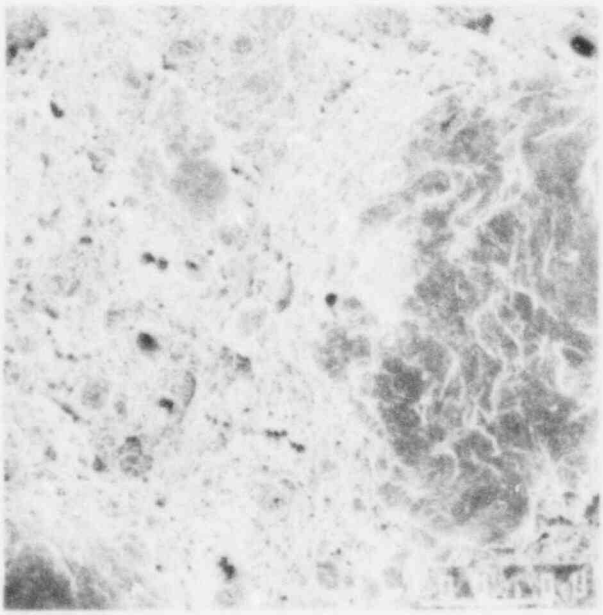

Figure 16. 200X
Higher Magnification Fractograph Showing Typical Ductile Fracture.

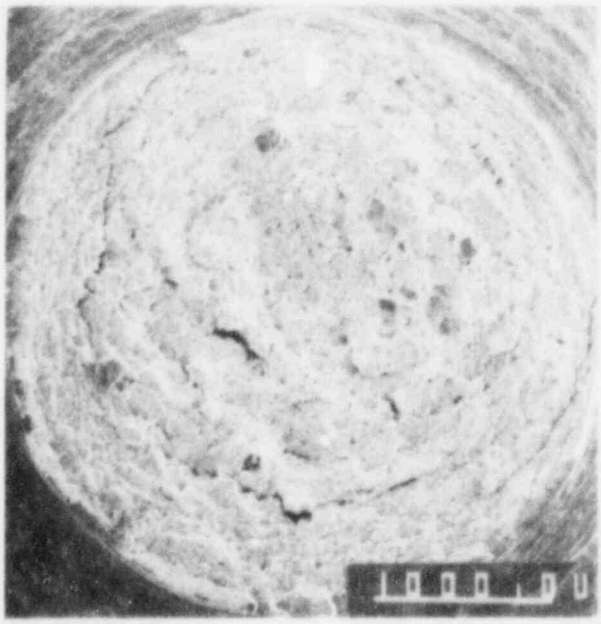

Figure 17. 27X
SEM Photo of Fracture Face for Specimen #2.

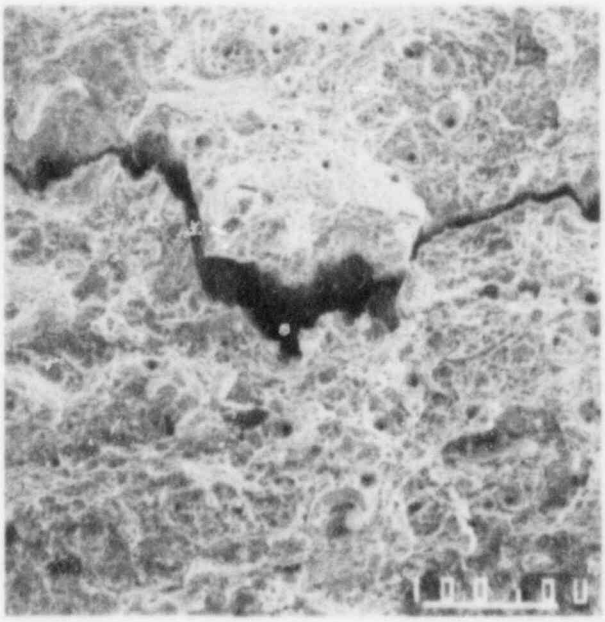

Figure 18. 200X
Higher Magnification Fractograph Showing Typical Ductile Fracture.

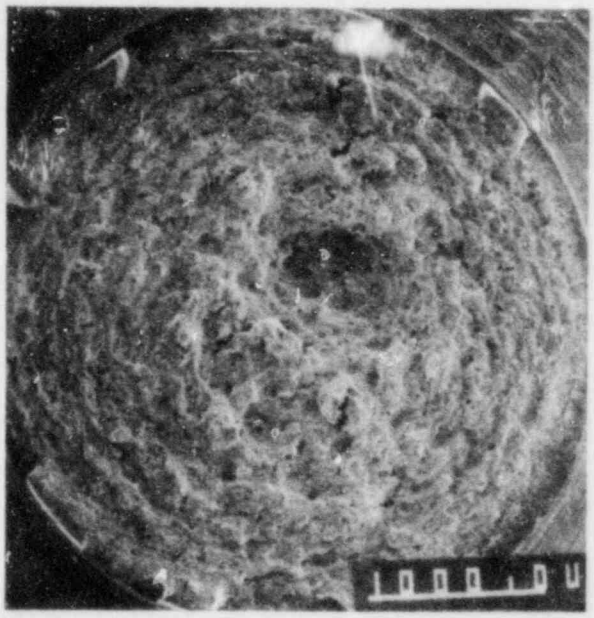

Figure 19. 27X
SEM Photo of Fracture Face for Specimen #3.

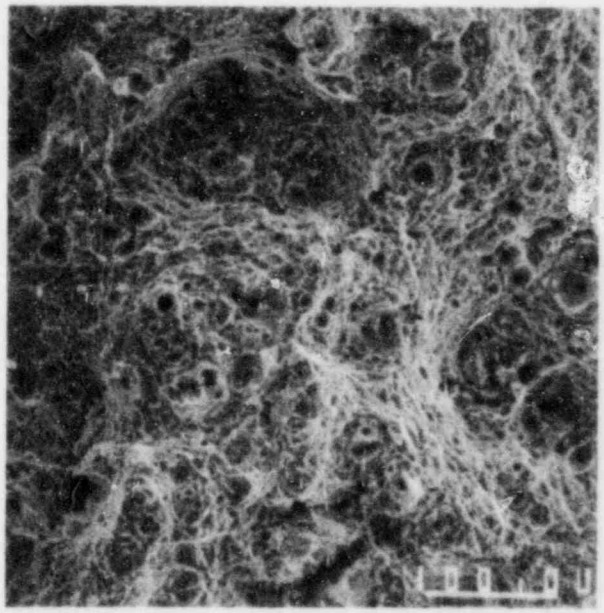

Figure 20. 200X
Higher Magnification Fractograph Showing Typical Ductile Fracture.

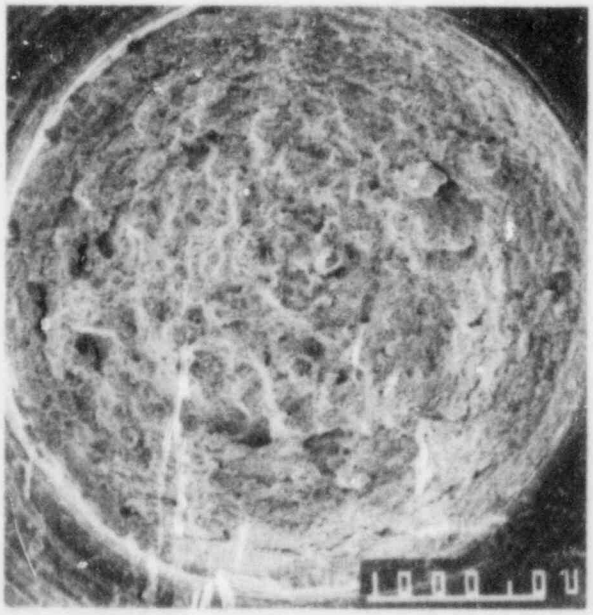

Figure 21. 27X
SEM Photo of Fracture Face for Specimen #4.

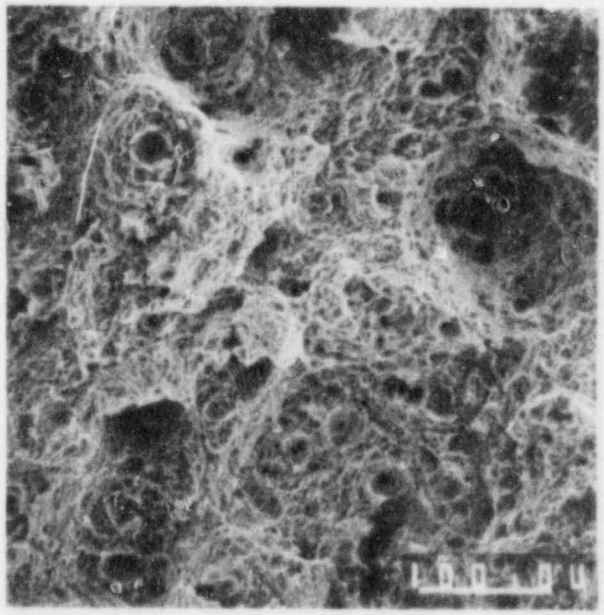

Figure 22. 200X
Higher Magnification Fractograph Showing Typical Ductile Fracture.

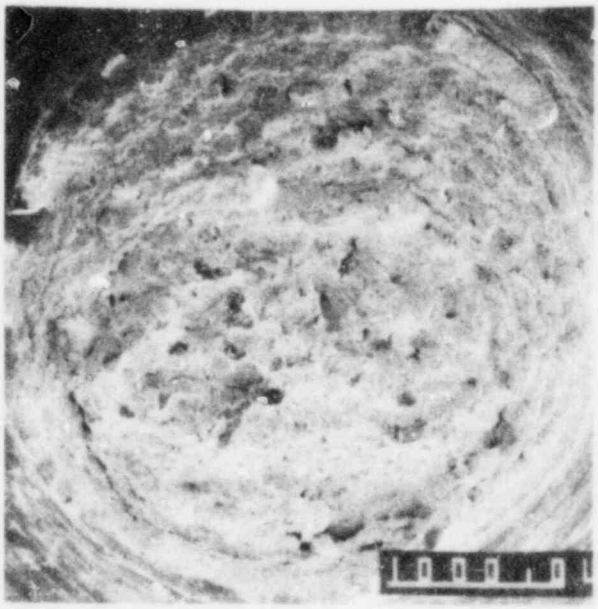

Figure 23. 27X
SEM Photo of Fracture Face for Specimen #5.

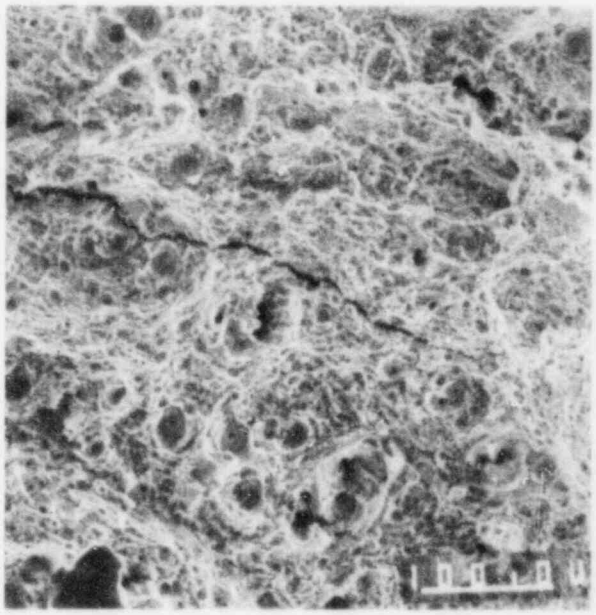

Figure 24. 200X
Higher Magnification Fractograph Showing Typical Ductile Fracture.

Figure 25. 27X
SEM Photo of Fracture Face for Specimen #6.

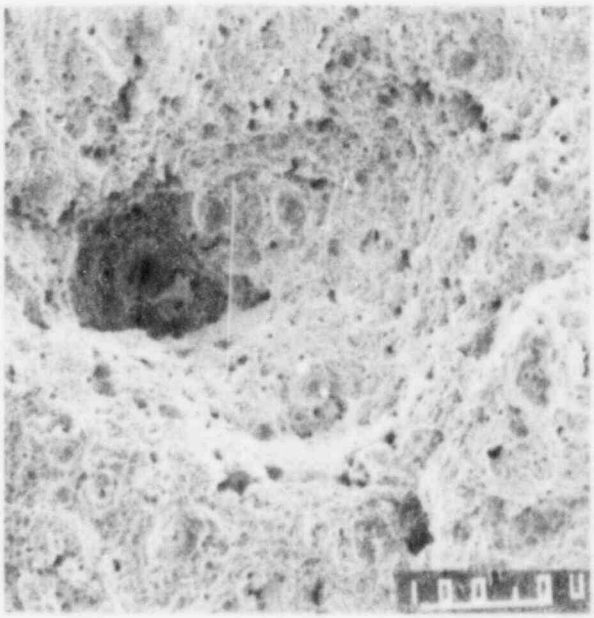

Figure 26. 200X
Higher Magnification Fractograph Showing Typical Ductile Fracture.

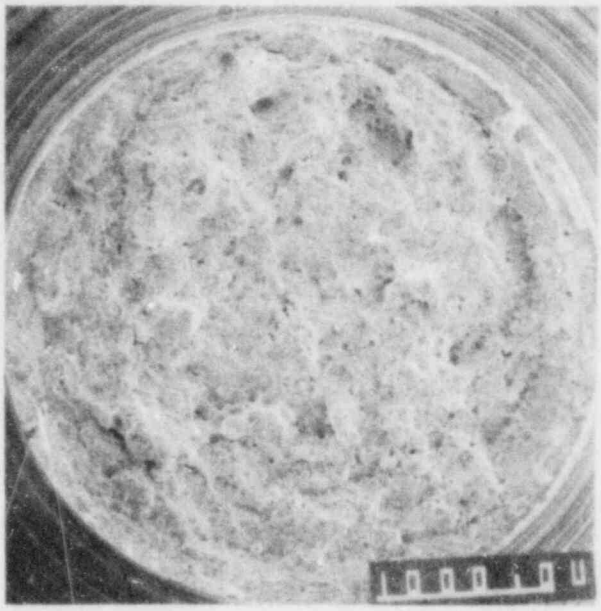

Figure 27. 27X
SEM Photo of Fracture Face for Specimen #7.

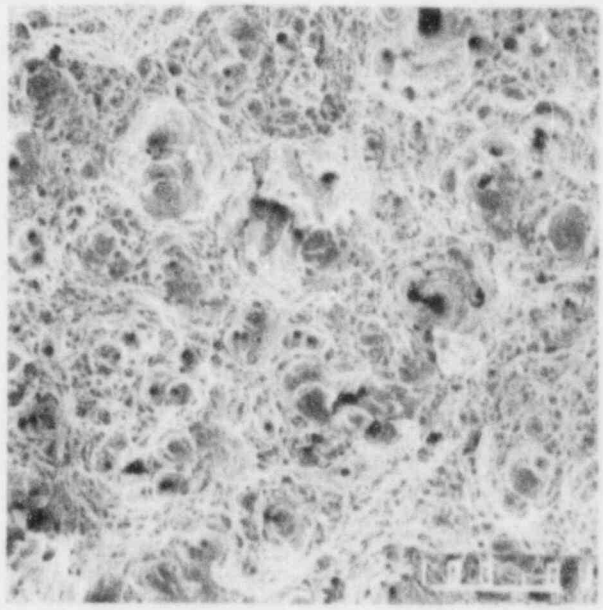

Figure 28. 200X
Higher Magnification Fractograph Showing Typical Ductile Fracture.

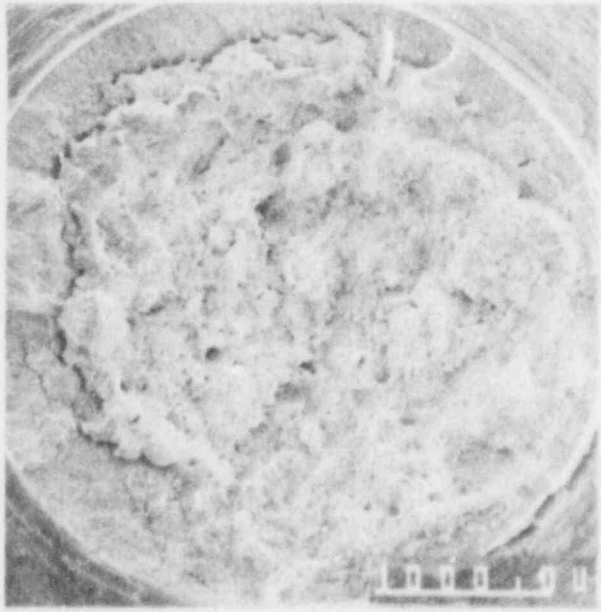

Figure 29. 27X
SEM Photo of Fracture Face for Specimen #8.

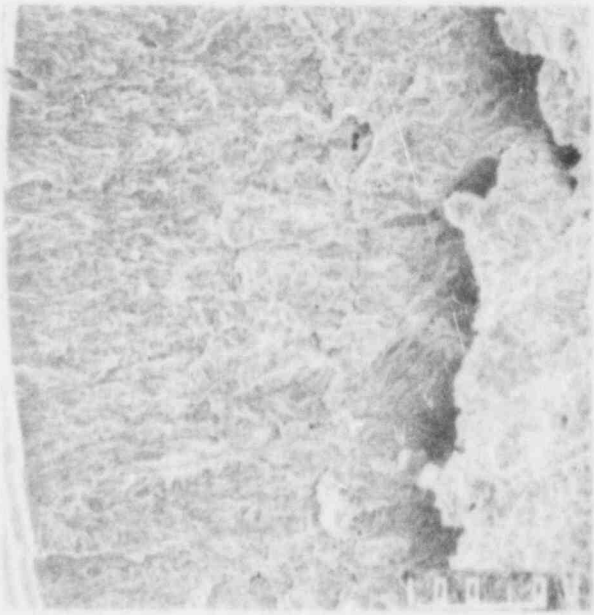

Figure 30. 200X
Higher Magnification Photo of Transgranular Area.

Figure 31. 27X
SEM Photo of Fracture Face for Specimen #9.

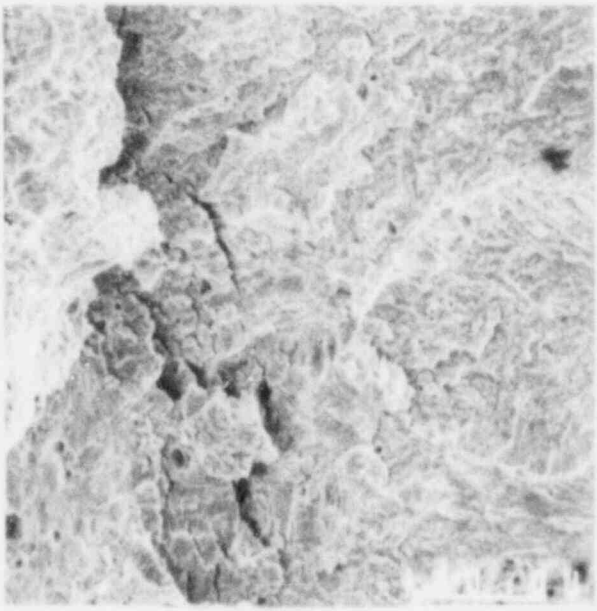

Figure 32. 200X
Higher Magnification Photo of Transgranular Area.

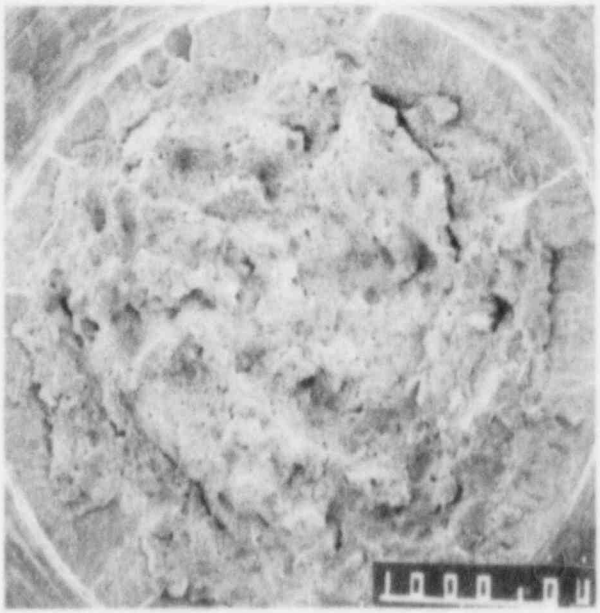

Figure 33. 27X
SEM Photo of Fracture Face for Specimen #10.

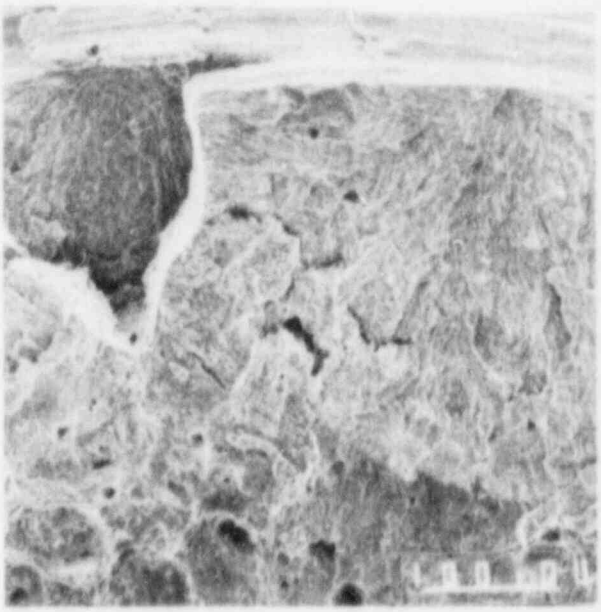

Figure 34. 200X
Higher Magnification Photo of Transgranular Area.

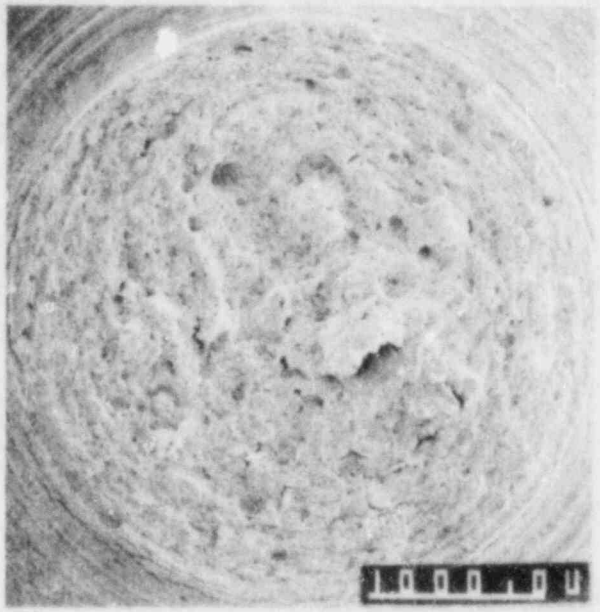

Figure 35. 27X
SEM Photo of Fracture Face for Specimen #11.

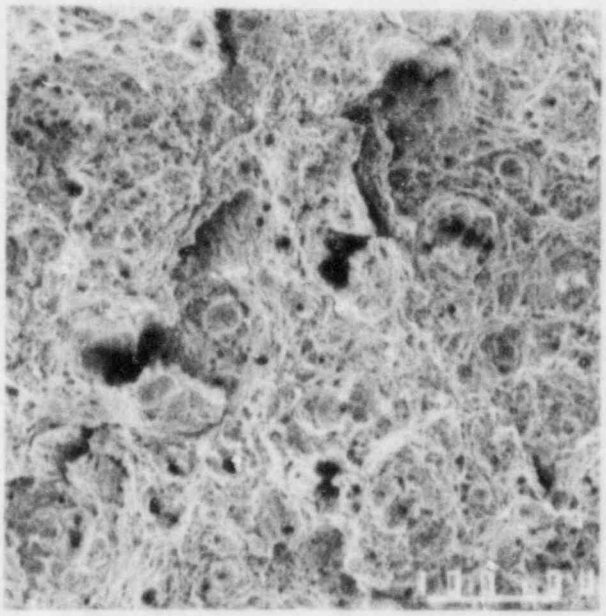

Figure 36. 200X
Higher Magnification Fractograph Showing Typical Ductile Fracture.

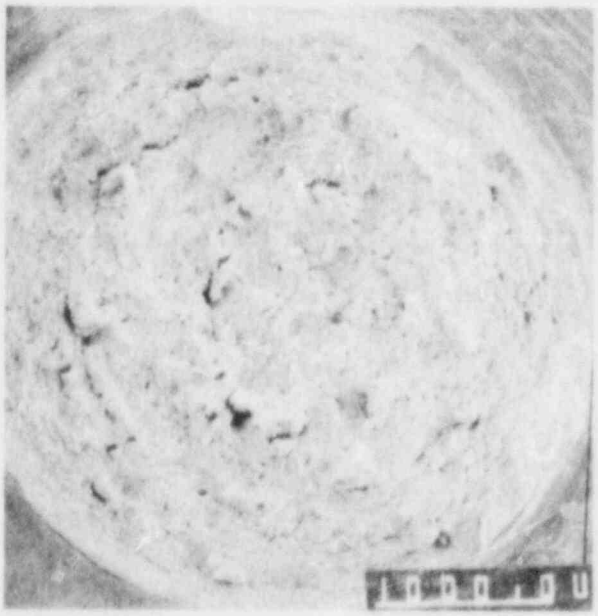

Figure 37. 27X
SEM Photo of Fracture Face for Specimen #12.

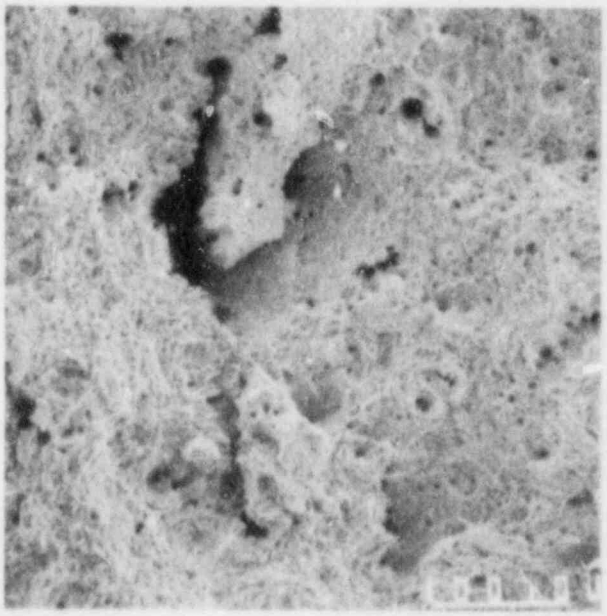

Figure 38. 200X
Higher Magnification Fractograph Showing Typical Ductile Fracture.

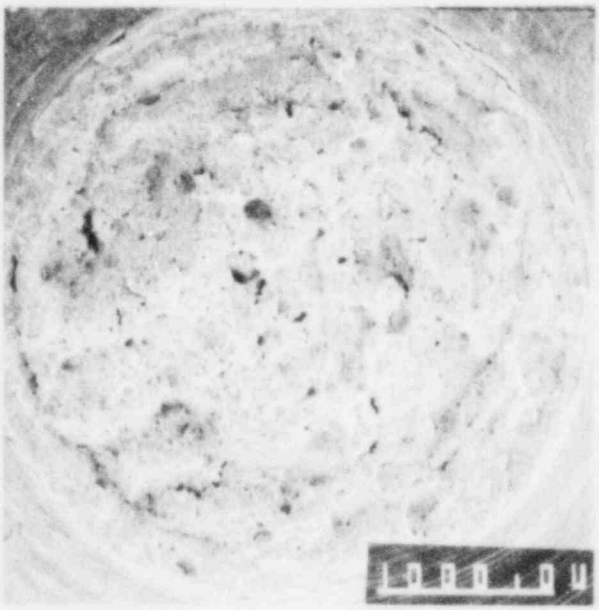

Figure 39. 27X
SEM Photo of Fracture Face for Specimen #13.

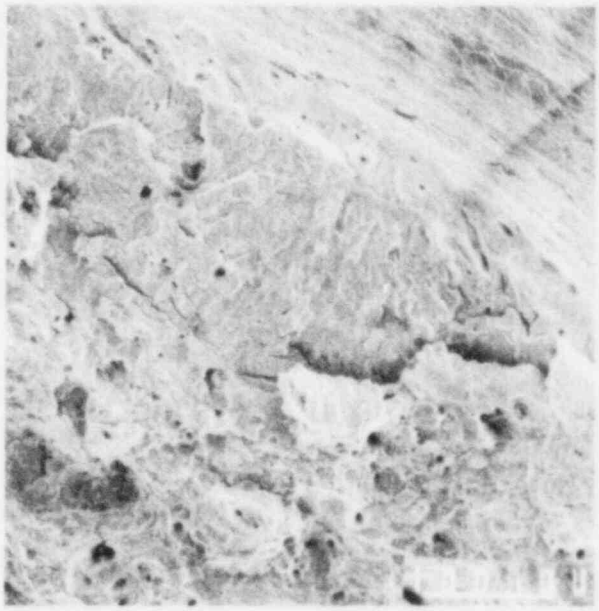

Figure 40. 200X
Higher Magnification Photo of Transgranular Area.

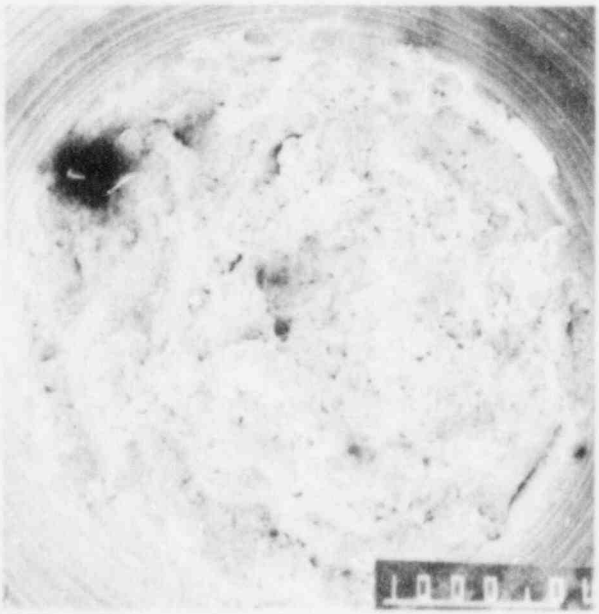

Figure 41. 27X
SEM Photo of Fracture Face for Specimen #14.

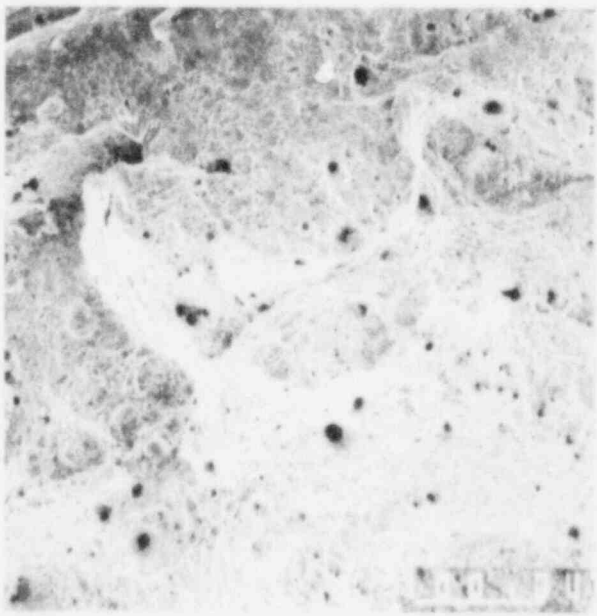

Figure 42. 200X
Higher Magnification Photo of Transgranular Area.

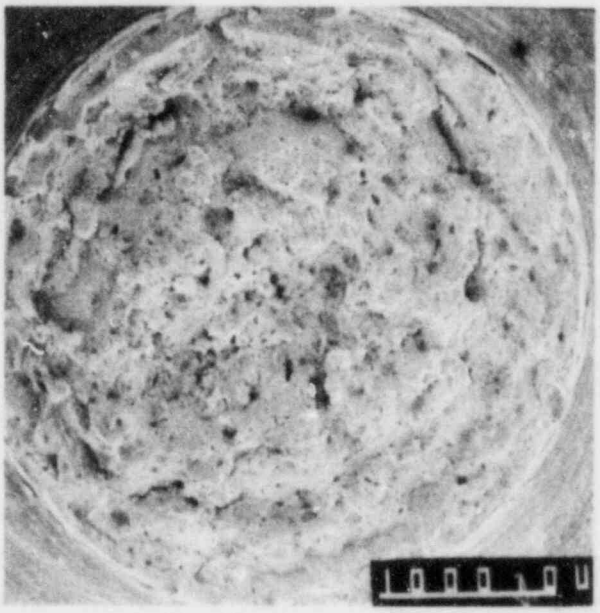

Figure 43. 27X
SEM Photo of Fracture Face for Specimen #15.

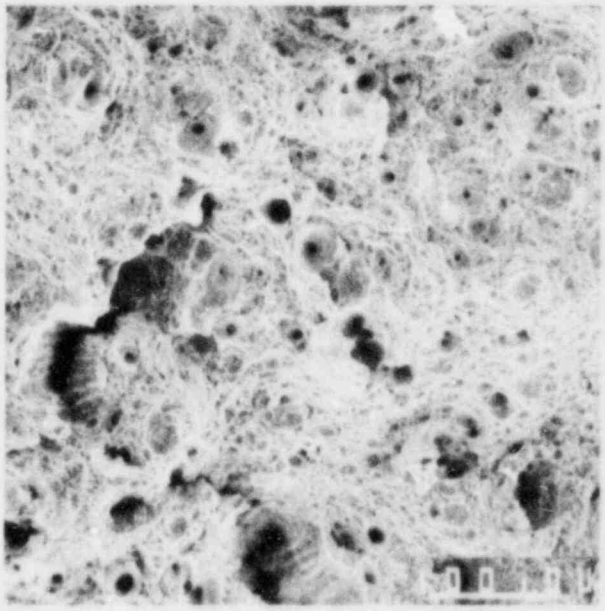

Figure 44. 200X
Higher Magnification Fractograph Showing Typical Ductile Fracture.

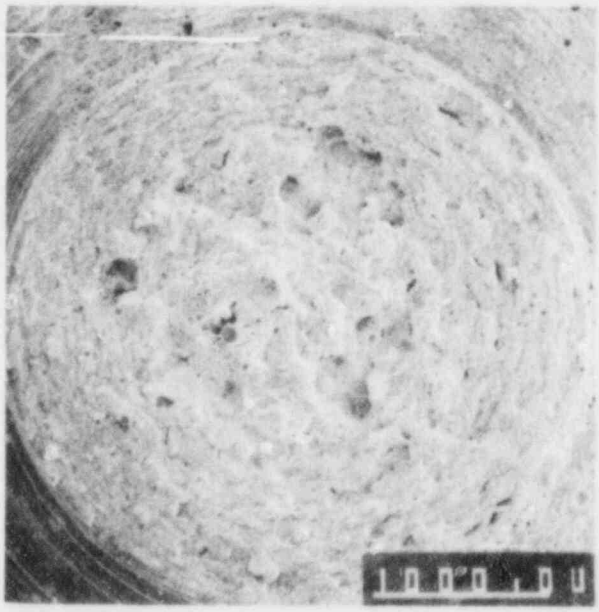

Figure 45. 27X
SEM Photo of Fracture Face for Specimen #16.

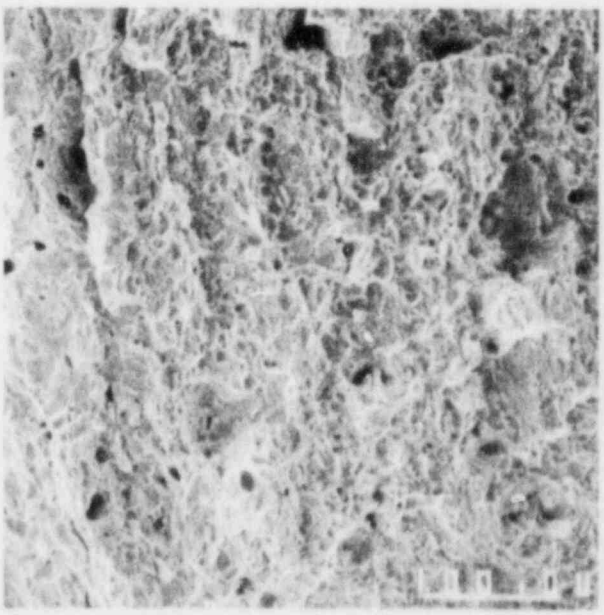

Figure 46. 200X
Higher Magnification Fractograph Showing Typical Ductile Fracture.

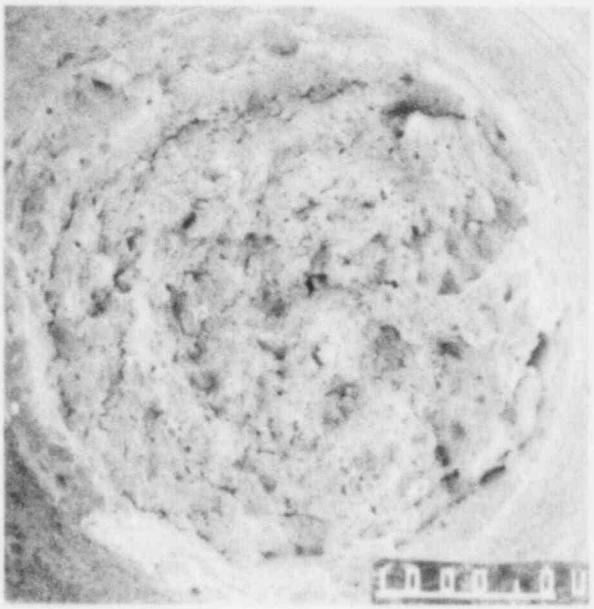

Figure 47. 27X
SEM Photo of Fracture Face for Specimen #17.

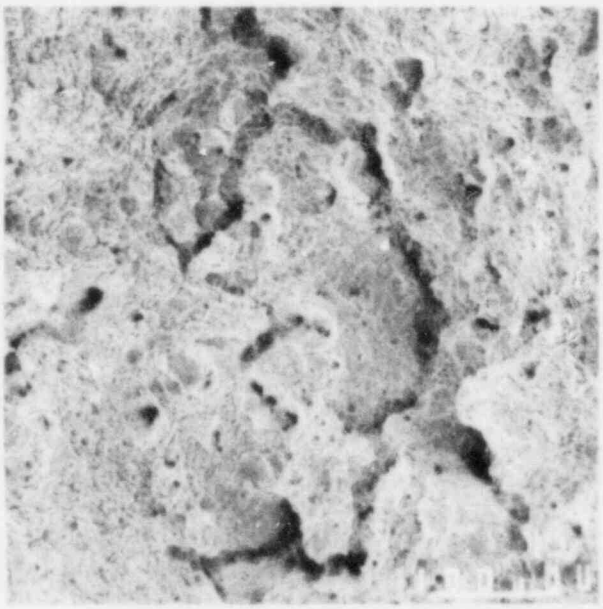

Figure 48. 200X
Higher Magnification Fractograph Showing Typical Ductile Fracture.

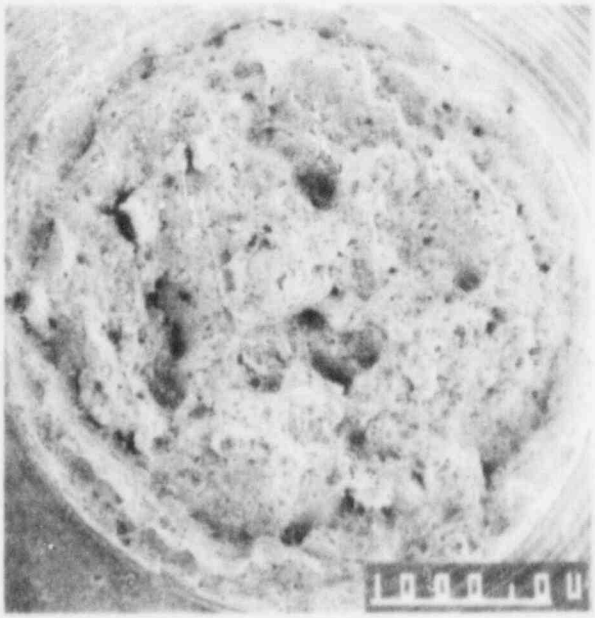

Figure 49. 27X
SEM Photo of Fracture Face for Specimen #18.

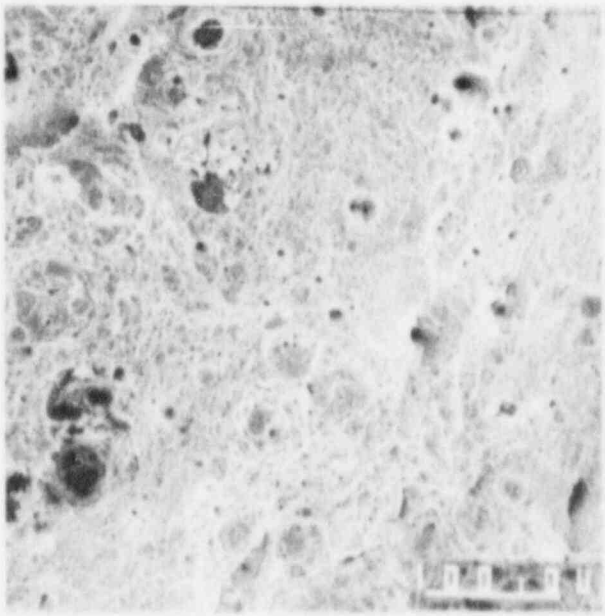

Figure 50. 200X
Higher Magnification Fractograph Showing Generally Ductile Failure.

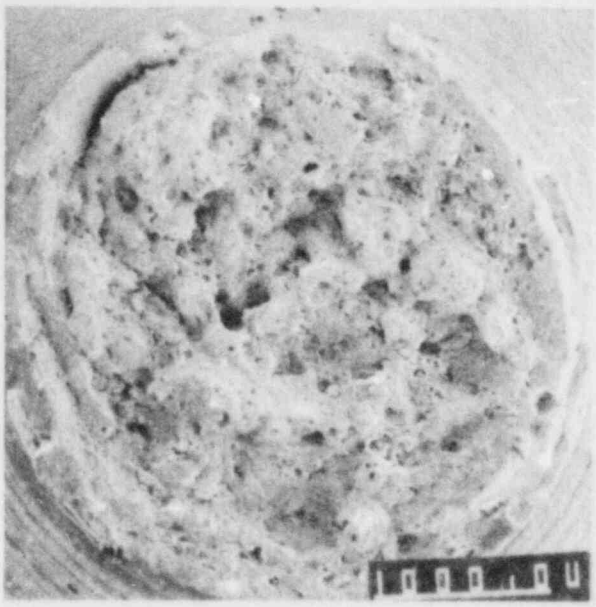

Figure 51. 27X
SEM Photo of Fracture Face for Specimen #19.

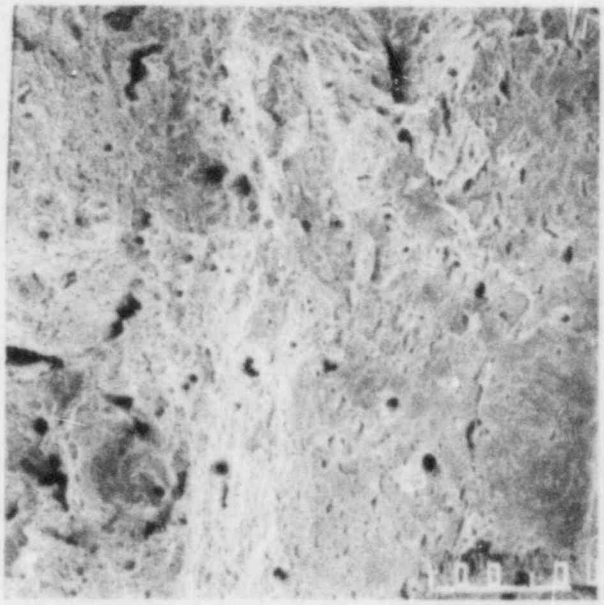

Figure 52. 200X
Higher Magnification Fractograph Showing Possible Transgranular Area.

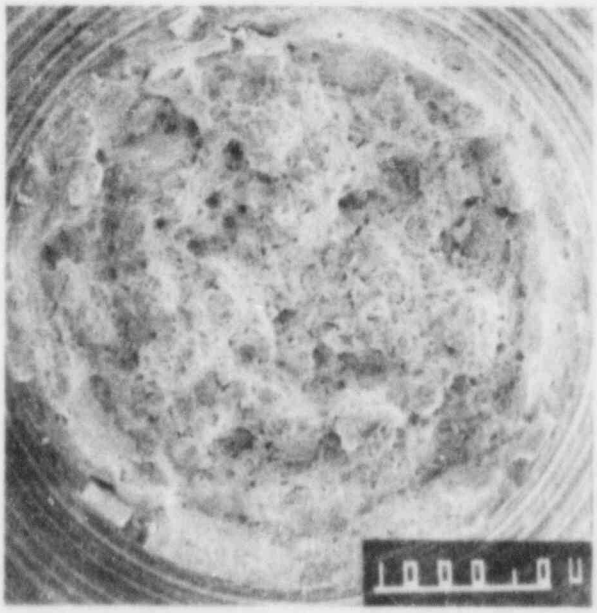

Figure 53. 27X
SEM Photo of Fracture Face for Specimen #20.

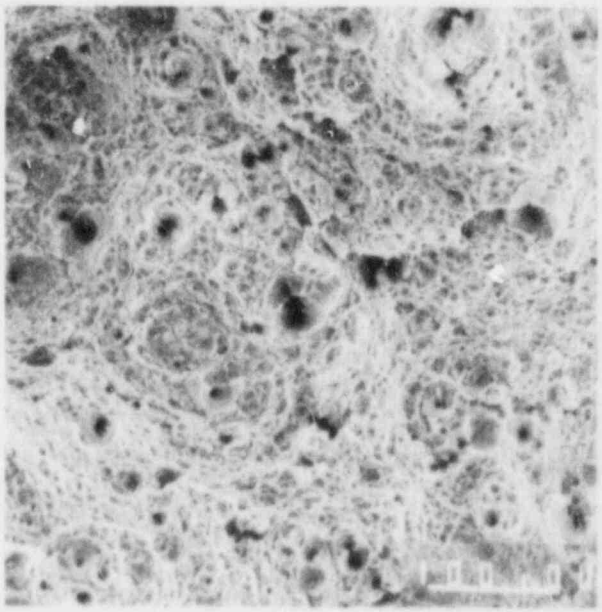

Figure 54. 200X
Higher Magnification Fractograph Showing Typical Ductile Fracture.

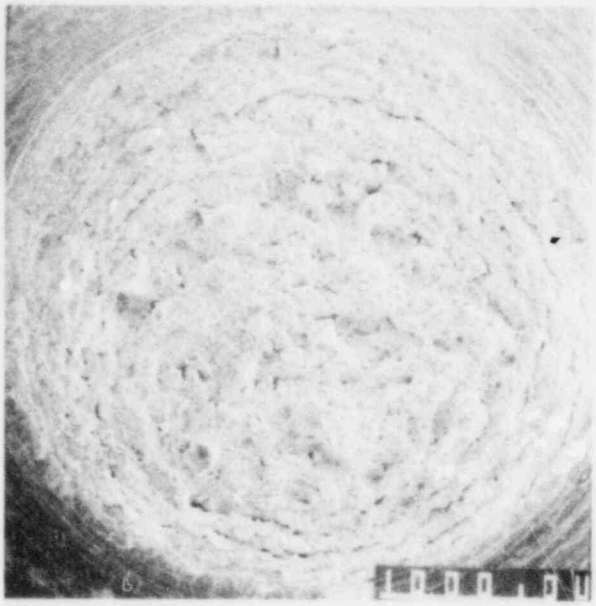

Figure 55. 27X
SEM Photo of Fracture Face for Specimen #21.

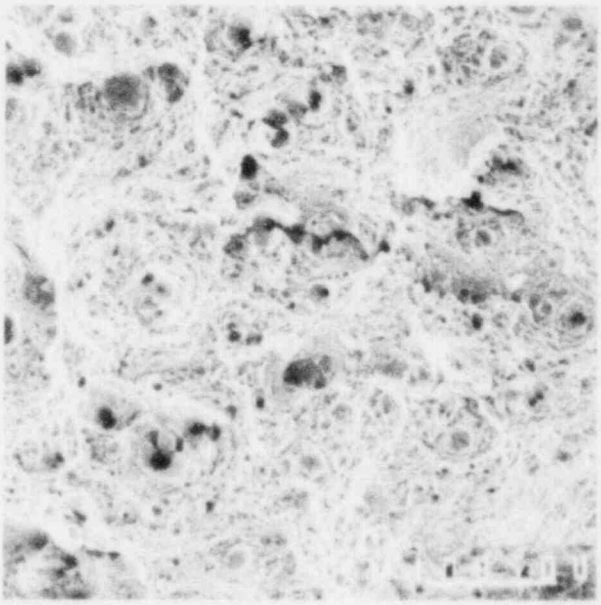

Figure 56. 200X
Higher Magnification Fractograph Showing Typical Ductile Fracture.

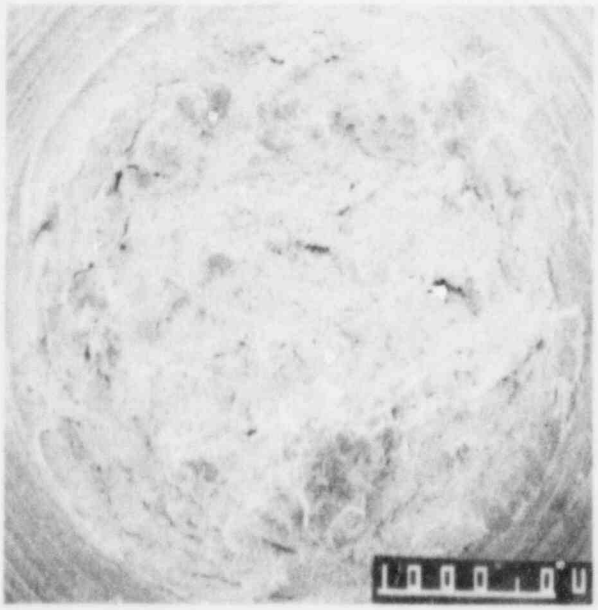

Figure 57. 27X
SEM Photo of Fracture Face for Specimen #22.

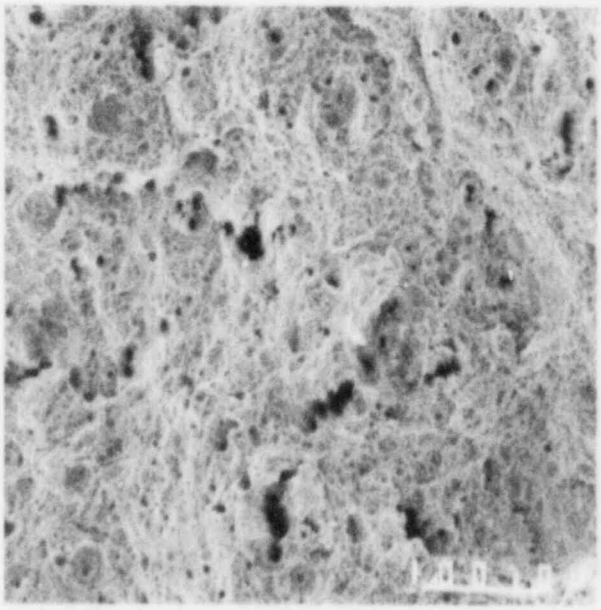

Figure 58. 200X
Higher Magnification Fractograph Showing Typical Ductile Fracture.

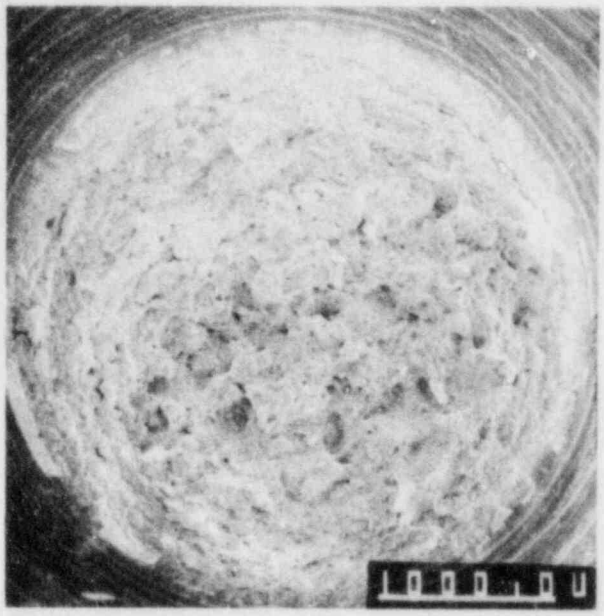

Figure 59. 27X
SEM Photo of Fracture Face for Specimen #23.

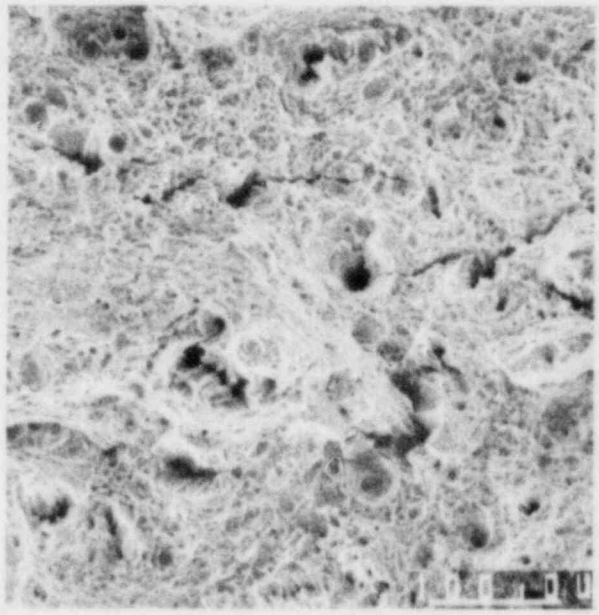

Figure 60. 200X
Higher Magnification Fractograph Showing Typical Ductile Fracture.

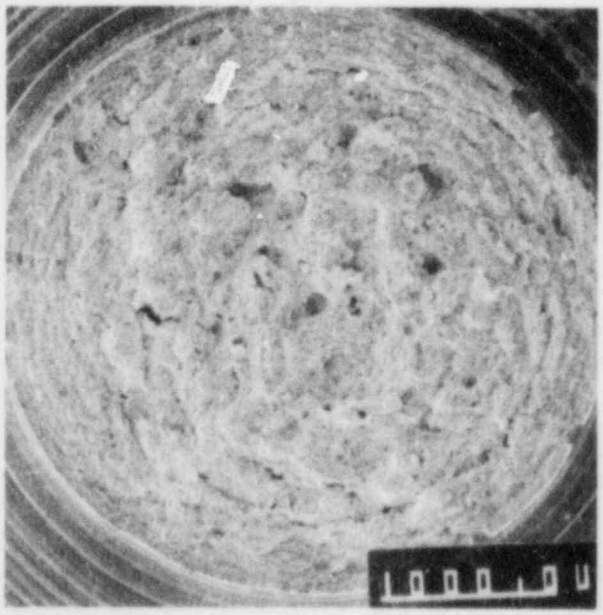

Figure 61. 27X
SEM Photo of Fracture Face for Specimen #24.

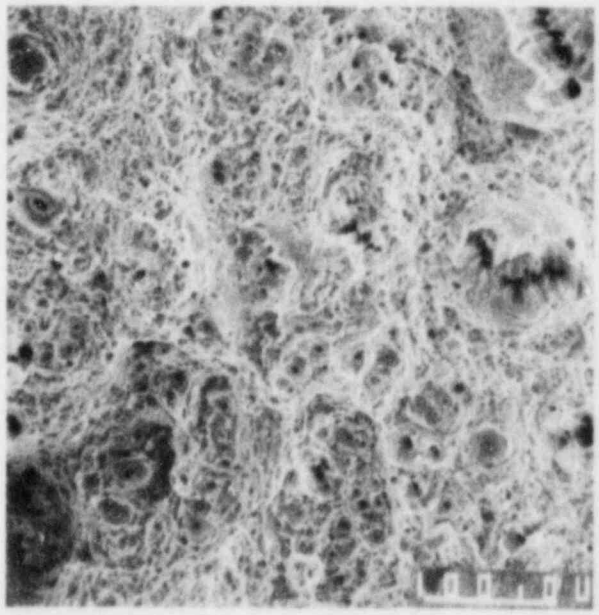

Figure 62. 200X
Higher Magnification Fractograph Showing Typical Ductile Fracture.

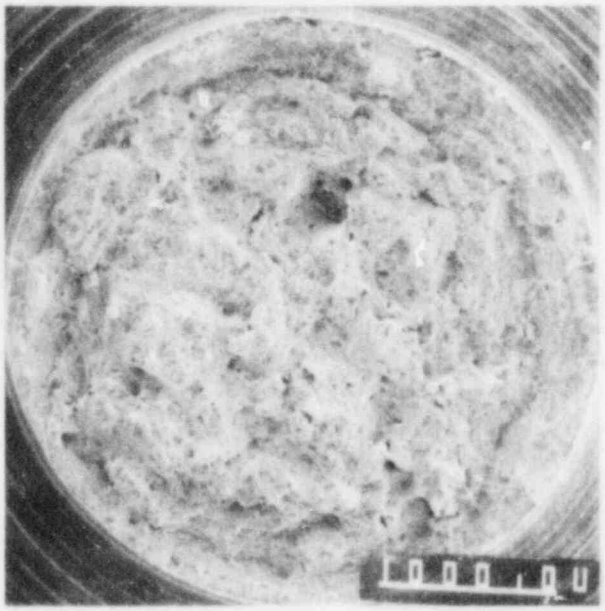

Figure 63. 27X
SEM Photo of Fracture Face for Specimen #25.

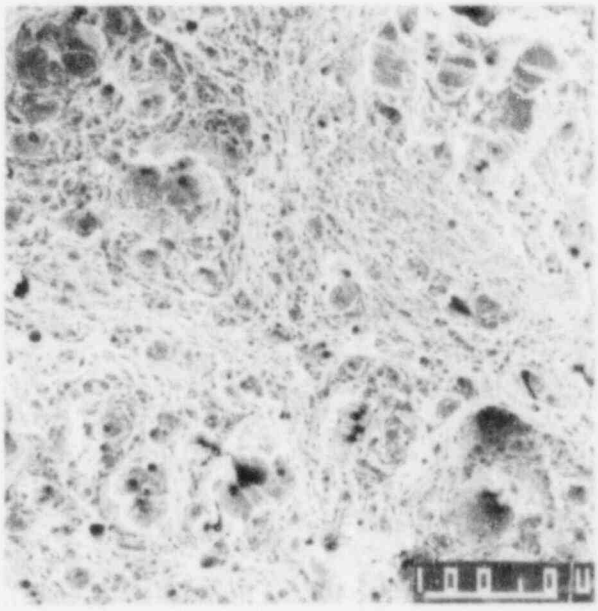

Figure 64. 200X
Higher Magnification Fractograph Showing Generally Ductile Fracture.

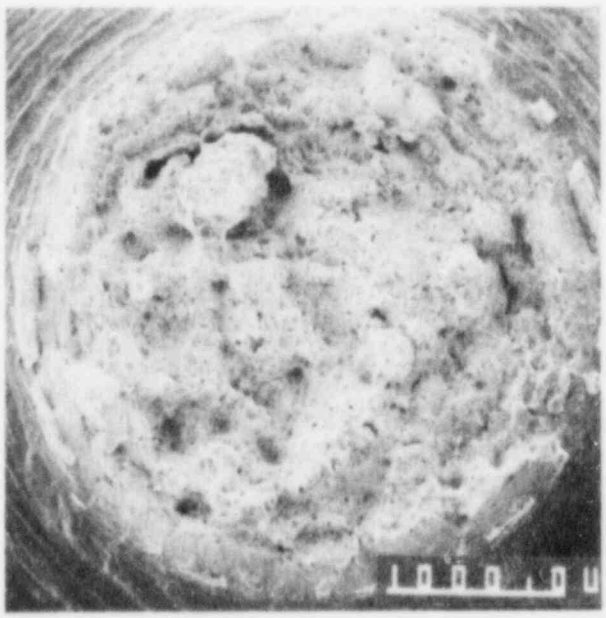

Figure 65. 27X
SEM Photo of Fracture Face for Specimen #26.

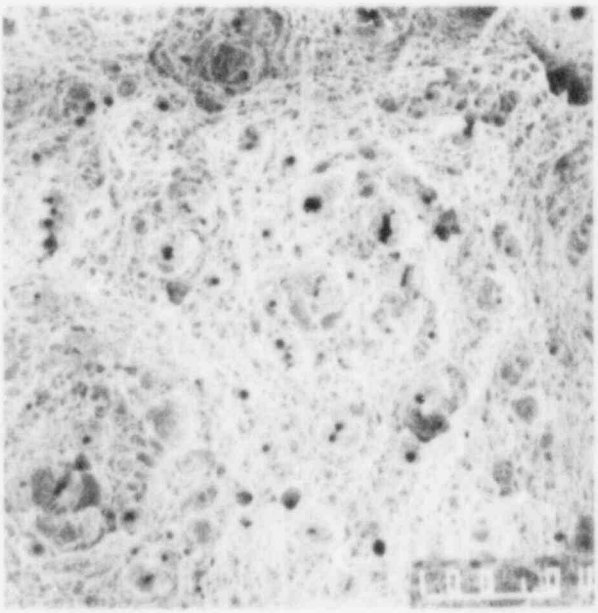

Figure 66. 200X
Higher Magnification Fractograph Showing Typical Ductile Fracture.

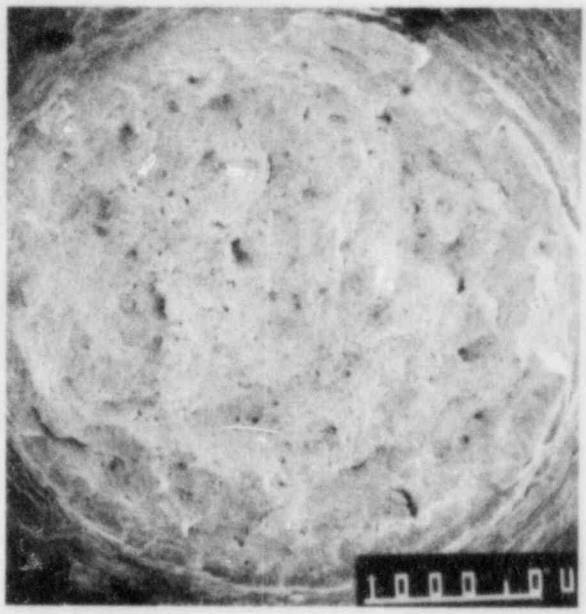

Figure 67. 27X
SEM Photo of Fracture Face for Specimen #27.

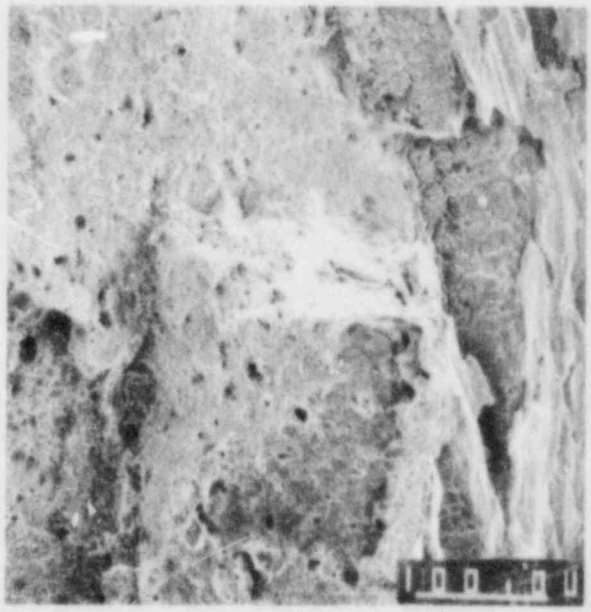

Figure 68. 200X
Higher Magnification Photo of Transgranular Area.

Figure 69. 27X
SEM Photo of Fracture Face for Specimen #28.

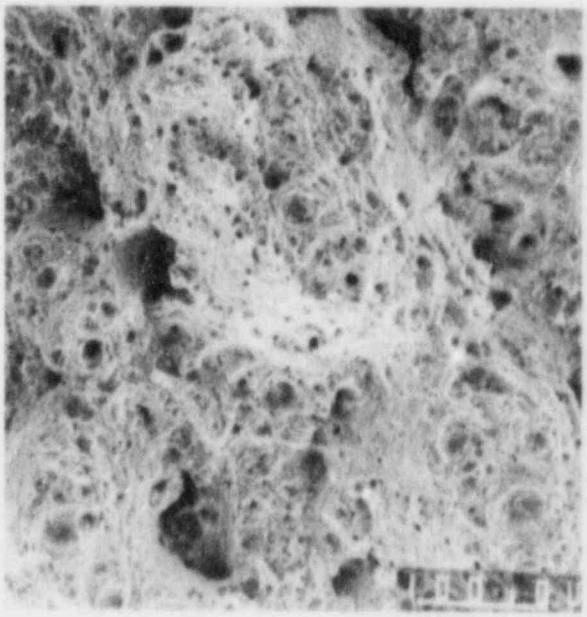

Figure 70. 200X
Higher Magnification Fractograph Showing Typical Ductile Fracture.

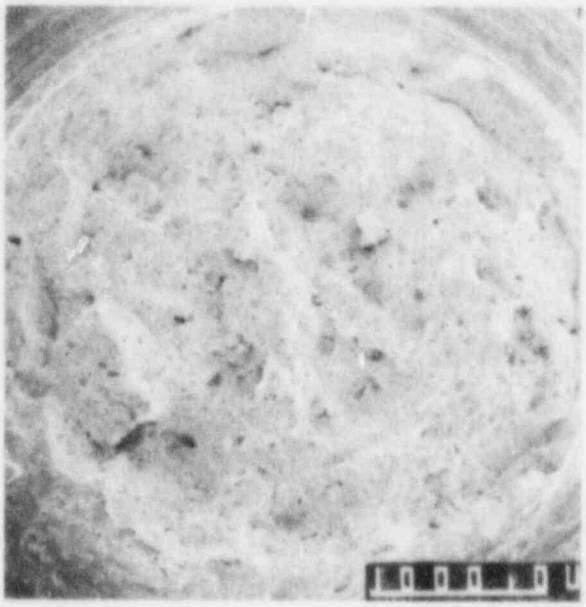

Figure 71. 27X
SEM Photo of Fracture Face for Specimen #29.

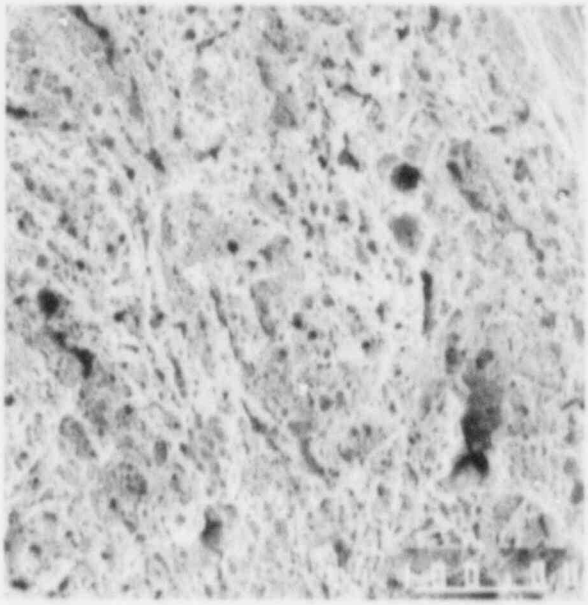

Figure 72. 200X
Higher Magnification Fractograph Showing Typical Ductile Fracture.

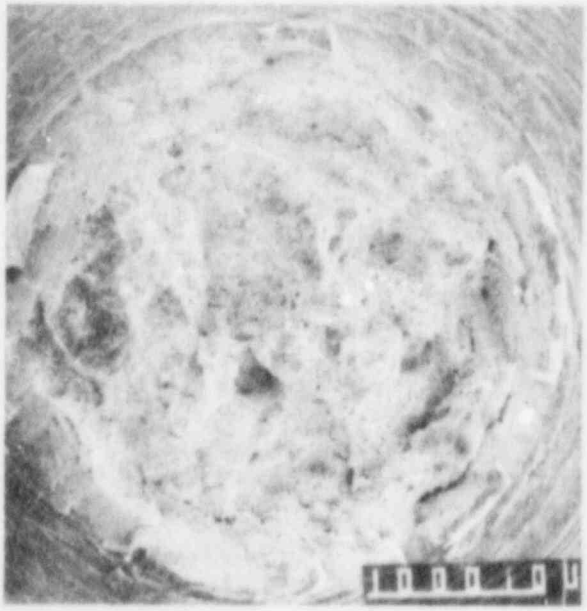

Figure 73. 27X
SEM Photo of Fracture Face for Specimen #30.

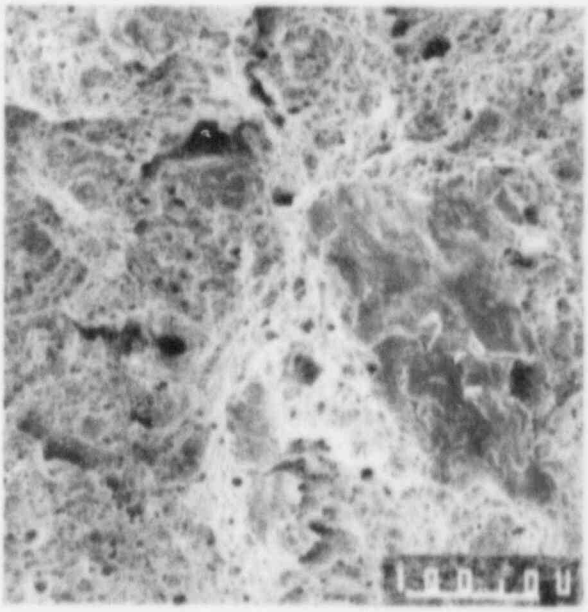

Figure 74. 200X
Higher Magnification Fractograph Showing Typical Ductile Fracture.

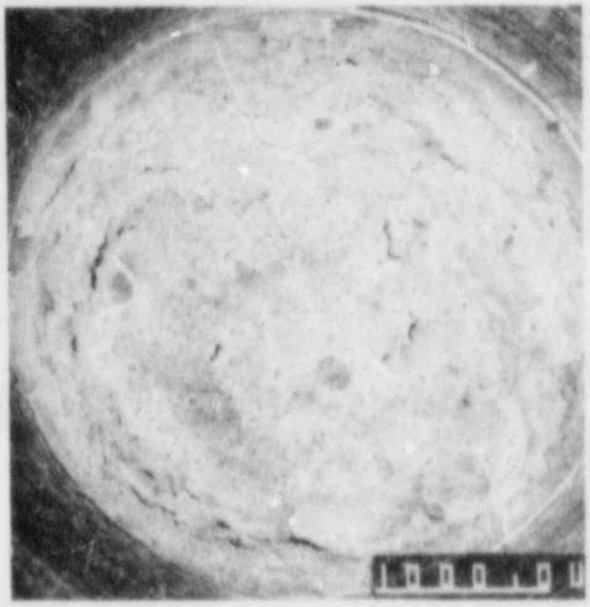

Figure 75. 27X
SEM Photo of Fracture Face for Specimen #31.

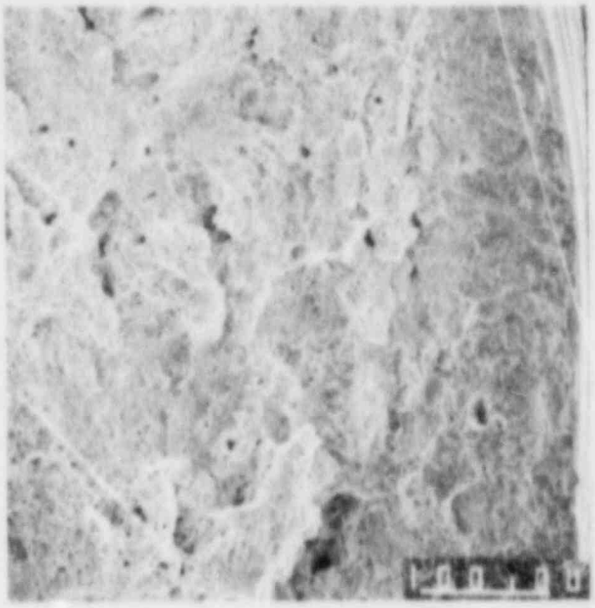

Figure 76. 200X
Higher Magnification Photo of Transgranular Area.

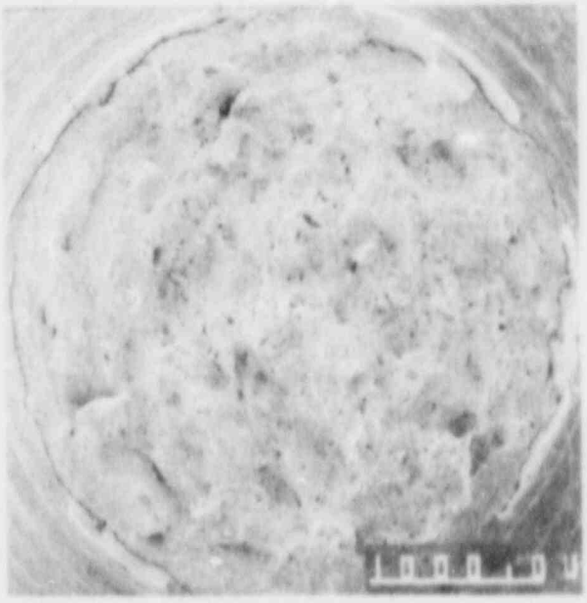

Figure 77. 27X
SEM Photo of Fracture Face for Specimen #32.

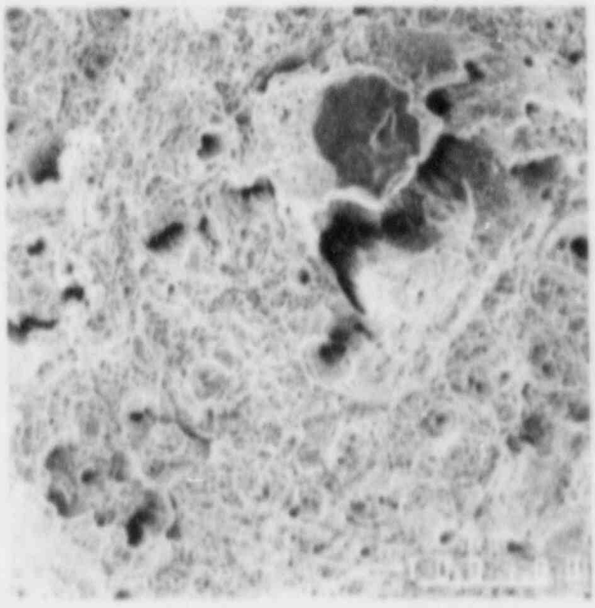

Figure 78. 200X
Higher Magnification Fractograph Showing Generally Ductile Failure.

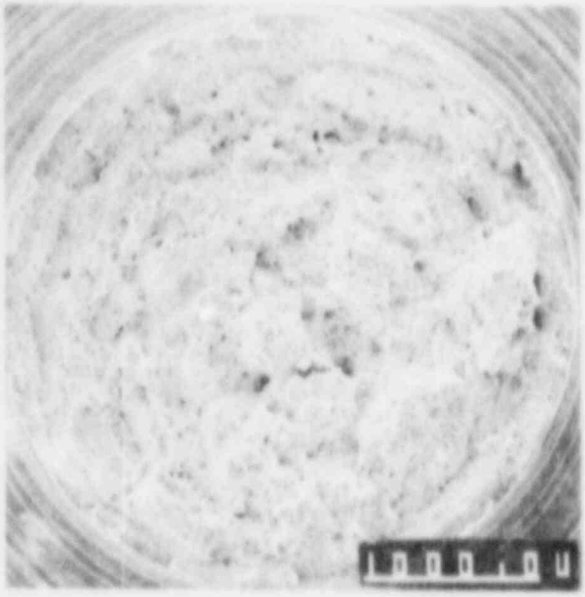

Figure 79. 27X
SEM Photo of Fracture Face for Specimen #33.

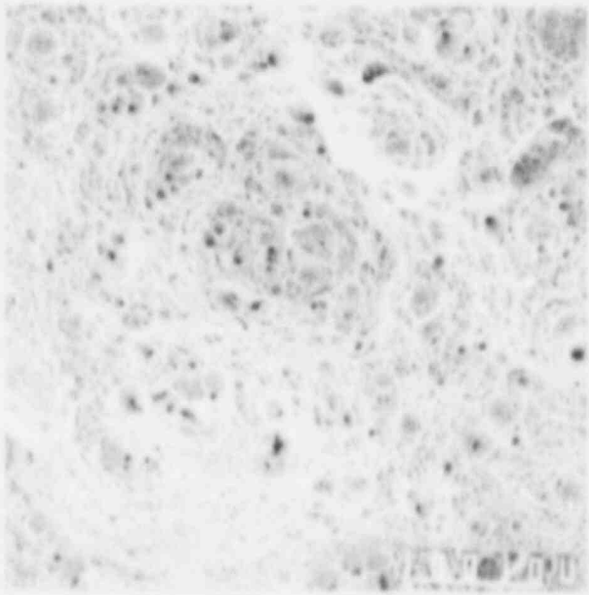

Figure 80. 200X
Higher Magnification Fractograph Showing Typical Ductile Fracture.

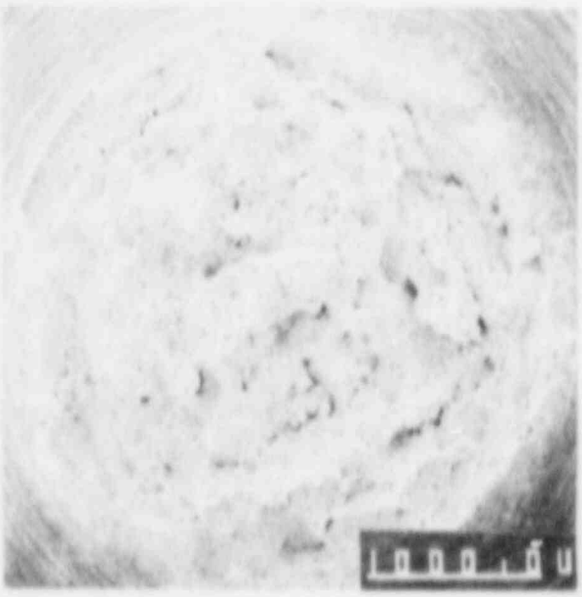

Figure 81. 27X
SEM Photo of Fracture Face for Specimen #34.

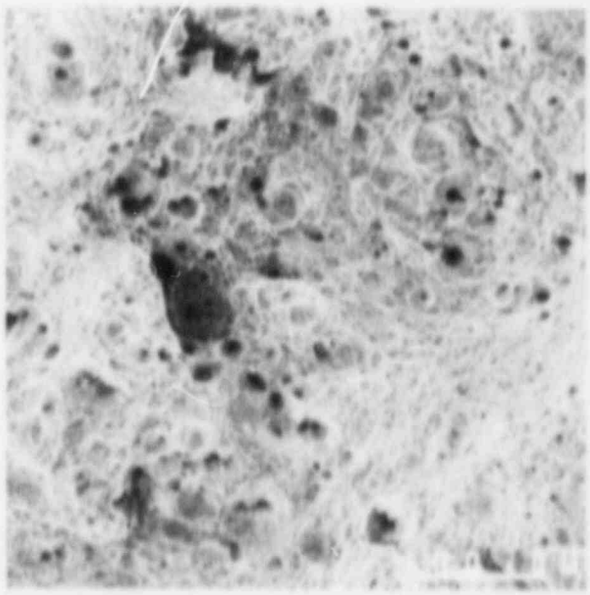

Figure 82. 200X
Higher Magnification Fractograph Showing Typical Ductile Fracture.

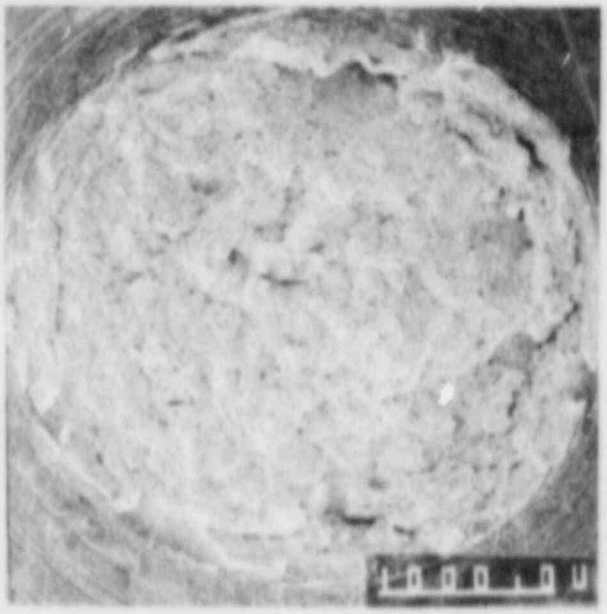

Figure 83. 27X
SEM Photo of Fracture Face for Specimen #35.

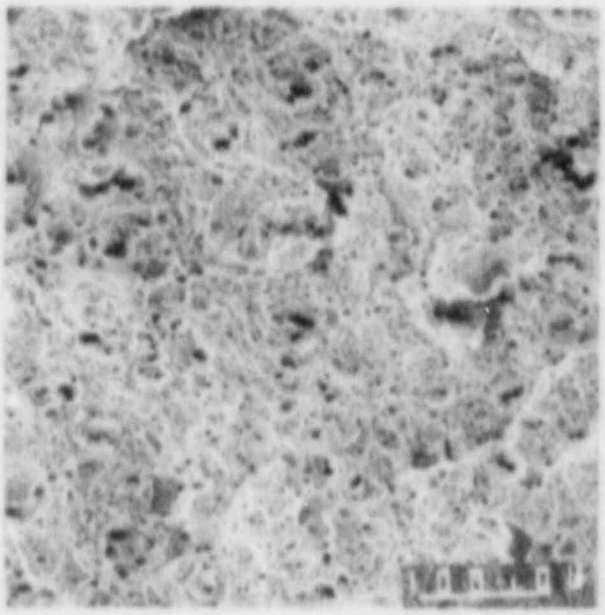

Figure 84. 200X
Higher Magnification Fractograph Showing Typical Ductile Fracture.

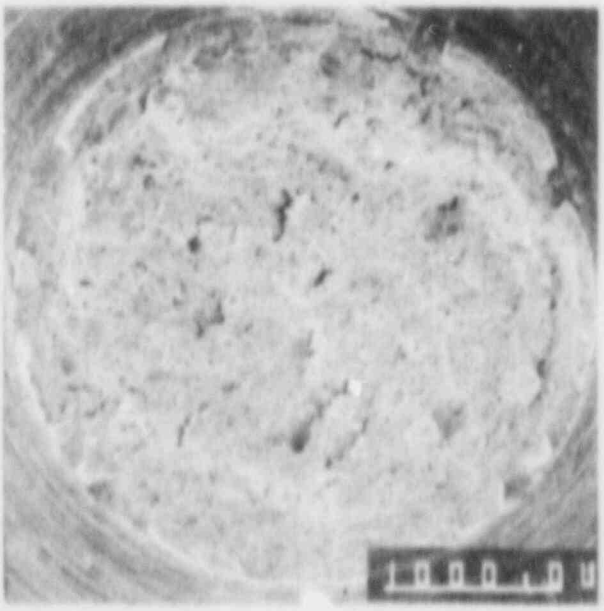

Figure 85. 27X
SEM Photo of Fracture Face for Specimen #36.

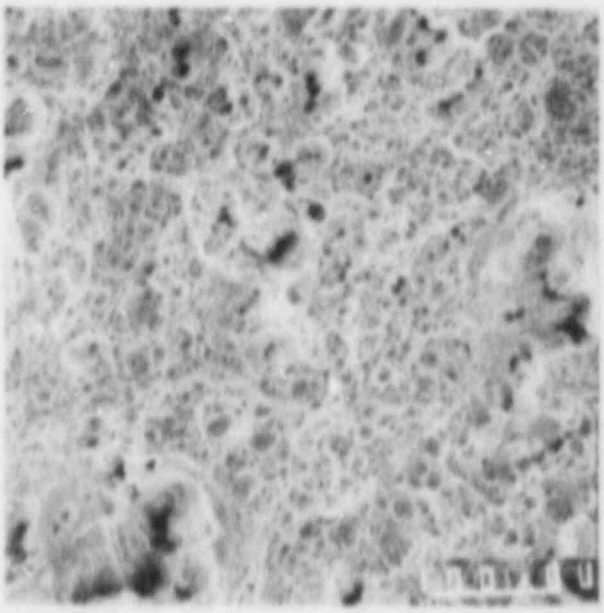

Figu.e 86. 200X
Higher Magnification Fractograph Showing Typical Ductile Fracture.

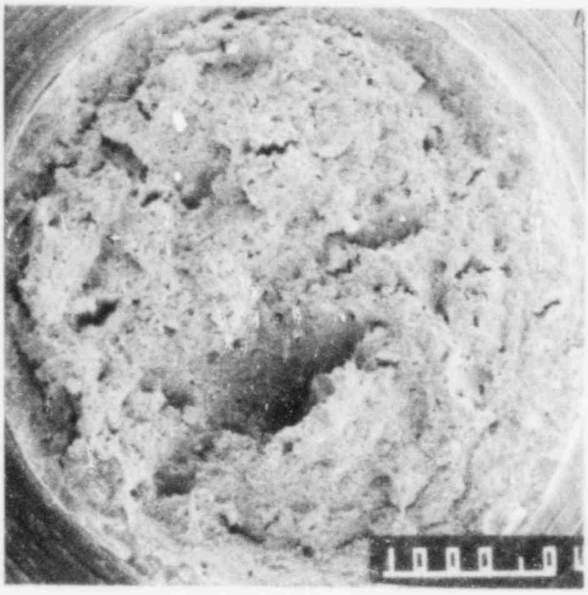

Figure 87. 27X
SEM Photo of Fracture Face for Specimen #37.

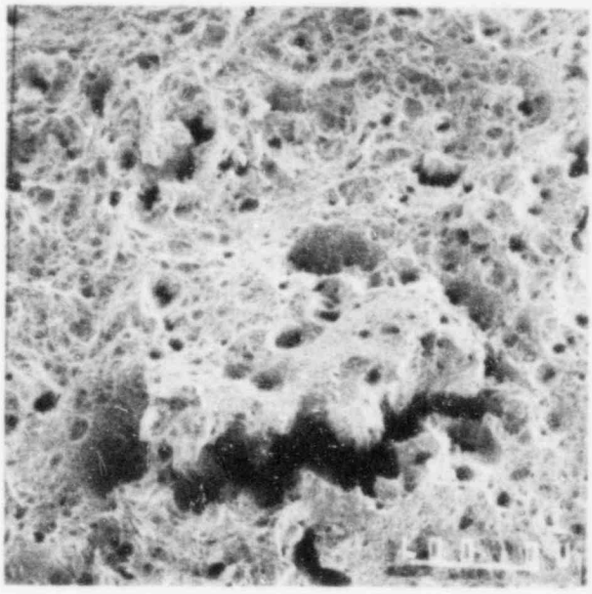

Figure 88. 200X
Higher Magnification Fractograph Showing Typical Ductile Fracture.

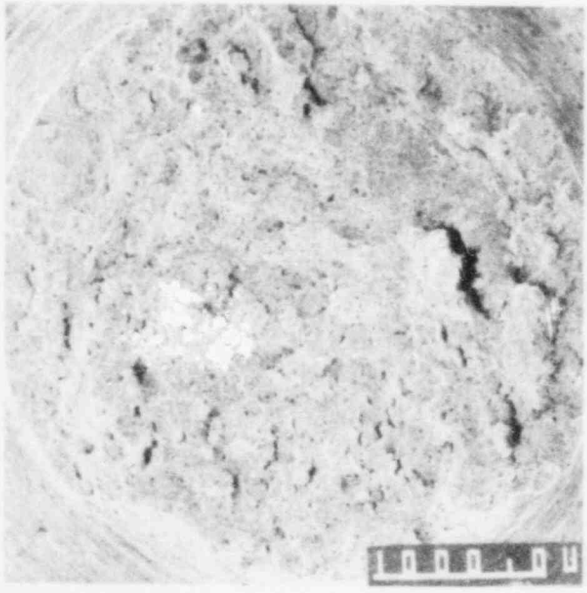

Figure 89. 27X
SEM Photo of Fracture Face for Specimen #38.

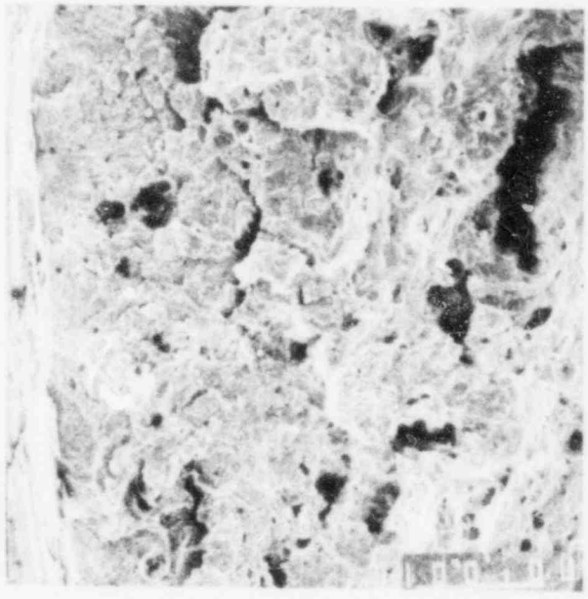

Figure 90. 200X
Higher Magnification Photo of Transgranular Area.

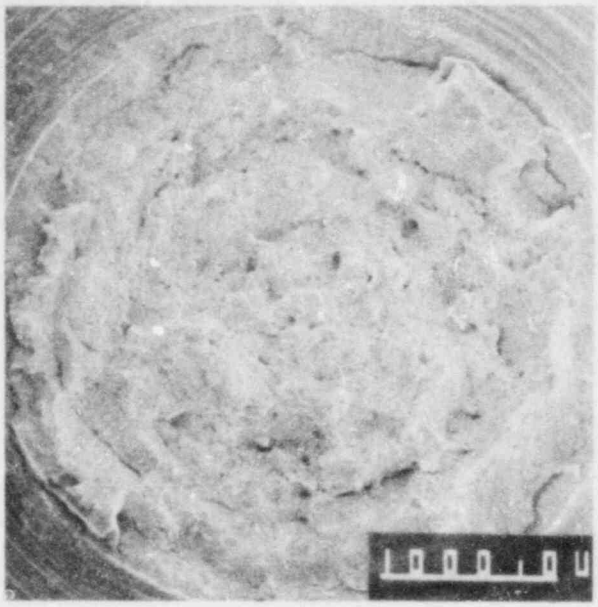

Figure 91. 27X
SEM Photo of Fracture Face for Specimen #39.

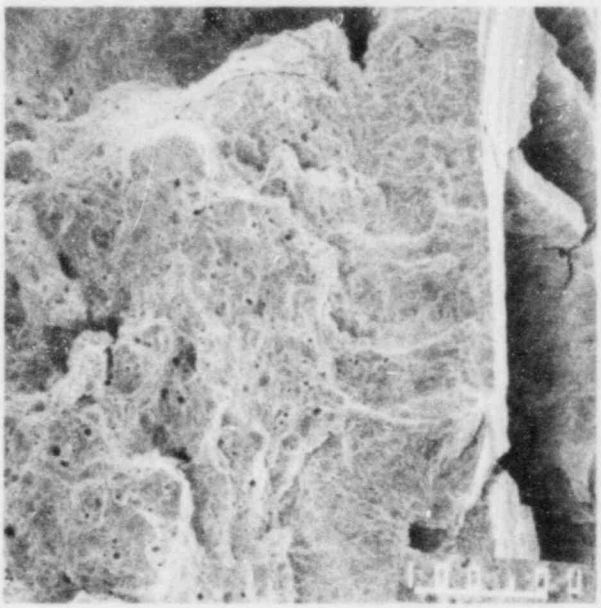

Figure 92. 200X
Higher Magnification Photo of Transgranular Area.

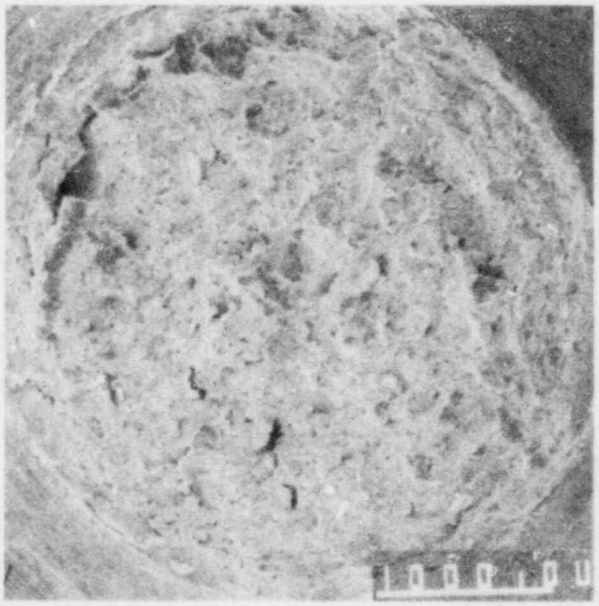

Figure 93. 27X
SEM Photo of Fracture Face for Specimen #40.

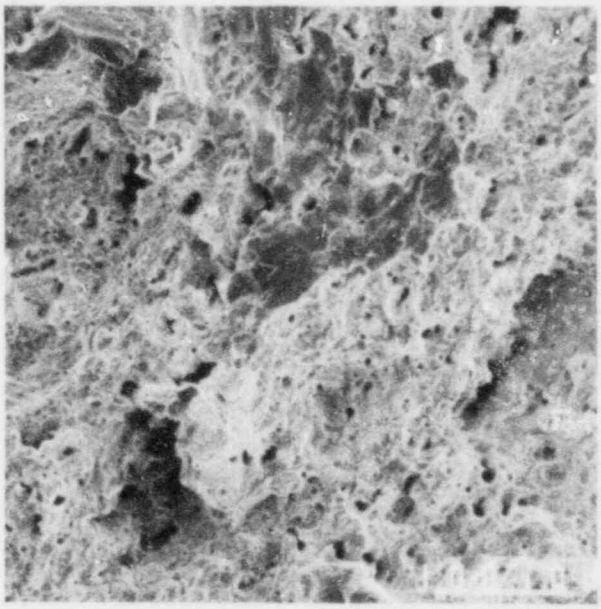

Figure 94. 200X
Higher Magnification Fractograph Showing Typical Ductile Fracture.

Figure 95. 27X
SEM Photo of Fracture Face for Specimen #41.

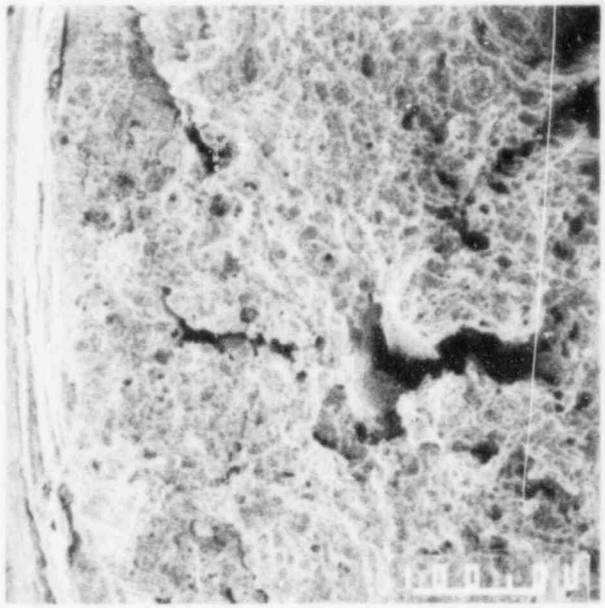

Figure 96. 200X
Higher Magnification Photo of Transgranular Area.

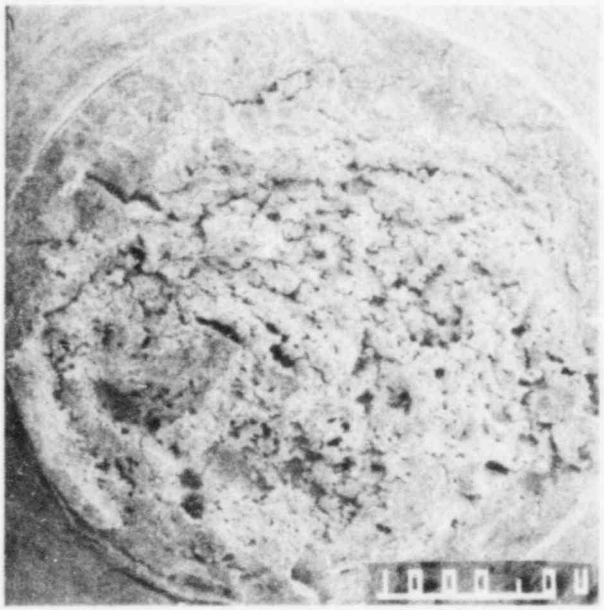

Figure 97. 27X
SEM Photo of Fracture Face for Specimen #42.

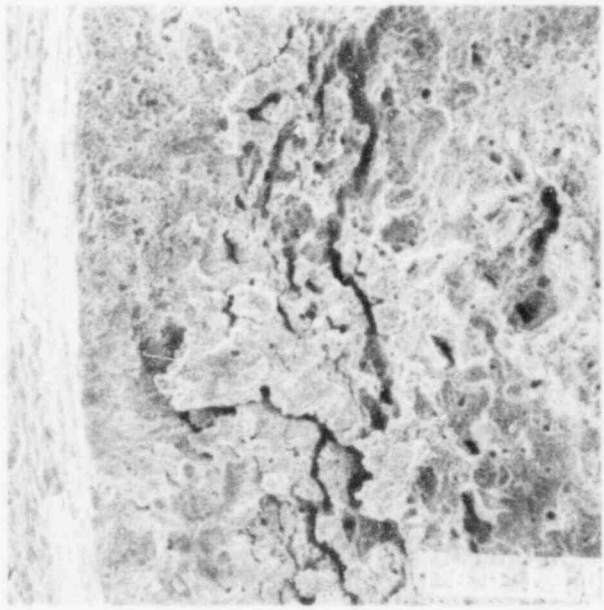

Figure 98. 200X
Higher Magnification Photo of Transgranular Area.

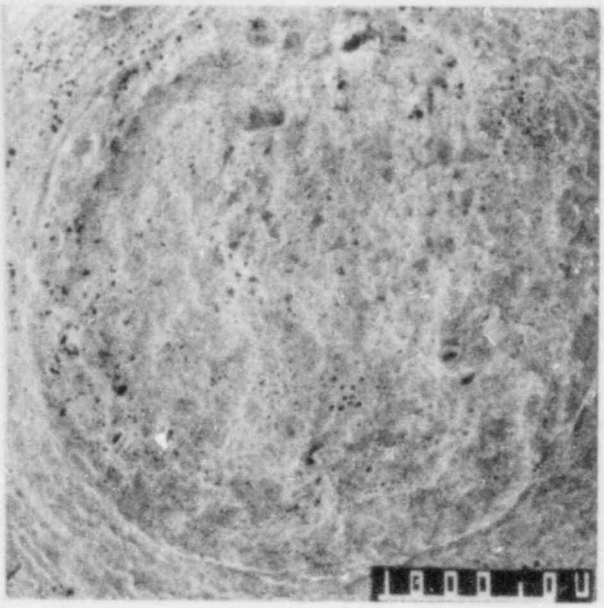

Figure 99. 27X
SEM Photo of Fracture Face for Specimen #43.

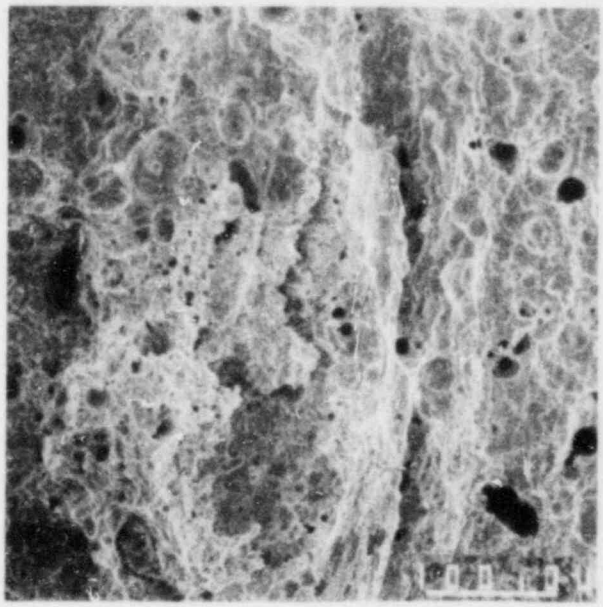

Figure 100. 200X
Higher Magnification Fractograph Showing Typical Ductile Fracture.

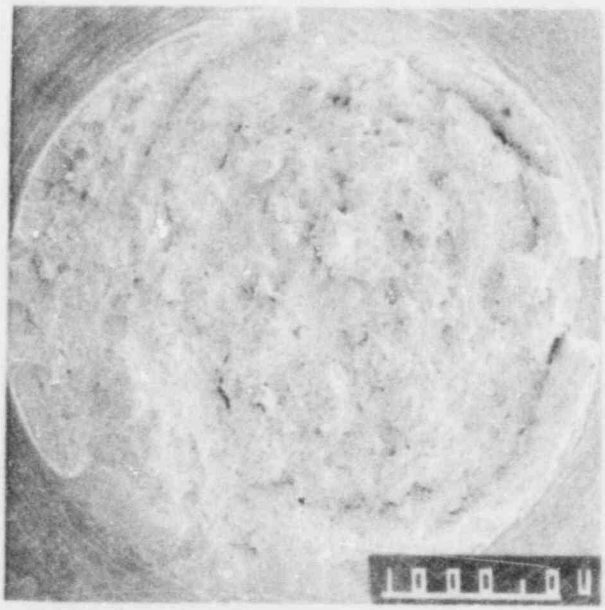

Figure 101. 27X
SEM Photo of Fracture Face for Specimen #44.

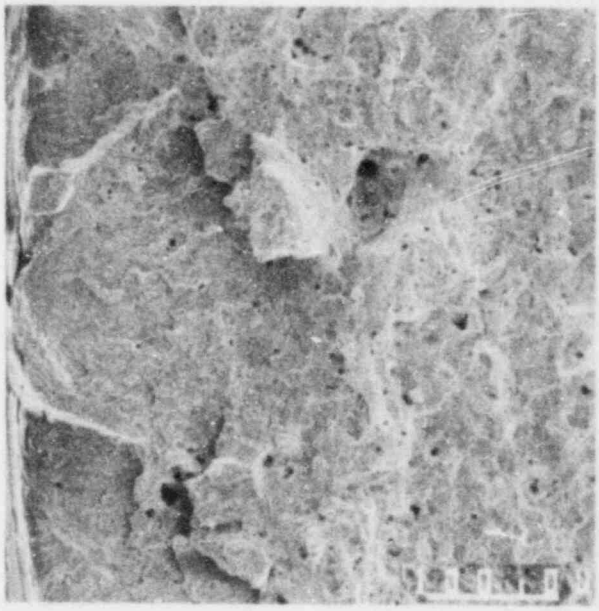

Figure 102. 200X
Higher Magnification Photo of Transgranular Area.

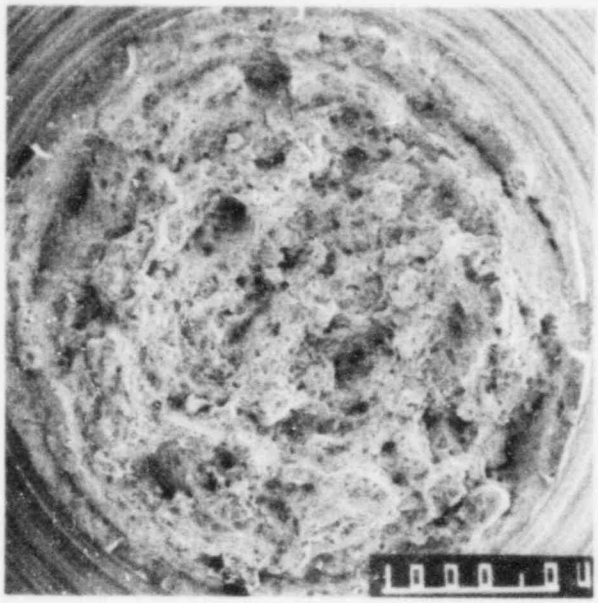

Figure 103. 27X
SEM Photo of Fracture Face for Specimen #45.

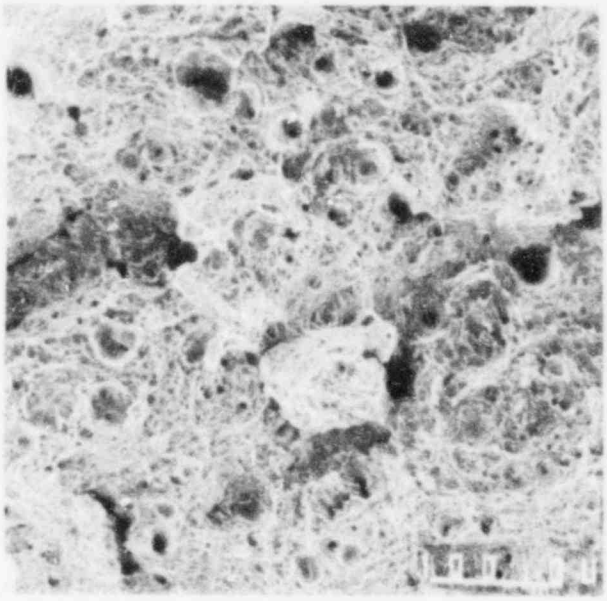

Figure 104. 200X
Higher Magnification Fractograph Showing Typical Ductile Fracture.

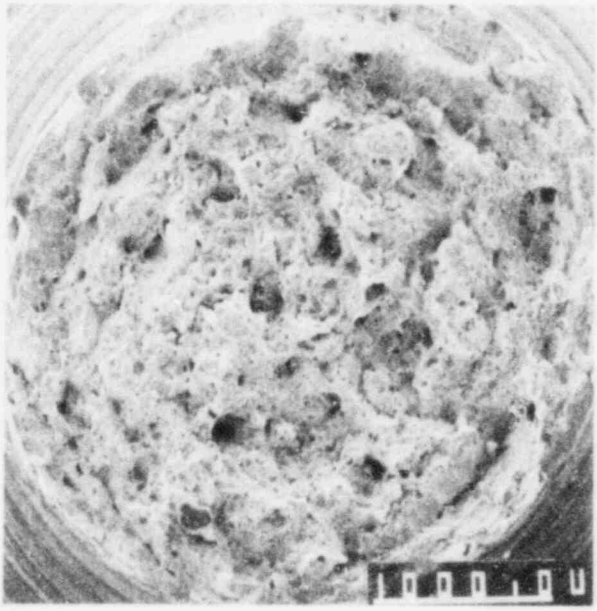

Figure 105. 27X
SEM Photo of Fracture Face for Specimen #46.

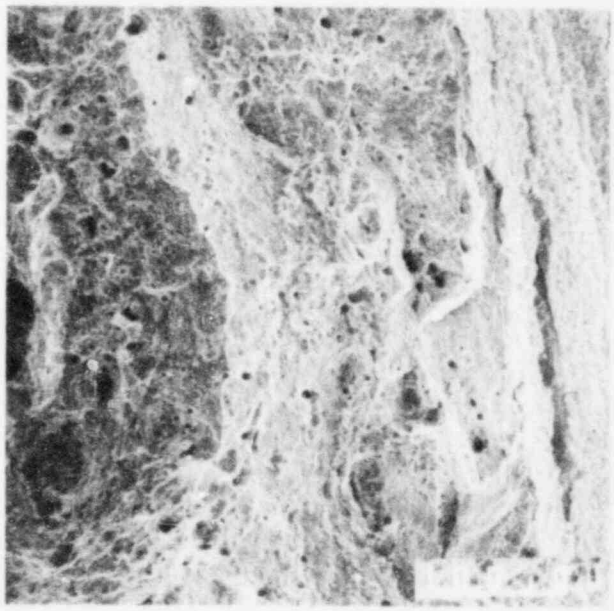

Figure 106. 200X
Higher Magnification Photo of Transgranular Area.

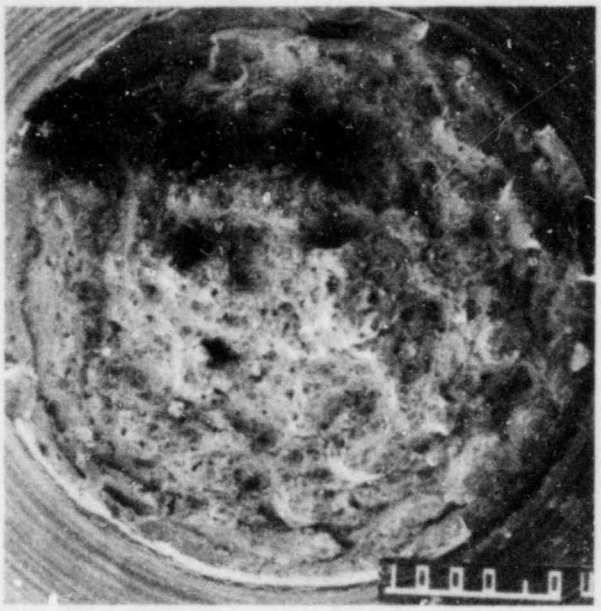

Figure 107. 27X
SEM Photo of Fracture Face for Specimen #47.

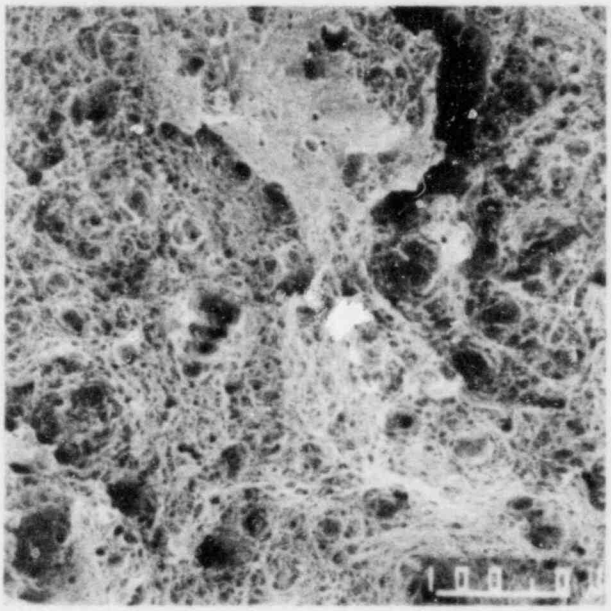

Figure 108. 200X
Higher Magnification Fractograph Showing Typical Ductile Fracture.

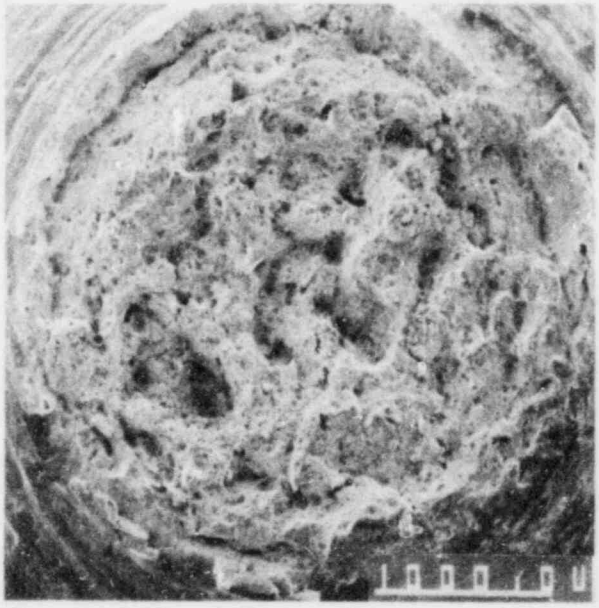

Figure 109. 27X
SEM Photo of Fracture Face for Specimen #48.

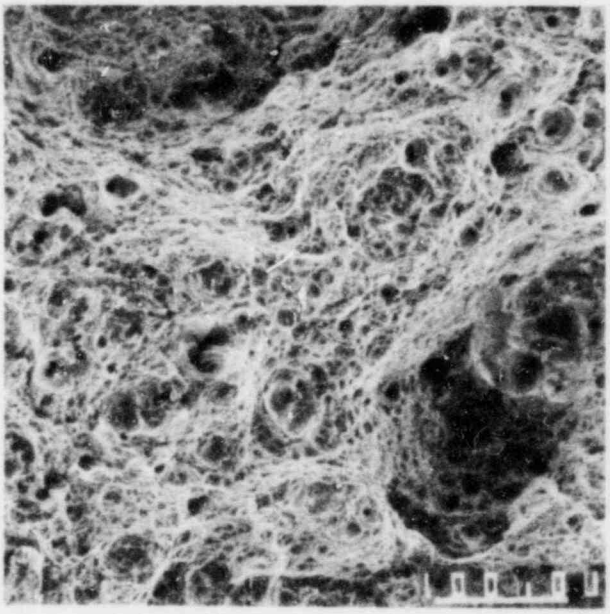

Figure 110. 200X
Higher Magnification Fractograph Showing Typical Ductile Fracture.

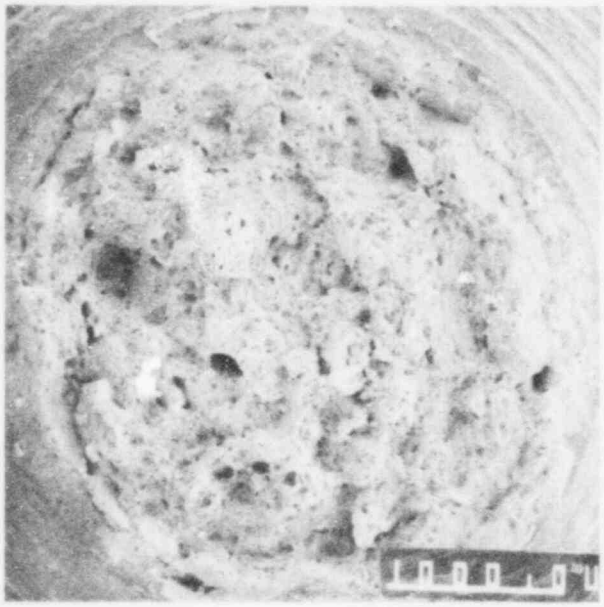

Figure 111. 27X
SEM Photo of Fracture Face for Specimen #49.

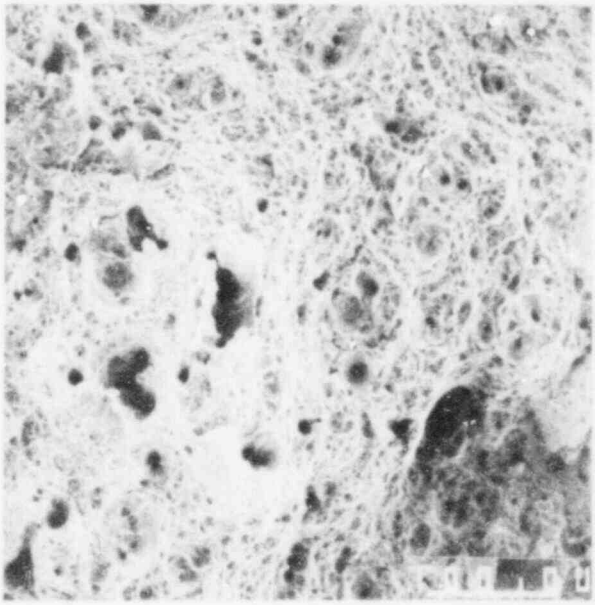

Figure 112. 200X
Higher Magnification Fractograph Showing Typical Ductile Fracture.

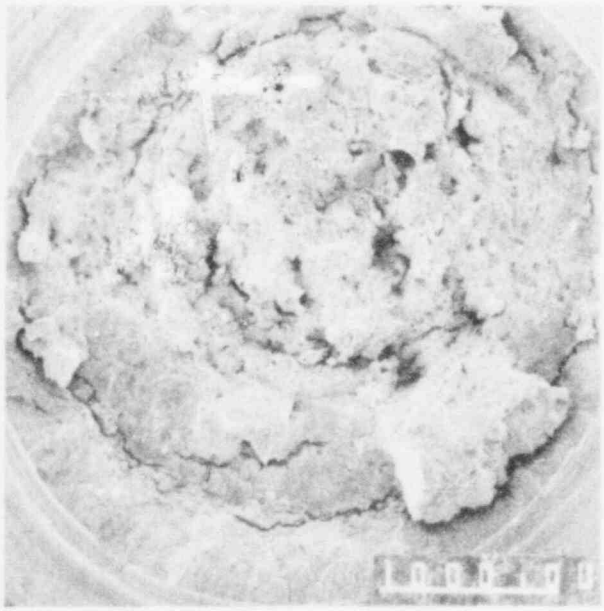

Figure 113. 27X
SEM Photo of Fracture Face for Specimen #50.

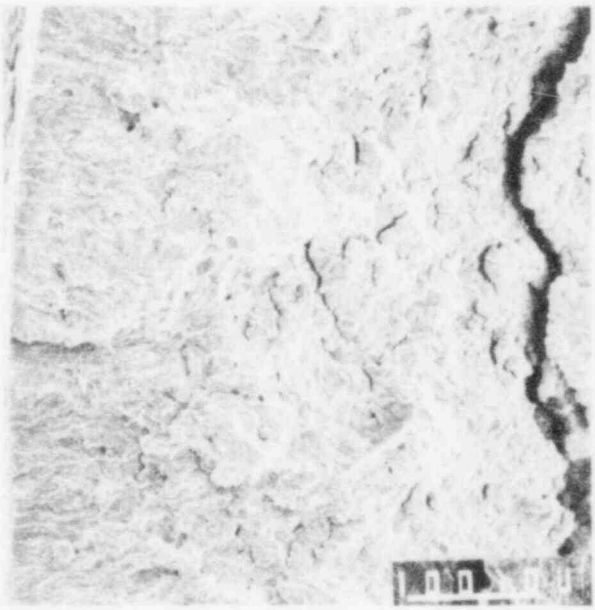

Figure 114. 200X
Higher Magnification Photo of Transgranular Area.

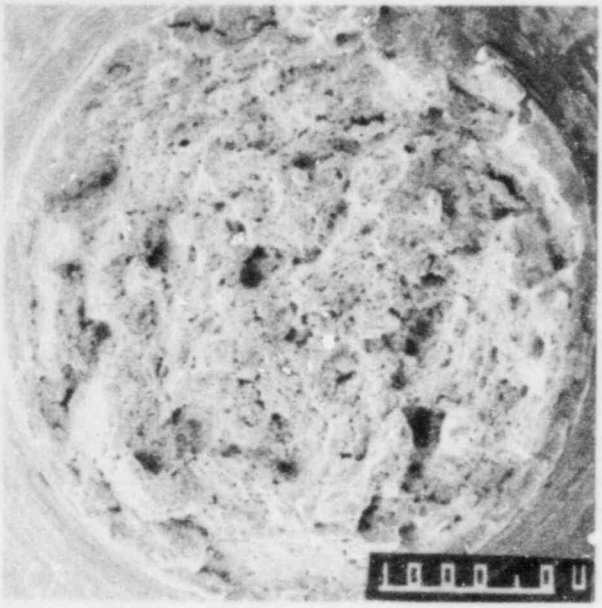

Figure 115. 27X
SEM Photo of Fracture Face for Specimen #51.

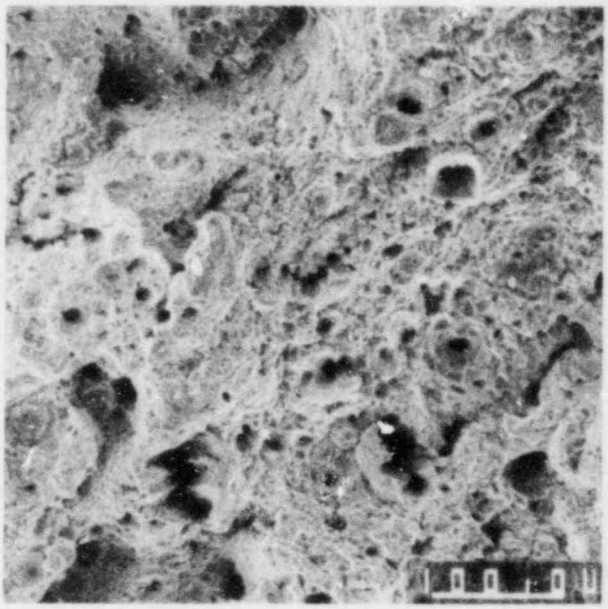

Figure 116. 200X
Higher Magnification Fractograph Showing Typical Ductile Fracture.

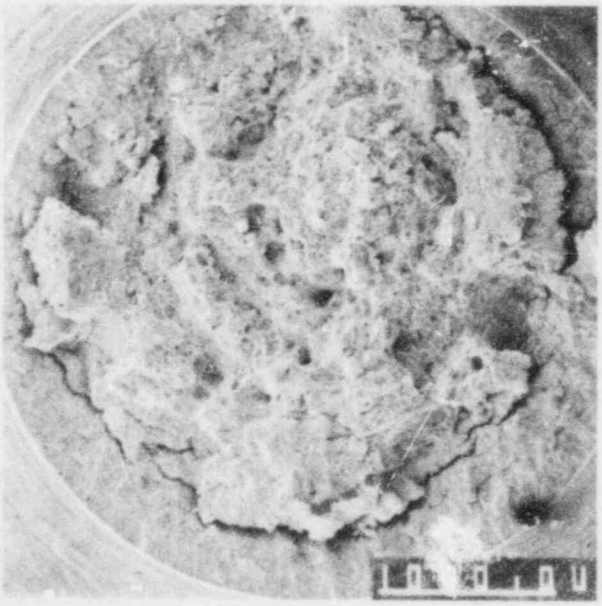

Figure 117. 27X
SEM Photo of Fracture Face for Specimen #52.

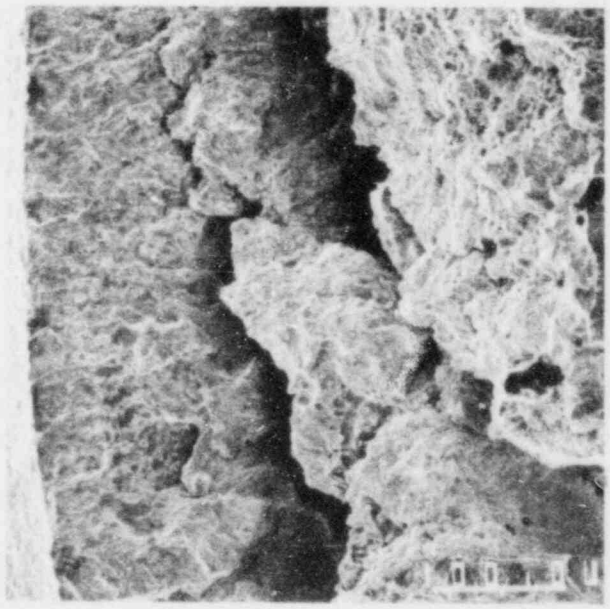

Figure 118. 200X
Higher Magnification Photo of Transgranular Area.

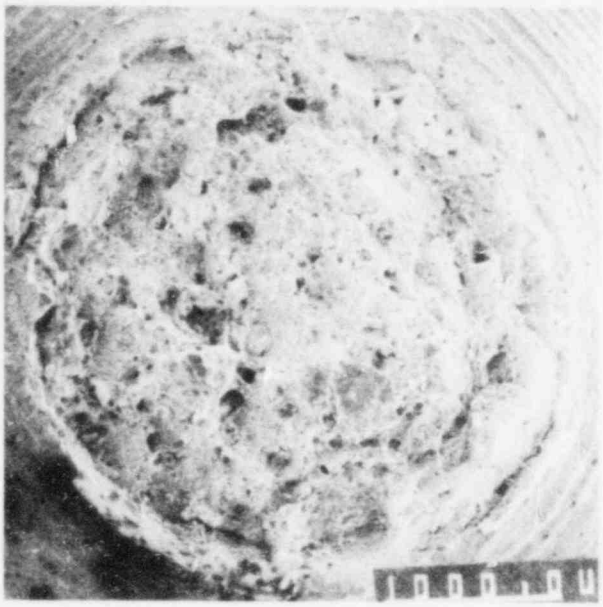

Figure 119. 27X
SEM Photo of Fracture Face for Specimen #53.

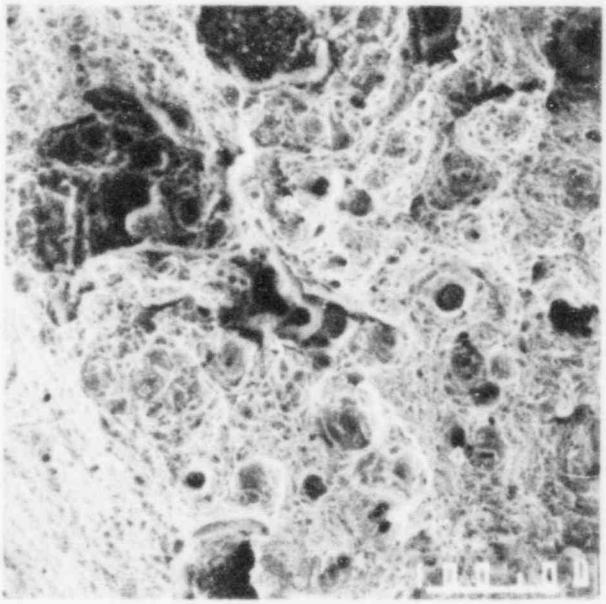

Figure 120. 200X
Higher Magnification Fractograph Showing Typical Ductile Fracture.

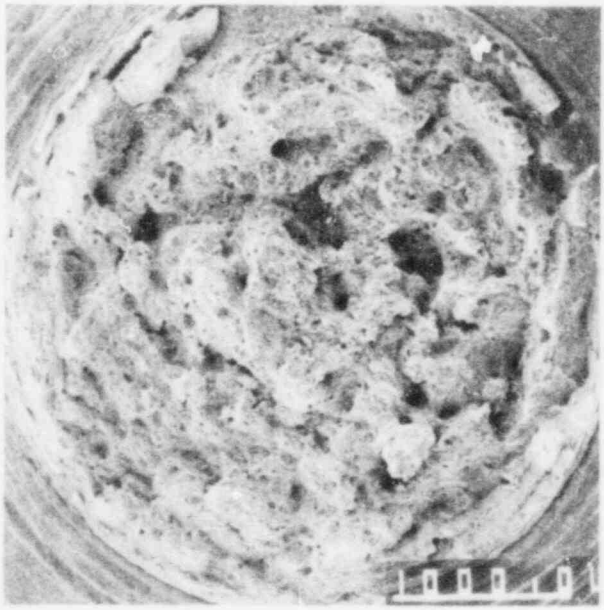

Figure 121. 27X
SEM Photo of Fracture Face for Specimen #54.

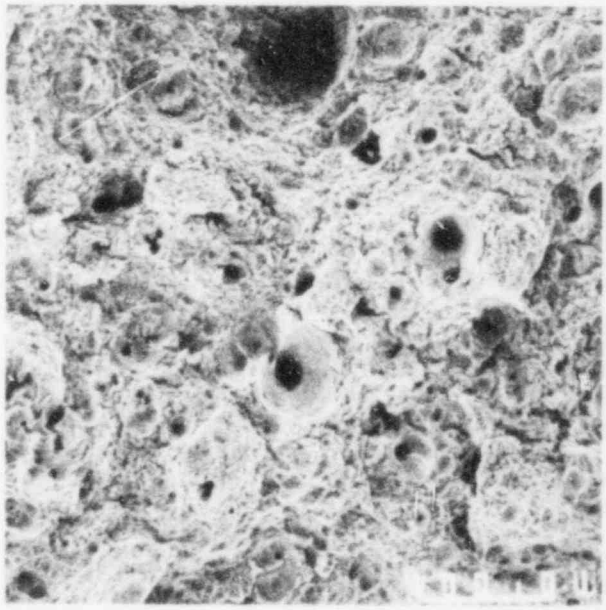

Figure 122. 200X
Higher Magnification Fractograph Showing Typical Ductile Fracture.

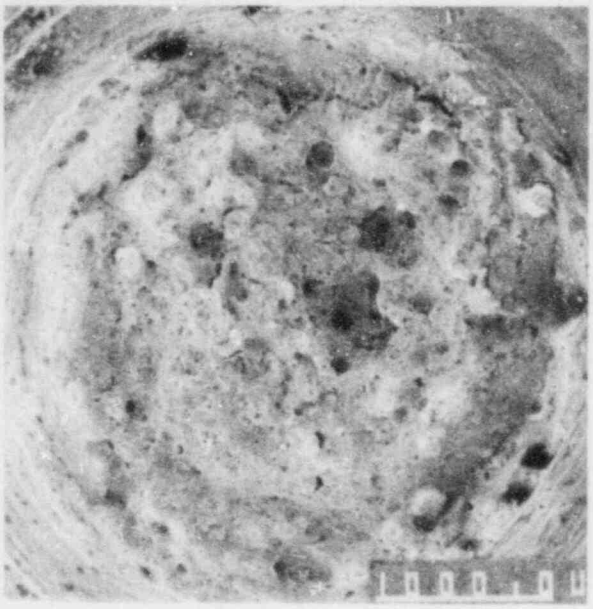

Figure 123. 27X
SEM Photo of Fracture Face for Specimen #55.

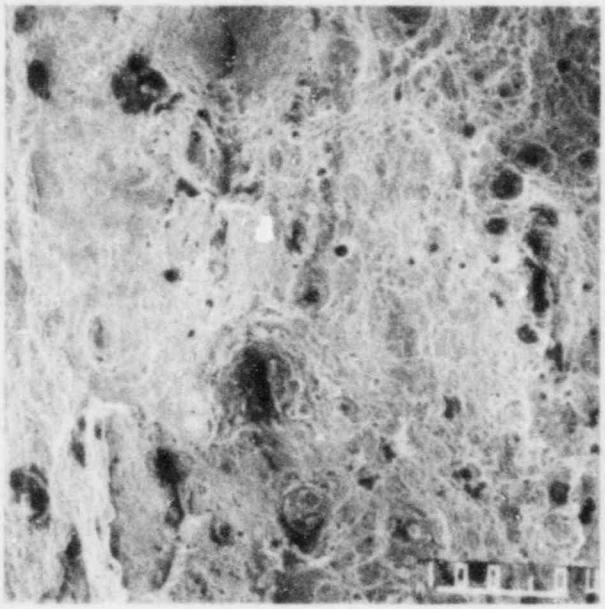

Figure 124. 200X
Higher Magnification Fractograph Showing Typical Ductile Fracture.

Figure 125. 27X
SEM Photo of Fracture Face for Specimen #56.

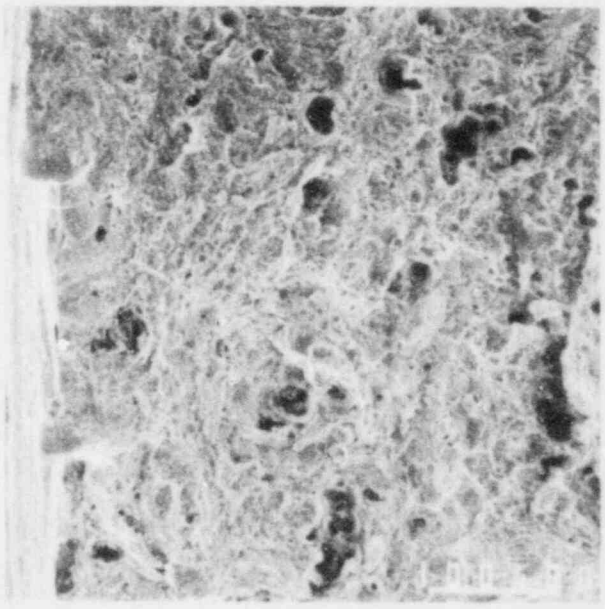

Figure 126. 200X
Higher Magnification Photo of Transgranular Area.

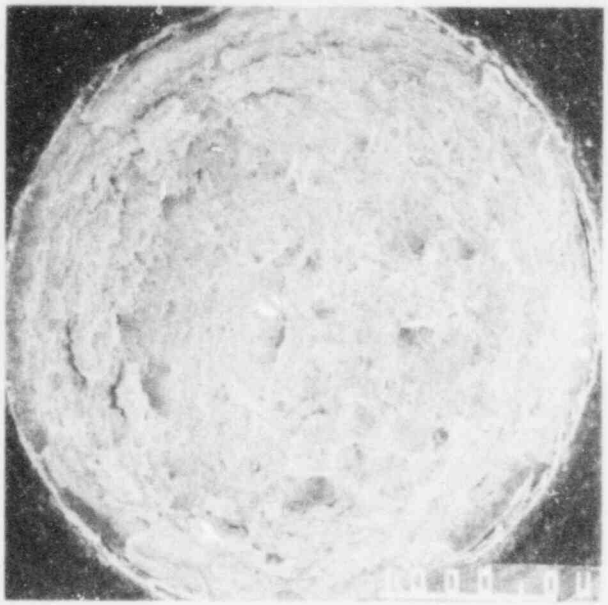

Figure 127. 27X
SEM Photo of Fracture Face for Specimen #57.

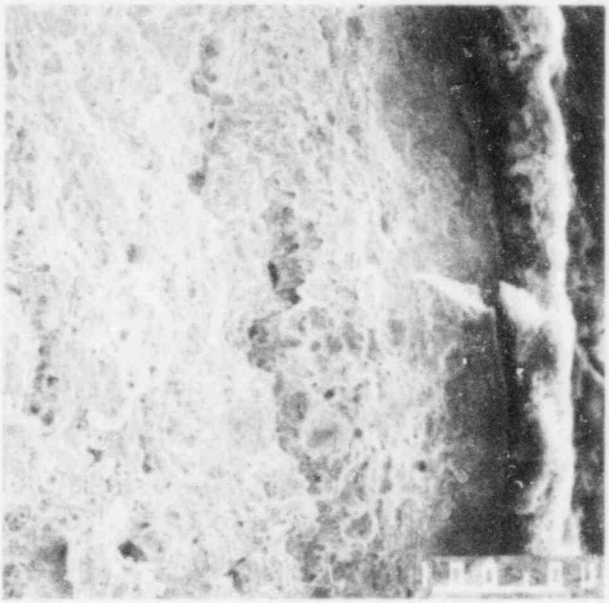

Figure 128. 200X
Higher Magnification Photo of Transgranular Area.

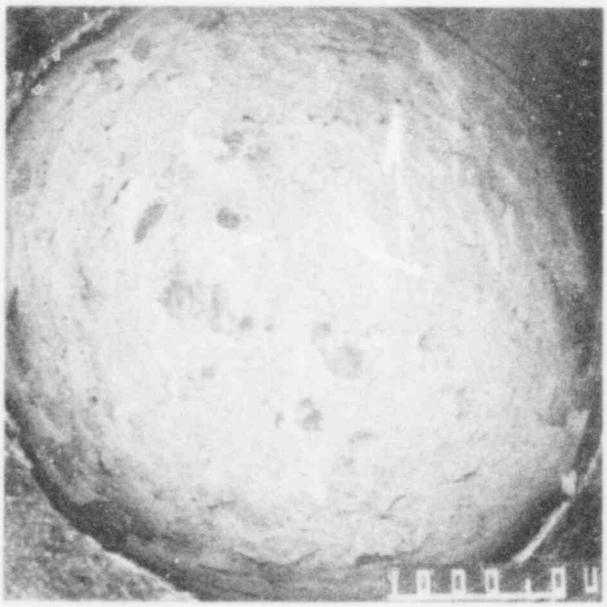

Figure 129. 27X
SEM Photo of Fracture Face for Specimen #58.

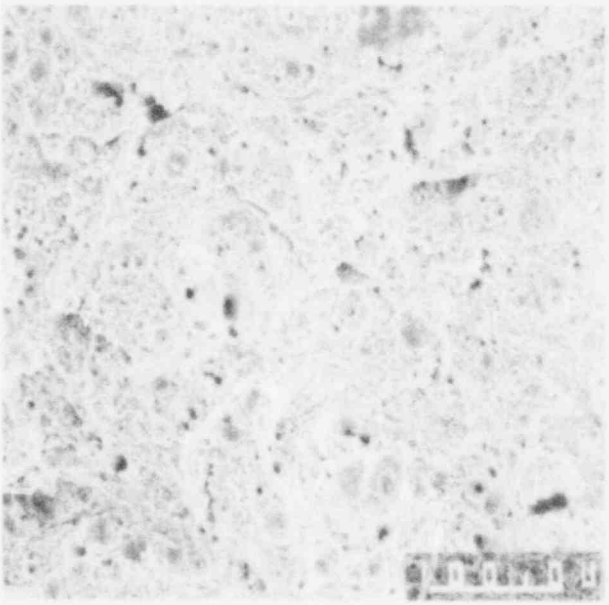

Figure 130. 200X
Higher Magnification Fractograph Showing Typical Ductile Fracture.

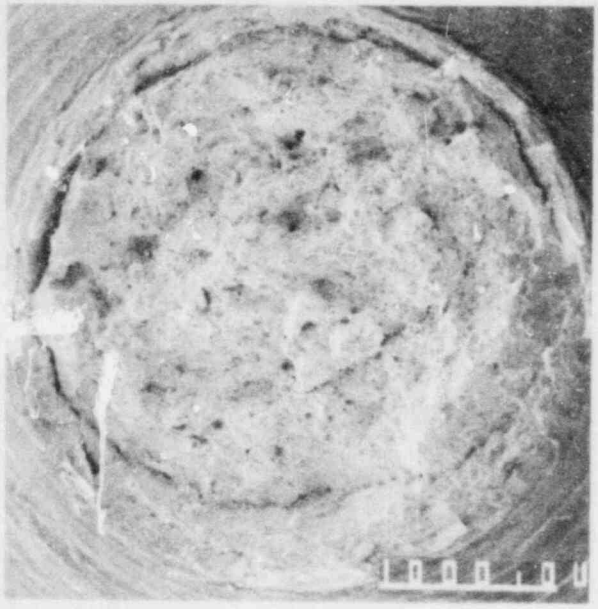

Figure 131. 27X
SEM Photo of Fracture Face for Specimen #59.

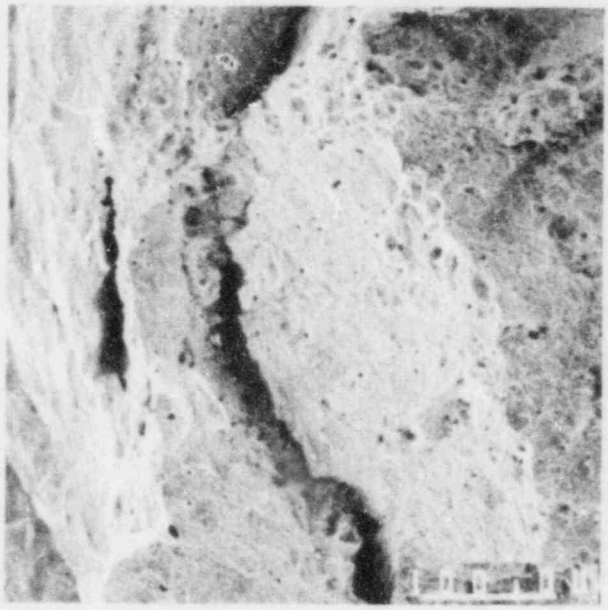

Figure 132. 200X
Higher Magnification Photo of Transgranular Area.

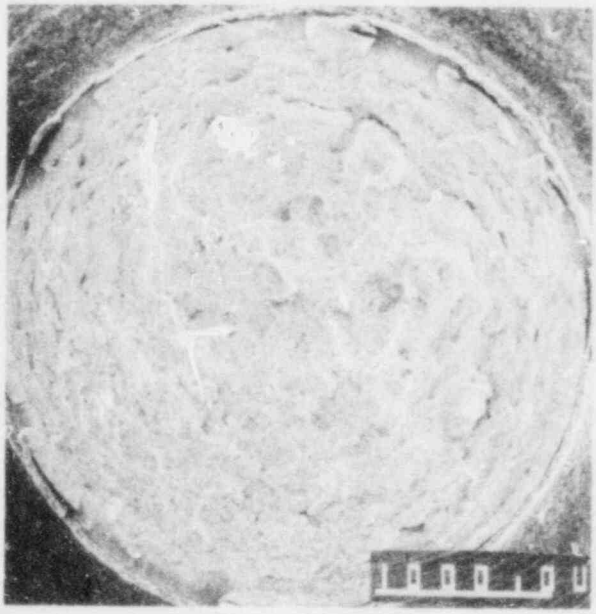

Figure 133. 27X
SEM Photo of Fracture Face for Specimen #60.

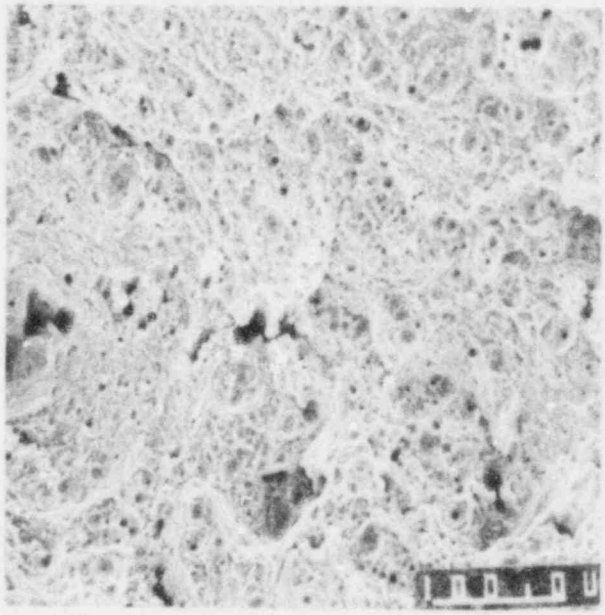

Figure 134. 200X
Higher Magnification Fractograph Showing Typical Ductile Fracture.

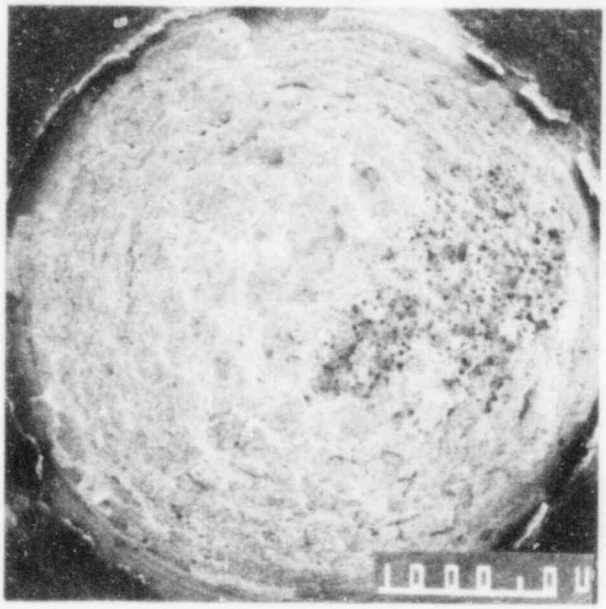

Figure 135. 27X
SEM Photo of Fracture Face for Specimen #61.

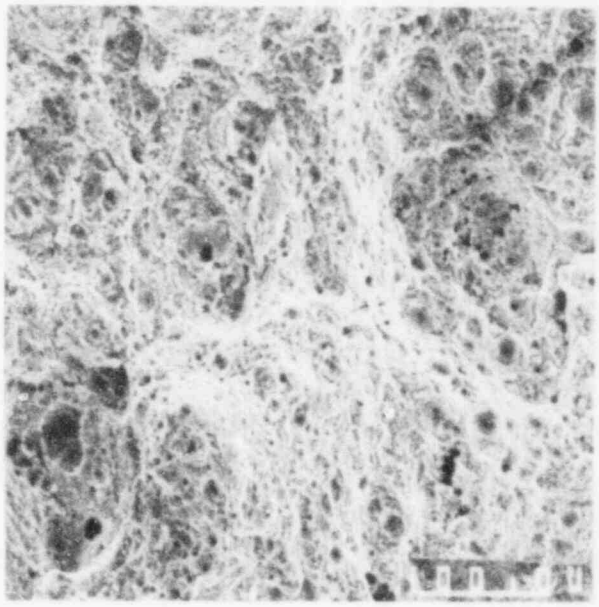

Figure 136. 200X
Higher Magnification Fractograph Showing Typical Ductile Fracture.

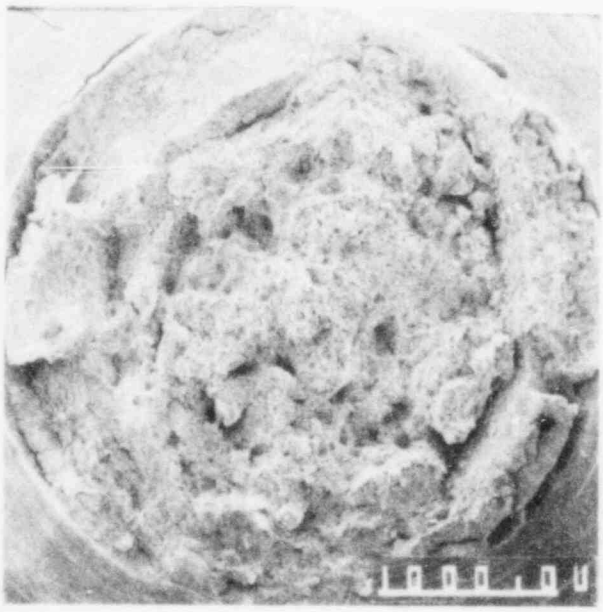

Figure 137. 27X
SEM Photo of Fracture Face for Specimen #62.

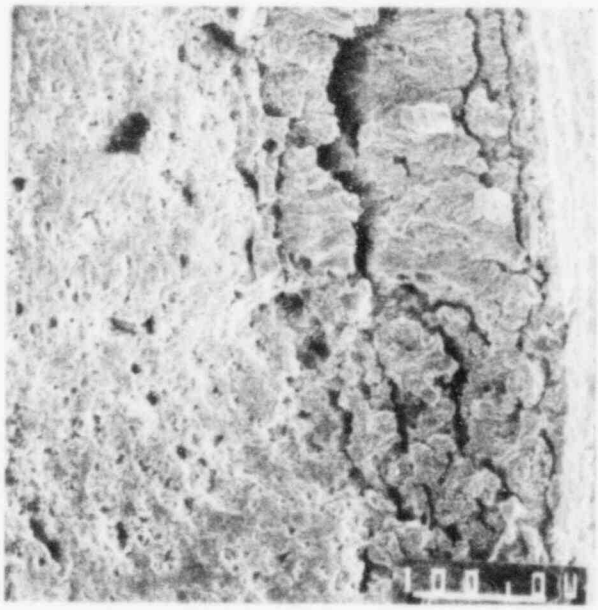

Figure 138. 200X
Higher Magnification Photo of Transgranular Area.

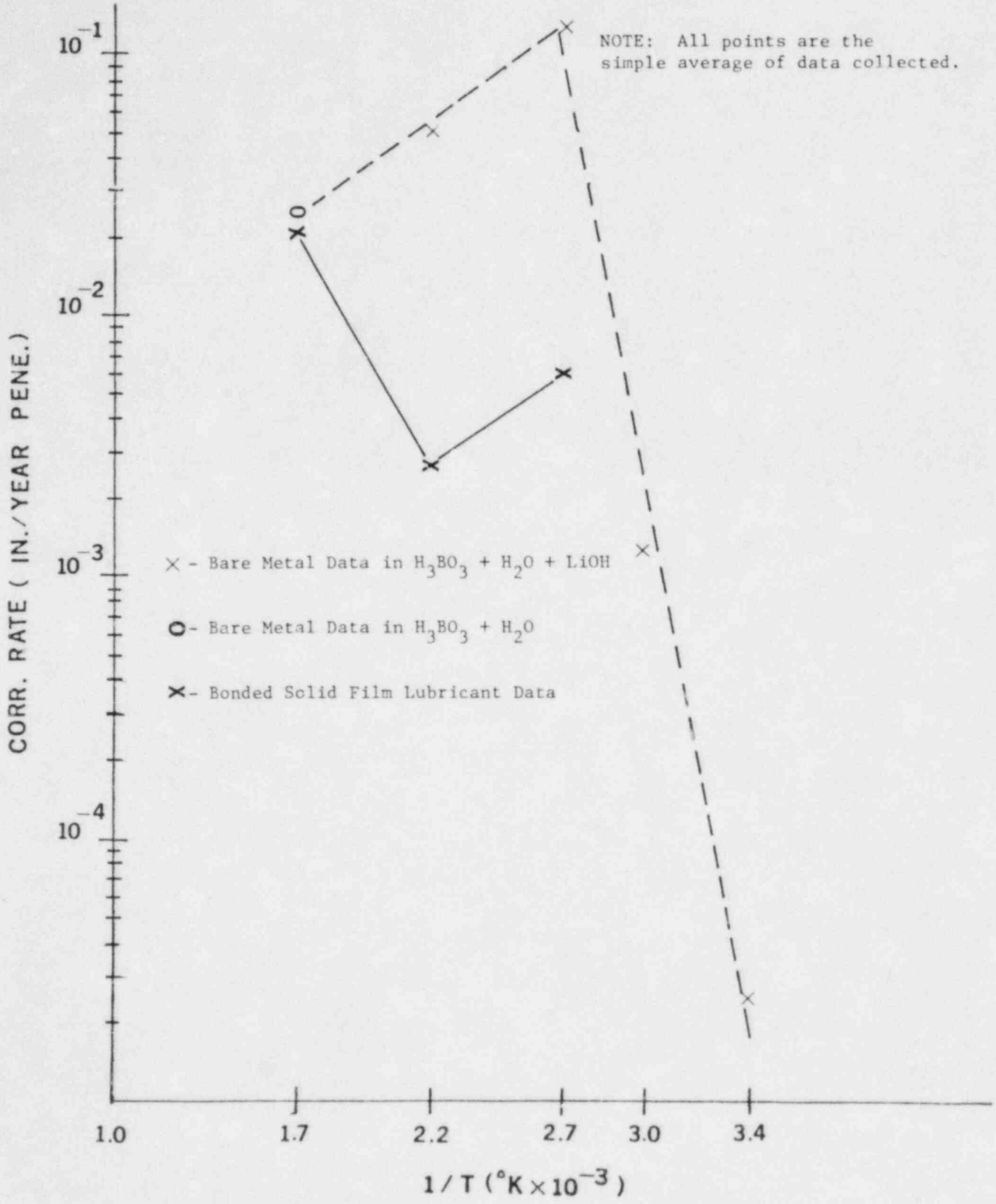

Figure 139 Graphical Representation of Weight Loss Experiments

NRC FORM 335 (7 77)

U.S. NUCLEAR REGULATORY COMMISSION

BIBLIOGRAPHIC DATA SHEET

1. REPORT NUMBER (Assigned by DDC)
NUREG/CR- 3766
BNL/NUREG- 51767

4. TITLE AND SUBTITLE (Add Volume No., if appropriate)
TESTING OF NUCLEAR GRADE LUBRICANTS AND THEIR EFFECT ON A540 B24 AND A193 B7 BOLTING MATERIALS

2. (Leave blank)

3. RECIPIENT'S ACCESSION NO.

7. AUTHOR(S)
Carl J. Czajkowski

5. DATE REPORT COMPLETED
MONTH: March
YEAR: 1984

9. PERFORMING ORGANIZATION NAME AND MAILING ADDRESS (Include Zip Code)
Brookhaven National Laboratory
Department of Nuclear Energy
Upton, New York 11973

DATE REPORT ISSUED
MONTH: March
YEAR: 1984

6. (Leave blank)

8. (Leave blank)

12. SPONSORING ORGANIZATION NAME AND MAILING ADDRESS (Include Zip Code)
Division of Engineering Technology
Office of Nuclear Reg. Research
Materials Engineering Branch
U.S. Nuclear Regulatory Commission, Washington, DC 20555

10. PROJECT/TASK/WORK UNIT NO.

11. CONTRACT NO.
A-3011

13. TYPE OF REPORT
Technical (Formal)

PERIOD COVERED (Inclusive dates)

15. SUPPLEMENTARY NOTES

14. (Leave blank)

16. ABSTRACT (200 words or less)

An investigation was performed on eleven commonly used lubricants by the nuclear power industry which included EDS analysis of the lubricants, notched-tensile constant extension rate testing of bolting materials with the lubricants, frictional testing of the lubricants and weight loss testing of a bonded solid film lubricant. The report concludes that there is a significant amount of variance in the mechanical properties of common bolting materials, that MoS_2 can hydrolyze to form H_2S at 100°C and cause stress corrosion cracking (SCC) of bolting materials. One of the most significant findings of this report is the observation that both A193 B7 and A540 B24 bolting materials are susceptible to transgranular stress corrosion cracking in demineralized H_2O at 280°C in notched tensile tests.

17. KEY WORDS AND DOCUMENT ANALYSIS

17a. DESCRIPTORS

lubricants
bolting materials
MoS_2
H_2S
transgranular stress corrosion cracking

17b. IDENTIFIERS/OPEN-ENDED TERMS

18. AVAILABILITY STATEMENT
Unlimited

19. SECURITY CLASS (This Report)
Unclassified

21. NO. OF PAGES

20. SECURITY CLASS (This Page)
Unclassified

22. PRICE
$

NRC FORM 335 (7 77)